Clemens Bell, BSc

FE-Analysis of Slope Stability Reinforced by Vegetation

MASTER'S THESIS

to achieve the university degree of

Master of Science

Master's degree programme: Civil Engineering, Geotechnics and Hydraulics

submitted to

Graz University of Technology

Supervisor

Ao.Univ.-Prof. Dipl.-Ing. Dr.techn. M.Sc. tit.Univ.-Prof. Helmut Schweiger
(Institute of Soil Mechanics and Foundation Engineering)

Second supervisor

Dr.techn. Indra Noer Hamdhan
(Bandung National Institute of Technology)

Graz, December 2015

Eidesstattliche Erklärung

Ich erkläre an Eides statt, dass ich die vorliegende Arbeit selbstständig verfasst, andere als die angegebenen Quellen/Hilfsmittel nicht benutzt, und die den benutzten Quellen wörtlich und inhaltlich entnommenen Stellen als solche kenntlich gemacht habe. Das in TUGRAZonline hochgeladene Textdokument ist mit der vorliegenden Masterarbeit identisch.

Graz, am _____ _____

(Unterschrift)

Statutory declaration

I declare that I have authored this thesis independently, that I have not used other than the declared sources / resources, and that I have explicitly marked all material which has been quoted either literally or by content from the used sources. The text document uploaded to TUGRAZonline is identical to the present master's thesis dissertation.

Graz, _____ _____

(Signature)

Preface of the author

There are so many people who supported me and contributed to the success of my studies and this master thesis. I want to express my gratitude to all of them.

I want to thank Ao.Univ.-Prof. Dipl.-Ing. Dr.techn. M.Sc. tit. Univ.-prof. Helmut Schweiger for the great opportunity to enable me writing my master thesis in Indonesia and his excellent guidance. I am also grateful to Dipl.-Ing. Patrick Pichler, BSc for his support and valuable suggestions.

Spacial thanks goes to Dr.techn. Indra Noer Hamdhan from Bandung National Institute of Technology (Indonesia) for his guidance and efforts to make my stay in Bandung as an interesting and diversified time, wherefrom I take countless great memories.

Most of all I want to thank my family for being the strongest backing one can have. You supported me in every single stage of my life and believed in me and my skills.

Abstract

Landslides are a worldwide and widespread problem and can be seen as a major form of natural hazards. They are most costly in terms of human life and economic loss. In recent years a lot of research has been done in order to understand the behaviour and mechanisms of landslides. In addition to sophisticated structural measures to enhance the stability of slopes, vegetation can be seen as a more economic and ecological approach. However, using vegetation as a reinforcing element is rarely included in slope stability analysis or in geotechnical design for slope stabilization.

This thesis gives a general overview on the mechanical and hydrological effects caused by the soil-root interaction. The focus is put on the mechanical description of roots and their implementation into a numerical model. Furthermore, the stability of a simple homogeneous slope including vegetation is studied by using a perpendicular root model. The behaviour of the model is analysed by conducting different case studies that represent the main factors of influence in slope stability (type of soil, inclination, water table, location of the vegetation and tension cracks).

Kurzfassung

Hangrutschungen sind ein weltweites und weitverbreitetes Problem mit großem Gefährdungspotential. Sie können verheerende Auswirkungen in Bezug auf das menschliche Leben und deren Wirtschaft haben. Im Bereich von Hangrutschungen ist in vergangener Zeit sehr viel Forschung betrieben worden, um das Verhalten und die Mechanismen verstehen zu können. Im Gegensatz zu aufwendigen baulichen Maßnahmen, um die Stabilität von Hängen gewährleisten zu können, kann die ingenieurtechnische Anwendung von Vegetation als einen ökologischeren und ökonomischeren Ansatz gesehen werden. Dennoch findet Vegetation selten Anwendung in der geotechnischen Planung und wird kaum in Berechnungen von Hangstabilitäten berücksichtigt.

Diese Arbeit beinhaltet einen allgemeinen Überblick über die mechanischen und hydrologischen Auswirkungen der Boden-Wurzel Interaktion. Der Fokus liegt dabei auf der mechanischen Beschreibung von Wurzeln und deren Anwendung in einem numerischen Modell. Die Stabilität eines homogenen Hanges mit Vegetation wird mit Hilfe eines senkrechten Wurzelmodells untersucht. Das Verhalten des Modells wurde anhand verschiedener Fallstudien untersucht. Diese beinhalten die gängigsten Einflussparameter für die Berechnung der Hangstabilität (Art es Bodens, Hangneigung, Wasserspiegel, Ort der Vegetation und Spannungsrisse).

Table of contents

List of figures

List of tables

List of symbols and abbreviations

Capital letters

A	[m²]	Cross-sectional area without roots
A_R	[m²]	Cross-sectional area of roots
C_d	[-]	Bulk surface resistance and earodynamic resistance coefficient
D	[m^3/s]	Drainage rate
E	[m^3/s]	Evaporation rate
E_{ref}	[N/m²]	Young's modulus
ET_0	[mm/h]	Potential evapotranspiration
ET_c	[mm/h]	Actual evapotranspiration
F	[m]	Diameter distribution function
F_I	[m^3/s]	Inflow of groundwater
F_O	[m^3/s]	Outflow of groundwater
F_p	[N]	Pullout force for an individual root
H	[m]	Global water level at the toe of the slope
I_T	[m^3/s]	Effective interception of vegetation
K_c	[-]	Crop specific evapotranspiration coefficient
K_w	[N/m²]	Bulk modulus of water
L	[m]	Length of root
P	[m^3/s]	Percolation rate
R_N	[MJ/kg]	Net radiation
S	[-]	Degree of saturation
S_e	[-]	Effective degree of saturation
SI	[m^3/s]	Supplemental irrigation rate in the soil system
S_{max}	[m^3/s]	Volume of extracted water
SR	[m^3/s]	Surface run off of water
S_{res}	[-]	Risidual saturation
S_{sat}	[-]	Saturation when the pores are fully filled with water
S_{acc}	[m^3/s]	Actual extraction rate under field conditions
T	[m^3/s]	Transpiration rate
T_a	[^oC]	Mean hourly air temperature
T_p	[m^3/s]	Potential transpiration rate
T_R	[N/m²]	Avarage tensile strength of roots
U_2	[m/s]	Wind speed at 2 meters above ground surface

Small letters

$\underline{\underline{k}}^{sat}$	[m/s]	Saturated permeability matrix
$\underline{\underline{k}}$	[m/s]	Tensor of permeability
$\underline{g}$	[m/s^2]	Vector of gravitational acceleration
$\underline{q}$	[m]	Unsaturated water flow
a	[m]	Parameter for defining the slope of the root water extraction function
b	[m]	Parameter for defining the slope of the root water extraction function
c'	[N/m²]	Effective cohesion
c_R	[N/m²]	Apparent cohesion due to roots
d	[m]	High of water table
f	[-]	Yield function
g_a	[-]	Fitting parameter related to the air entry value of the soil
g_c	[-]	Fitting parameter used in the general Van Genuchten equation
g_n	[-]	Fitting parameter as a function of the water extraction rate
k_{rel}	[m/s]	Relative permeability (permeability at a given saturation)
l	[kPa/^{o}C	Slope of saturated vapour pressure curve
n	[-]	Porosity of the soil
o_a	[kPa]	Actual vapour pressure
o_s	[kPa]	Saturated vapour pressure
p'	[N/m^2]	Mean effective stress
p_a	[N/m^2]	Pore air pressure
p_w	[N/m²]	Pore water pressure/ suction pore pressure
q	[N/m^2]	Deviatoric stress
r	[m]	Depth below ground surface, radius of root
r_{max}	[m]	Maximum root depth
t	[s]	Time
u	[N/m²]	Pore water pressure

Greek letters

φ	[^{o}]	Friction angle
φ'	[^{o}]	Effective friction angle
γ_p	[kPa/ ^{o}C]	Psychrometric constant
γ_{sat}	[N/m^3]	Saturated soil unit weight
γ_{unsat}	[N/m^3]	Unsaturated soil unit weight
γ_w	[N/m^3]	Unit weight of water
$\underline{\varepsilon}$	[-]	Vector of strain
$\underline{\varepsilon}^e$	[-]	Vector of elastic strain

$\underline{\varepsilon}^{p}$	[-]	Vector of plastic strain
ρ_w	[kg/m^3]	Density of water
σ_1'	[N/m^2]	Minor principal effective stress
σ_3'	[N/m^2]	Major principal effective stress
ϕ_p	[N/m^2]	Suction pore pressure head
ω	[MJ/kg]	Latent heat vapouration
α	[-]	Pore water suction dependent function
θ	[^{o}]	Shearing angle of the roots
σ	[N/m^2]	Total stress
σ'	[N/m^2]	Effective stress
τ	[N/m^2]	Total shear stress
υ	[-]	Poisson's ratio
χ	[-]	Matric suction coefficient
ψ	[-]	Dilatancy angle
ψ_{max}	[m]	Maximum pore pressure head
ψ_{min}	[m]	Minimum pore pressure head
ϕ	[m]	Diameter of the roots

Abbreviations

CIMIS	California Irrigation Management Information System
FAO	United Nations Food and Agriculture Organization
FBM	Fiber Bundle Model
FE	Finite Element
FEM	Finite Element Method
MC	Mohr-Coulomb
MORECS	Meteorological Office Rainfall and Evaporation Calculation System
PM	Penman-Monteith
RAR	Root Area Ratio
RWUM	Root Water Uptake Model
SWCC	Soil Water Characteristic Curve
USDA	United States Department of Agriculture

1 Introduction

Landslides are a worldwide and widespread problem. These natural hazards are most costly in terms of human life and economic loss. Therefore, it can be considered as one of the key topics in geotechnical engineering. In recent years a lot of research has been done in order to understand the behaviour and mechanisms of landslides. There are several factors that can trigger landslides such as geological activity, hydrological influence and human interference. However, seepage and rainfall can be seen as the main factors (Likitlersuang et al. 2015).

Using vegetation as a reinforcing element is a more economic and ecological approach to enhance the stability of slopes compared to sophisticated slope stabilization by structural measures. Vegetation supports the draining of the soil before and after a rainfall event, increases soil suction, reduces pore pressures and strengthens the soil due to its roots.

In this work an overview about the mechanical and hydrological behaviour of a rooted soil is given. Further, stability analysis on a simple homogeneous slope are carried out by using the finite element software PLAXIS and a perpendicular root model for calculating the strength parameter due to the roots. The Objective of the thesis is the analyses of the basic behaviour of a slope with a vegetation cover. This is done by conducting different case studies, which represents the main factors of influence in slope stability (type of soil, inclination, water table, location of the vegetation and tension cracks).

2 Slope reinforcement using vegetation

The focus in this chapter is put on the mechanical and hydrological effect provided by the root system. Moreover, some techniques are shown how to implement a root system into a numerical model. For the sake of convenience and a better understanding a brief review about unsaturated soil behaviour is given in chapter 2.2.1.

Further information about the characteristics, root morphology and effects on the soil reinforcement is provided by e.g., Mickovski (2009), Simon & Collison (2002) Islam & Sahin (2013), Fan & Lai (2013), Faisal & Normaniza (2008) and Likitlersuang et al. (2015).

2.1 Mechanical effects provided by the root system

Chirico et al. (2013) describe two main positive effects caused due to the soil-root interaction:

- **A geo-mechanical effect:**
  The geo-mechanical effect is related to the reinforcement provided by the root network that explores the soil in the vadose zone (unsaturated zone) in order to maximize the efficiency in water uptake.

- **A soil-hydrological effect:**
  As a result of the root water uptake, suction is generated which causes negative pore water pressures and this has a positive effect on the stability of slopes (chapter 2.2).

The reinforcement mechanics of a soil-root matrix can be compared with reinforced concrete structures using steel. Soil can absorb forces by compression but can't significantly handle tension forces. On the contrary, roots can resist tensile forces while having no resistance if compressed. The main properties that are influencing the mechanical behaviour of the soil-root system are the soil strength, the single root strength, the interface strength between soil and roots and the root spatial structure (Waldron & Dakessian 1981 and Schwarz et al. 2010).

Experimental data from direct shear tests on blocks of soil containing roots have shown that the presence of roots have an increasing influence on the soil cohesion but just a small effect on the friction angle (Wu et al. 1988, Faisal & Normaniza 2008). Figure 1 shows the result of a direct shear test and the effect of increased cohesion while leaving its friction angle unaffected. This effect can be implemented in the Mohr-

Coulomb failure criterion trough an “apparent cohesion” term (Gentile et al.1998) (Eq.(1)). This means that the cohesion of the rooted soil contains two different parts of cohesion, the effective cohesion of the soil without roots and the additional cohesion (apparent cohesion) due to the presence of roots.

$$\tau = (c' + c_R) + \sigma' \tan \varphi' \tag{1}$$

For the unsaturated part of the soil the effective stress can be written as:

$$\sigma' = (\sigma - p_a) + \chi\,(p_a - p_w) \tag{2}$$

Implementing equation (2) in equation (1) the shear strength for the unsaturated part of the soil becomes:

$$\tau = (c' + c_R) + [(\sigma - p_a) + \chi\,(p_a - p_w)] \tan \varphi' \tag{3}$$

τ	[kN/m^2]	Shear stress on the failure plane
c'	[kN/m^2]	Effective cohesion
c_R	[kN/m^2]	Apparent cohesion
σ'	[kN/m^2]	Effective stress normal to the shear plane
σ	[kN/m^2]	Total stress normal to the shear plane
φ'	[^{0}]	Effective friction angle of the soil
p_a	[kN/m^2]	Pore air pressure
p_w	[kN/m^2]	Pore water pressure
χ	[-]	Matric suction coefficient

See chapter 3.1.2 for more information about the stress analysis of unsaturated soils.

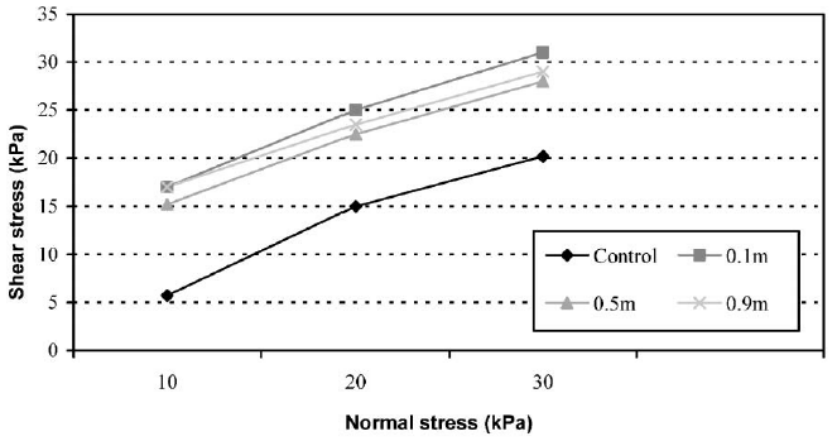

Fig. 1 Direct shear tests from 12 months old Vetiver plants under soil suction-free conditions, control represents the soil without roots, 0.1/0.5/0.9 represents the rooted soil in particular depths (Faisal & Normaniza 2008)

2.1.1 Perpendicular root model

The model is assuming that all roots are perpendicular to the shearing plane (Fig. 2). Due to the fact that roots have no significant bending stiffness, tension is transferred to them as the soil is sheared. Furthermore the tension in the roots while shearing can be expressed as a tangential component resisting shear and a normal component increasing the confining pressure on the shear plane (Waldron 1977).

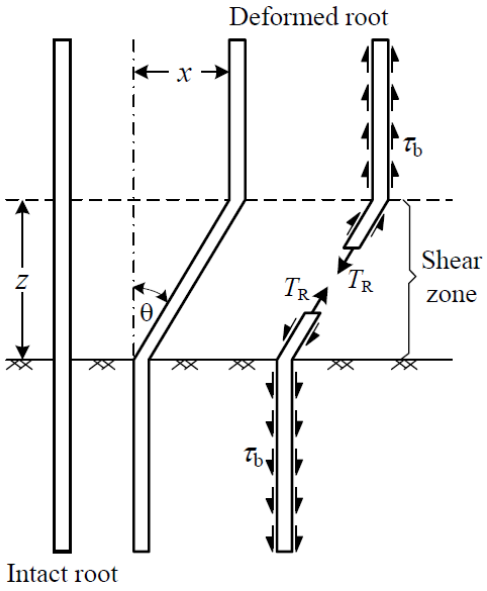

Fig. 2 Interface between soil and root (Likitlersuang et al.2015)

Considering the above-mentioned simplifications, the apparent cohesion can be formulated with equation (4):

$$c_R = T_R(\sin\theta + \cos\theta \tan\varphi)\frac{A_R}{A} \tag{4}$$

T_R is the average tensile strength of roots per unit area of soil (kN/m^2), A_R/A is the root area ratio (ratio of roots to non-rooted soil in a cross sectional area of the soil), θ is the shearing angle of the roots (degrees) and φ is the friction angle of the soil (degrees).

The shearing angle θ (Eq. (4)) is unknown and difficult to determine because it is depending on the shear path of the sliding plane. For this Wu et al. (1979) carried out a sensitivity analysis for the term $(\sin\theta + \cos\theta \tan\varphi)$ shown in equation (4) for normal variations of θ and φ (40-90˚ and 25-40˚ respectively). The values are ranging from 1.1 to 1.3. An average value of 1.2 was selected by Wu et al. (1979).

Therefore, equation (4) can be simplified and written as:

$$c_R = 1.2\, T_R\, \frac{A_R}{A} \tag{5}$$

As the diameter and the concentration of the roots are generally decreasing with depth, the root area ratio (RAR, A_R/A) is changing. Furthermore the RAR is showing a very high variability with species, location and depth (Gentile et al. 2010). If the variation of the RAR is known over depth, equation (5) can be written as:

$$c_R(\mathrm{z}) = 1.2\, T_R\, \frac{A_R(z)}{A} \tag{6}$$

Equation (5) constitutes a simplified model for the apparent cohesion and is based on following assumptions:

- All roots are orientated perpendicular to the shear plane.
- The full tensile strength of all roots is mobilized at the time when the soil fails.
- The roots are failing due to exceeding the tensile strength and are not pulled out of the soil.
- The tensile strength of the roots is constant and not changing with diameter.

Considering the tensile strength is dependent on the root diameter, equation (5) can be formulated as (Cazzufi & Crippa 2005):

$$c_R(\mathrm{z}) = 1.2 \left(\int_{\phi_{min}}^{\phi_{max}} T_R\,(\phi)\, F(\phi)\, d(\phi) \right) \frac{A_R(z)}{A} \tag{7}$$

The diameter of the roots is varying between ϕ_{max} and ϕ_{min}, T_R is the maximum tensile stress and $F(\phi)$ is the diameter distribution function of the particular species. For the diameter distribution experimental studies have been carried out to investigate the correlation between the diameter of the roots and its related tensile strength (Fig. 3). These studies have shown that smaller root diameters correspond to higher tensile strength and the data can be interpolated by an exponential negative function shown by Cazzuffi & Crippa (2005). Two different growth conditions have been taken for the studies. First, plants grown in natural conditions (defined as S-Plants) and second, plants grown in pots (defined as P-Plants). Both types of samples have the same age.

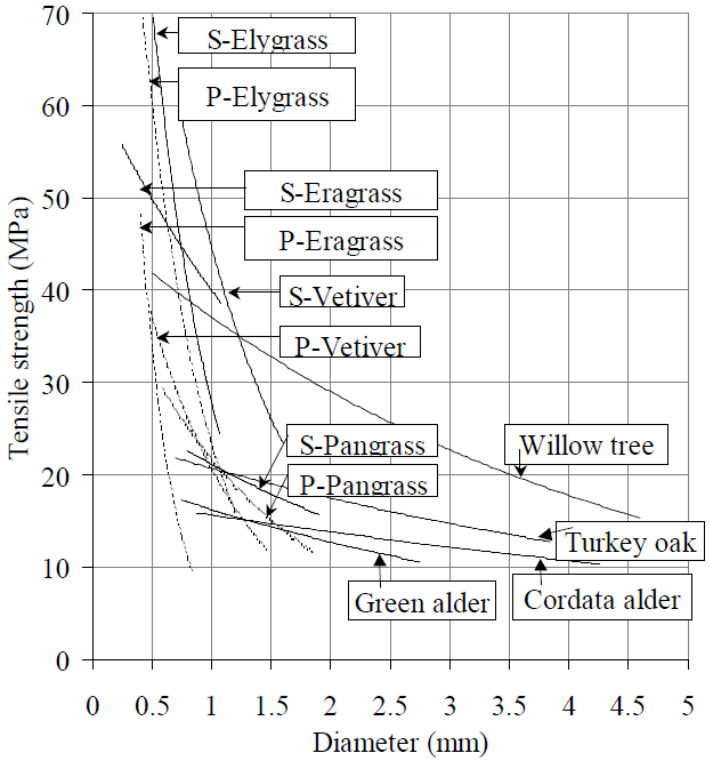

Fig. 3 Maximum tensile strength vs. root diameter for specific tested plants (Cazuuffi & Crippa 2005)

2.1.2 Root models considering progressive failure and root-pullout

As a consequence of the above-mentioned simplifications by using the perpendicular root model the apparent cohesion tends to be overestimated. Field and laboratory tests carried out by Pollen (2004), Pollen & Simon (2004) and Thomas & Pollen (2009) confirmed the effect of this overestimation when using the perpendicular root model. To overcome these simplifications Thomas & Pollen (2009) are calculating the apparent cohesion by using a fibre-bundle model (FBM). This model uses a dynamic approach with progressive root failure to overcome the assumption that all roots break simultaneously. If a fibre (root) is breaking because of exceeding its tensile strength, the stress that was carried by the broken fibre is now redistributed to the intact fibres. The model takes into account that roots with a greater cross-sectional area receive a greater proportion of the total applied load (the load is divided that every fibre receives equal stress) as well as the root orientation relative to the failure plane and the angle of the shear distortion.

When shearing a root-reinforced soil, two main mechanical mechanisms of root failure occur: (1) root breaking and (2) root-pullout (Pollen, 2006). The perpendicular root model (chapter 2.1.1) and the fibre-bundle model (chapter 2.1.2) are describing root breaking without considering the effect of root-pullout. According to Pollen (2006) the root-pullout force is dependent on the soil shear strength and the soil matric suction and can be formulated as (Pollen 2006):

$$F_p = \mathrm{S} \cdot \mathrm{L} \cdot 2\pi\mathrm{r} \tag{8}$$

F_p is the pullout force for an individual root [N], S is the soil shear strength [kPa], r is the radius of the root [m] and L is the length of the root [m]. Pollen (2006) has shown that the inclusion of root pullout is particularly important. Especially for critical stability conditions when perpendicular root models tend to overestimate the reinforcing effect of roots.

For further information Pollen (2006) shows a developed function for the pullout forces while taking suction and negative pore water pressures into account. Chirico et al. (2013) show an eco-hydrological model developed from Wu et al. (1979) which is calculating the *RAR(z)* taking local climatic conditions and soil water retention properties into account.

2.2 Hydrological effects of the soil-root interaction

The hydrological effect of a vegetated slope can be generally divided into two main effects: (a) the influence of the unsaturated behaviour of the soil and (b) the influence of the vegetation to the hydrological behaviour. For the sake of completeness and a better understanding, a short review about the unsaturated soil behaviour in terms of the unsaturated groundwater flow and the influence of the suction pore pressure on the saturation is given in chapter 2.2.1. Further, chapter 2.2.2 deals with the influence of the vegetation on the hydrological behaviour of soils.

It should be noted that in the following chapter only the main equations are shown. A full description can be found in Hamdhan (2012).

2.2.1 A brief review on unsaturated soil behaviour

Based on Darcy's law (1856) for a water flow in saturated soils, equation (9) shows the unsaturated flow $\underline{q}$ in a porous medium:

$$\underline{q} = \frac{\underline{\underline{k}}}{\rho_w g}\left(\underline{\nabla} p_w + \rho_w \underline{g}\right) \tag{9}$$

where,

$$\underline{\underline{k}} = k_{rel}\,\underline{\underline{k}}^{sat} \tag{10}$$

The permeability $k_{rel}\,(S)$ is defined as the ratio of the permeability at a given saturation to the permeability in the saturated state and $\underline{\underline{k}}^{sat}$ is the saturated permeability matrix. ρ_w is the density of water and $\underline{g}$ is the vector of gravitational acceleration $(0, -g, 0)^T$. The term $\rho_w g$ is used by assuming hydrostatic conditions. Therefore the flow is not affected by the gradient of water pore pressures in vertical directions. $\underline{\nabla} p_w$ is the gradient of the water pore pressure which generates the groundwater flow.

For a better representation of the physical behaviour of an unsaturated groundwater flow, the compressibility of water and the change of soil porosity (compression of soil due to combined action of effective stress and pore pressure) is taken into account, while neglecting the deformations of solid particles, the gradient of water density and the displacements of solid particles for transient groundwater flow. Implementing the unsaturated groundwater flow (Eq. (9)) and the above mentioned considerations into the continuity equation, it can be formulated as equation (11). The continuity equation

is according to the mass concentration and describes that the water outflow from the volume is equal to the change in the mass concentration.

$$\underline{\nabla}^T \left[\frac{k_{rel}}{\rho_w g} \underline{\underline{k}}^{sat} \left(\nabla p_w + \rho_w \underline{g}\right)\right] - \mathrm{n}\left(\frac{S}{K_w} - \frac{\partial S}{\partial p_w}\right)\frac{\partial p_w}{\partial t} = 0 \tag{11}$$

The porosity of the soil is described by *n* and *S* is the saturation. The compressibility of the water is defined by the bulk modulus K_w.

In steady state conditions (variation of pore pressure with respect to time is zero, $\partial p_w/\partial t = 0$) the continuity equation becomes:

$$\underline{\nabla}^T \left[\frac{k_{rel}}{\rho_w g} \underline{\underline{k}}^{sat} \left(\nabla p_w + \rho_w \underline{g}\right)\right] = 0 \tag{12}$$

Using equation (12) the suction pore pressure p_w can be calculated. As the saturation of the soil is dependent on the pore pressure, a hydraulic model described by the Soil Water Characteristic Curve (SWCC) is presenting this behaviour. The SWCC defines the water store capacity of a soil for a given soil suction (Ng & Pang 2000).

A common and widely used formulation of the SWCC is proposed by Van Genuchten (1980). The Van Genuchten model relates the saturation to the pressure head ϕ_p and has three parameters for describing the shape of the SWCC:

$$\mathrm{S}(\phi_p) = S_{res} + (S_{sat} - S_{res})\left[1 + \left(g_a|\phi_p|\right)^{g_n}\right]^{g_c} \tag{13}$$

where,

$$\phi_p = -\frac{p_w}{p_w g} \tag{14}$$

p_w is the suction pore pressure, S_{res} is residual saturation (describes the part of the pore fluid which remains in the pores) and S_{sat} is the saturated condition.

g_a, g_n, and g_c are fitting parameters. The parameter g_a is related to the air entry value of the soil and has to be measured. g_n is a function of the rate of water extraction from the soil once the air entry value has been exceeded. The parameter is specific to a material and has to be measured. g_c is a fitting parameter and in PLAXIS it is used to convert the Van Genuchten model into a two-parameter equation (Eq. (15)):

$$g_c = -\frac{1-g_n}{g_n} \tag{15}$$

The derivative of the degree of saturation in a two-parameter formulation with respect to the suction pore pressure is:

$$\frac{\partial S(p_w)}{\partial p_w} = (S_{sat} - S_{res}) \left[\frac{1-g_n}{g_n}\right] \left[g_n \left(\frac{g_a}{\gamma_w}\right)^{g_n} p_w^{(g_n-1)}\right] \left[1 + \left(g_a \frac{p_w}{\gamma_w}\right)^{g_n}\right]^{\left(\frac{1-2g_n}{g_n}\right)} \tag{16}$$

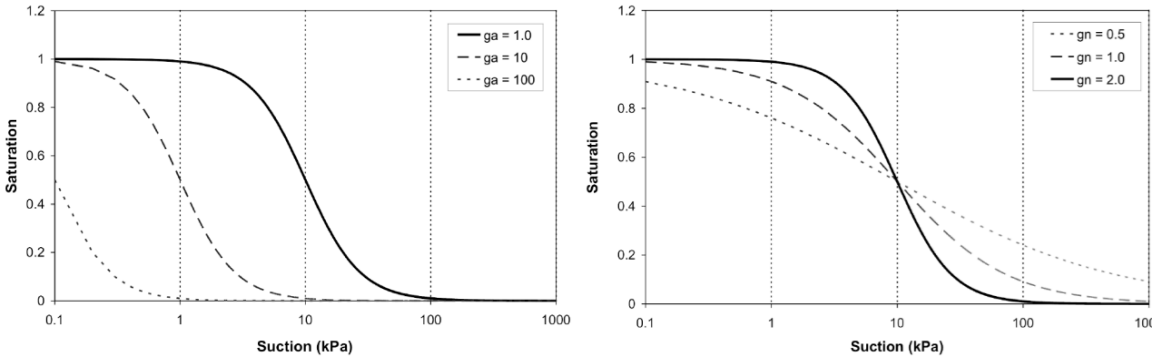

Fig. 4 Effect of the Van Genuchten relations on the SWCC (Brinkgreve et al. 2014a)

Fig. 4 shows the degree of saturation at different suction pore pressures and the influences of the fitting parameters g_a and g_n on the SWCC. If the saturation is smaller than one (S < 1), suction is generated, which is a beneficial parameter because it increases the shear strength of the unsaturated soil. On the contrary, if positive pore pressures are generated, the shear strength of the soil will be reduced (see also chapter 3.1.2, Stress analysis).

2.2.2 Contribution of vegetation to the hydrological behaviour of soils

Vegetation extracts its required water from the soil due to its roots. Therefore a beneficial hydrological impact results due to decreasing moisture content and further with time a lower phreatic water level (Selby, 1993). As a consequence the matric suction is increased and as a result the shear strength (Simon & Collison 2002). The driving force that transfers the water from the soil system to the atmosphere is the transpiration (defined as water vaporized from the plant). Therefore, the interaction between soil, vegetation and the atmosphere plays an important role in the root water uptake model (Fatahi 2007).

Fatahi (2007) describes the effect of decreasing discharge of the roots by increasing soil suction. As soil suction is the resisting force for the movement of water, it also affects the transpiration rate. Therefore, soil suction can be seen as a reduction factor for the potential transpiration rate which can be related to the moisture content for the root water uptake (Fig. 5)

The preview chapter 2.2.1 was showing the correlation of the suction pore pressure p_w and the degree of saturation influenced by the soil characteristics. But furthermore, the suction pore pressure and therefore the matric suction are also influenced by environmental factors (infiltration due to precipitation, evaporation and boundary drainage conditions including the location of groundwater level).

By having no infiltration and transpiration the matric suction profile will come to a hydrostatic equilibrium. As a consequence there is no water flux up- or downwards from the ground surface. Infiltration in the unsaturated part of the soil will reduce the matric suction because of an increasing saturation (downward flux). When having transpiration (extraction of moisture) due to the root water uptake, matric suction will be increased (upward flux). See figure 5 for an explanation of the matric suction profile for horizontally layered unsaturated soils.

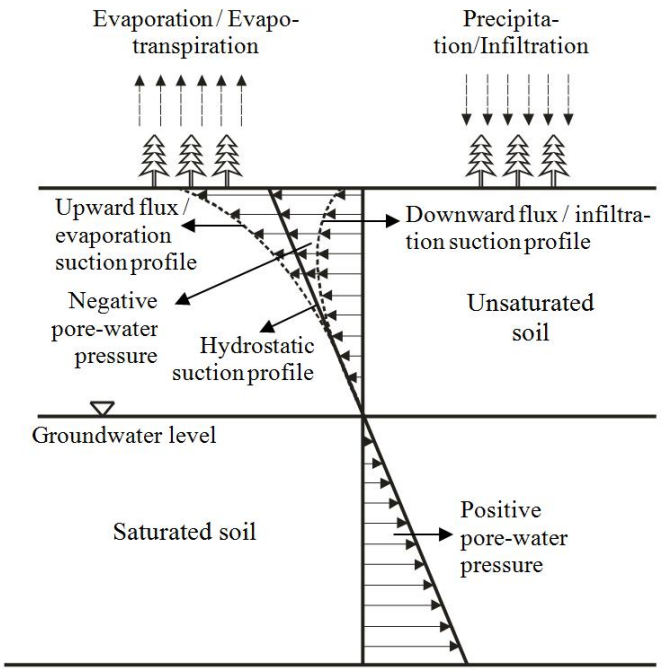

Fig. 5 Matric suction profile for unsaturated soil profiles under various surface flux boundary conditions (Fredlund 1996)

In order to analyse the effect of vegetation on the ground, the transpiration rate must be included in the flow equation and the knowledge of the initial water content and the quantities of water, entering and leaving the soil system, is required. For solving the equation, a coupled flow and deformation analysis must be performed (Fatahi 2007). Fig. 6 shows a soil system with its hydrological factors of influence.

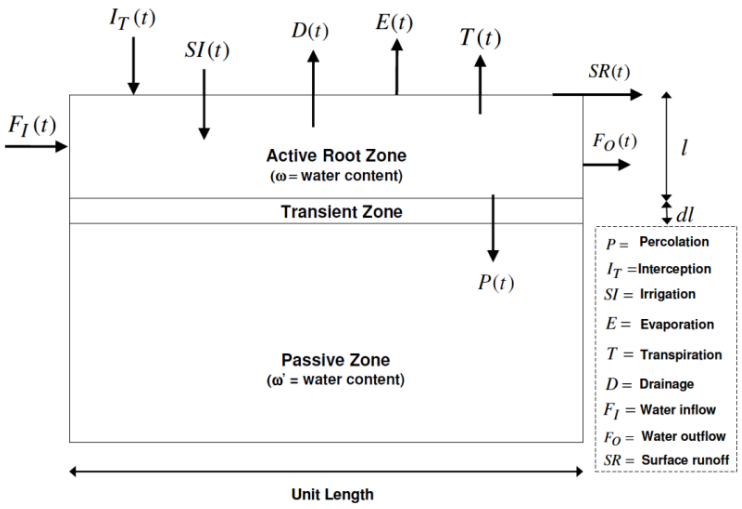

Fig. 6 Soil system with hydrological factors of influence (Fatahi 2007)

F_I(t) is the inflow of groundwater flow, $I_T(t)$ is the effective interception, which reaches the soil system (Precipitation below the canopy), $SI(t)$ is the supplemental irrigation rate in the soil system, $D(t)$ is the drainage rate, $E(t)$ is the evaporation rate, $T(t)$ describes the transpiration rate, $P(t)$ is the percolation rate, $SR(t)$ is the surface run off and $F_O(t)$ is the outflow of groundwater. The rooted zone is defined as the active zone and the passive zone is the soil without roots. Fatahi (2007) is showing in his work the most common models for the root water uptake.

As most of the parameters are already implemented in numerical models, the description of the transpiration ($T(t)$) from the root water uptake is still a challenge as it depends on a number of parameters (climatic conditions, root architecture, soil parameters, hydraulic parameters and characteristics of the vegetation).

Simon & Collison (2002) described that the canopy interception is negligible (case study for winter/early spring when the deciduous trees where dormant) compared to the effect of water extraction by roots. The process of water uptake is primarily governed by the root density, conductivity of the soil-root system and the availability of water (Nyambayo & Potts 2009).

For investigating the hydrological influence of roots Simon & Collison (2002) developed a case study on stream bank stability occupied by different types of vegetation species. They were using the Mohr-Coulomb failure criterion for the limit equilibrium analysis for the saturated part. For the unsaturated part of the soil they used the Fredlund et. al (1979) criteria and for the root reinforcement the criteria from Waldron (1977). Both criteria are explained in chapter 2.1. The factor of safety was calculated by using the model to assess each attribute (root reinforcement, surcharge and modified pore water pressure) separately and in combination (Simon & Collison 2002). With this approach Simon & Collison were able to illustrate the influence of adding different attributes to the safety analysis (Fig. 7). One of the main outputs of this case study was that for some cases the hydrologic effects can be more beneficial than the mechanical effect. It has to be mentioned that this result is dependent on a lot of different input factors. Data from an unusually dry season is used, so the result is strongly dependent to its mechanical and hydraulic conditions. But however, this case study shows that hydrological effects shouldn't be neglected.

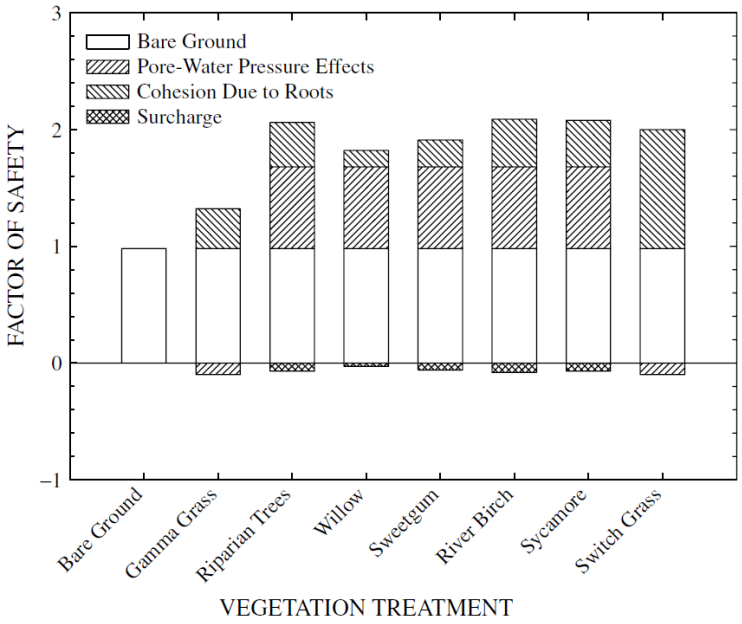

Fig. 7 Minimum factor of safety for special species during a dry year, subdivided by vegetation effects (Simon & Collison 2002)

2.2.3 Mathematical description of Root Water Uptake Model (RWUM)

According to Nyambayo & Potts (2009) RWUM's that do not involve plant-specific parameters in their algorithms are more versatile, as they can be applied to a wider range of vegetation types. On this account, a mathematical model of RWUM is shown which is proposed by Feddes et al. (1978) with modification to the proposed model from Prasad (1988). The model proposes the following one-dimensional linear RWUM:

$$S_{max} = \mathrm{a} - \mathrm{b} \cdot \mathrm{r} \tag{17}$$

where S_{max} represents the volume of extracted water per unit volume of soil, per unit time and is the maximum water extraction rate at depth r below ground surface. This extraction rate can occur if the soil moisture content is unlimited. The parameters *a* and *b* are defining the shape of the root water extraction function (Fig. 8). Therefore, below the maximum root depth, r_{max}, the water uptake is assumed to be zero and equation (17) becomes:

$$S_{max} = \mathrm{a} - \mathrm{b} \cdot \mathrm{r} = 0 \quad \text{for } \mathrm{r} \geq \mathrm{r_{max}} \tag{18}$$

By integrating equation (18) over the whole root depth, the total potential transpiration rate T_p can be obtained:

$$T_p = \int_0^{r_{max}} S_{max} \ \mathrm{dr} = \int_0^{r_{max}} a - b \cdot r \ \mathrm{dr} \tag{19}$$

Integrating equation (19) yields the shape coefficients *a* and *b*:

$$a = \frac{2\,T_p}{r_{max}} \quad \text{and} \quad b = \frac{2\,T_p}{r^2{}_{max}} \tag{20}$$

Now, the sink term S_{max} for unlimited soil moisture conditions can be determined by substituting these coefficients into equation (17):

$$S_{max} = \frac{2\,T_p}{r_{max}}\left(1 - \frac{r}{r_{max}}\right) \tag{21}$$

Under field conditions the degree of saturation is varying and dependent on the pore water pressure described by the SWCC. If the saturation is decreasing and therefore the matric suction is increasing, the actual transpiration is lower than the potential one. To be able to predict a more realistic root water uptake under these limiting conditions Feddes et al. (1978) proposed to add an additional factor α into the sink term (Eq. (21)) which is defining the extraction rate of water by different suction levels:

$$S_{acc}(\mathrm{r}) = \alpha\, S_{max} = \alpha\, \frac{2\,T_p}{r_{max}}\left(1 - \frac{r}{r_{max}}\right) \tag{22}$$

Equation (22) represents a one dimensional linear RWUM where S_{acc} is the actual extraction rate under field conditions (volume of water per unit volume of soil, per unit time) and α is a pore-water suction dependent function (unit less) (Fig. 9).

The actual rate of evapotranspiration T at time t can be calculated by the spatial integral of the volumetric rate of water uptake $S_{acc}(r)$ over the entire depth:

$$\mathrm{T(t)} = \int_{r_{max}}^{0} S_{acc}(r)\,dr \tag{23}$$

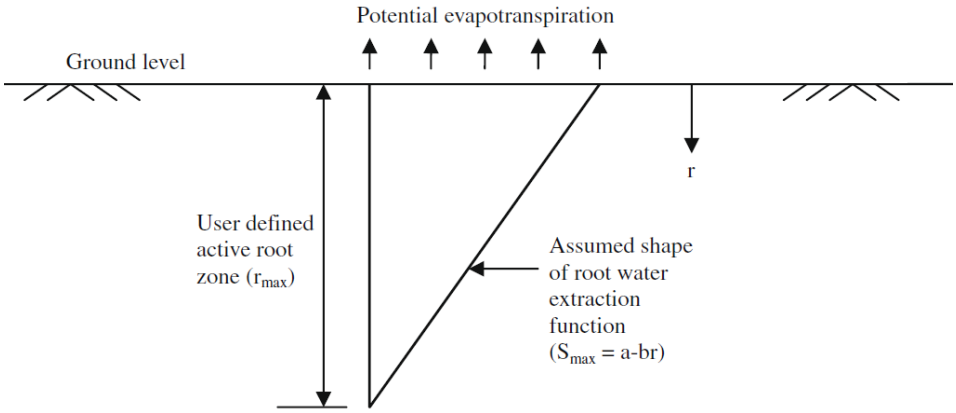

Fig. 8 Assumed shape of root water extraction function in the rooted zone (Nyambayo & Potts 2009)

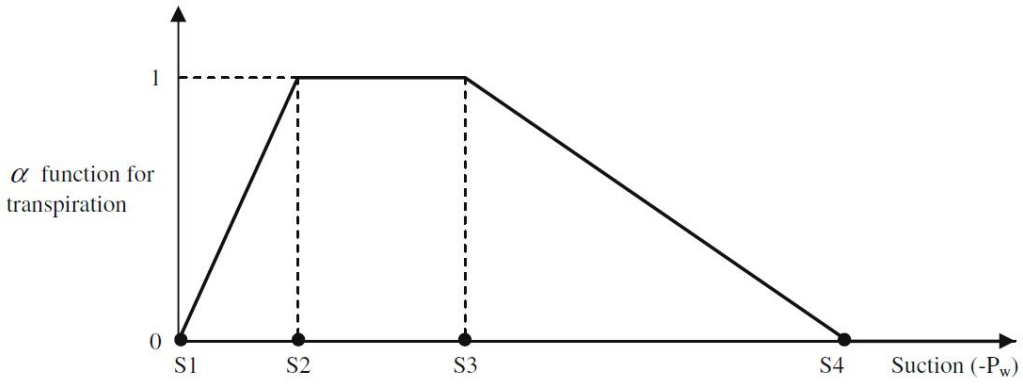

Fig. 9 Linear variation of α function dependent on the pore water pressure (Nyambayo & Potts 2009)

S4 is defined as the wilting point (minimal point of soil moisture the plant requires not to wilt) and the root water uptake is assumed to be zero at suctions higher than the wilting

point as well as for suctions below the anaerobiosis point *S1* (conditions when roots are unable to function). The root water uptake is assumed to be constant between the points *S2* and *S3*. A linear variation of α as a function of pore water suction is assumed between *S1* and *S2* and between *S3* and *S4* (Nyambayo & Potts 2009).

2.2.4 Determination of the actual evapotranspiration

Usually transpiration and evaporation is merged together to one parameter and expressed as evapotranspiration (ET_0). It is assumed that the potential transpiration T_p is equal to the actual evapotranspiration.

As it is very difficult to formulate an equation to estimate the actual evapotranspiration under different sets of conditions, the idea of reference crop evapotranspiration was developed. That means that standardized grass surfaces with well-known biophysical characteristics are used as a reference for the calculations. Using these known parameters and the measured climatic data, the ET_0 can be calculated. Then, a crop specific evapotranspiration coefficient (K_c) is used to calculate the actual evapotranspiration (ET_c) for a specific crop (Eq. (24)). Crop coefficients are established through a series of field measurements and vary by time of the year (Eching & Moellenberndt 2000). Now, the ET_c can be used for the root water uptake model, shown in the previous chapter 2.2.3.

$$ET_c = K_c \cdot ET_0 \tag{24}$$

For determining the potential evapotranspiration it is recommended to take use of meteorological calculation systems.

One of these is the Meteorological Office Rainfall and Evaporation Calculation System (MORECS). It is widely used in the United Kingdom and computes the values of potential evapotranspiration for a variety of plants. Detailed information about MORECS is provided by Hough & Jones (1997) and Hough et al. (1997). Another calculation system is the California Irrigation Management Information System (CIMIS)[1]. It estimates the reference evapotranspiration (ET_0) using the Penman-Monteith equation (PM) (Eq. (25)) and weather data (air temperature, relative humidity, wind speed and solar radiation). Moreover, Allen et al. (1998) is providing a guideline for calculating crop evapotranspiration from meteorological data and crop coefficients. In this guideline several different approaches are shown for calculating the

[1] California Departement of Water Resources: Determining the potential evapotranspiration. http://www.cimis.water.ca.gov/. Date of access: 21.10.2015

evapotranspiration. The United Nations Food and Agriculture Organization (FAO) recommend using the PM equation provided by Allen et al. (1998) (Eq. (25)).

$$ET_0 = \frac{l(R_N - G)}{\omega\left[l + \gamma_p(1 + C_d U_2)\right]} + \frac{\omega \frac{37}{T_a + 237.16} U_2 (o_s - o_a)}{l + \gamma(1 + C_d U_2)} \tag{25}$$

where l is the slope of the saturated vapour pressure curve [kPa/˚C], R_N is the net radiation [MJ/m^{2}h] and relates the amount of incoming radiation to the amount of radiation returning from the surface, γ_p is the psychrometric constant which relates the partial pressure of water in air to the air temperature [kPa/˚C], T_a is the mean hourly air temperature [˚C], U_2 is the wind speed at 2 meters above ground surface [m/s], o_s is the saturated vapour pressure [kPa], o_a is the actual vapour pressure [kPa], ω is the latent heat vapouration [MJ/kg] and C_d is the bulk surface resistance and aerodynamic resistance coefficient [-].

2.3 Considerations about rainfall infiltration

Rainfall infiltration can be seen as one of the main triggering factor in slope stability and is important to be considered in terms of a long-term stable design (Harry et al. 2007). Rainfall induced landslides are characterized by a failure surface parallel to the ground surface (Ali et al. 2014).

In the unsaturated part of the soil, above the water table, negative pore water pressures contribute toward higher shear strengths, which have a positive effect on the stability of the slope. The behaviour of the matric suction by changing saturation is described by the SWCC (Fig. 4). Infiltration of rainwater reduces the negative pore water pressures and increases the soil unit weight due to an increased saturation. Both of these effects have a destabilizing influence (Ali et. al 2014).

In a dry period a slope is drying due to a water loss because of evapotranspiration. This causes an upward flux of water and further an increased matric suction. Evapotranspiration also takes part while having rainfall infiltration and slowing the progressive wetting of the slope. The wetting front propagates in a direction normal to the slope surface (Ali et. al 2014). This can explain having shallow failure depth with a failure plane parallel to the ground surface.

An important hydraulic factor is the infiltration capability of the soil. It determines the amount of water entering the soil under a given rainfall event. If the rainfall intensity exceeds the infiltration capability of the soil, no more water can be absorbed from the soil and surface run-off takes place. The soil infiltration capability is mainly affected by the water content of the soil, the permeability of the soil and the topography of the slope (Gavin & Xue, 2008).

The main factors of influence are the characteristics of the rainfall (duration, intensity and pattern), the saturated hydraulic conductivity of the soil, the slope geometry, the initial conditions and the boundary conditions.

2.3.1 Hydrological impact of rainfall infiltration

As already discussed, the water uptake of roots can be seen as a function of the pore water pressures and therefore of the saturation. As a conclusion, the water uptake is not a constant factor while having rainfall events. They are changing the saturation pattern and are dependent on soil properties and climatic conditions (evaporation & transpiration). This is the reason why it is difficult to take evapotranspiration into

account. But critical conditions can be assumed with an infiltration high enough to compensate the stabilizing effect of the water uptake.

Rainfall infiltration can be classified in terms of the infiltration behaviour into two cases.

- **Rainfall intensity smaller than the saturated hydraulic conductivity (Fig. 10)**
  The matric suction is decreasing in the unsaturated part of the soil but cannot disappear. Therefore, no surface run-off takes place and the rainwater infiltrates fully into the soil.

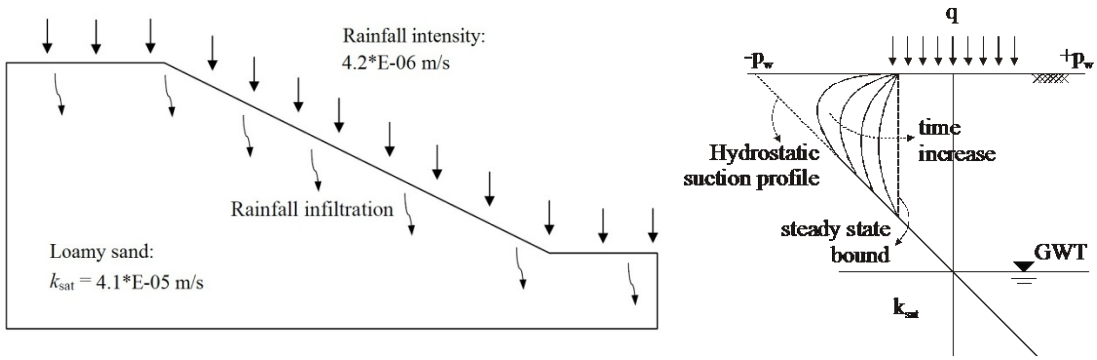

(a) (b)

Fig. 10 Case 1: Rainfall intensity smaller than the saturated hydraulic conductivity ($q < k_{sat}$); (a) modified from Sasekaran (2011), (b) from Hamdhan (2012)

- **Rainfall intensity higher than the saturated hydraulic conductivity (Fig. 11)**
  If fully saturated conditions are reached, the saturated part of the soil cannot absorb all of the rainwater anymore and surface run-off takes place.

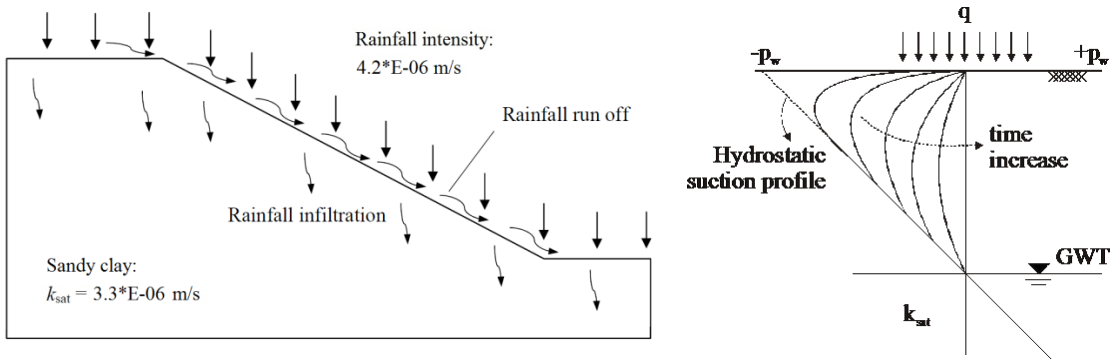

(a) (b)

Fig. 11 Case 2: Rainfall intensity higher than the saturated hydraulic conductivity ($q > k_{sat}$); (a) modified from Sasekaran (2011), (b) from Hamdhan (2012)

If evapotranspiration due to vegetation is not considered in the FE simulation, vegetation has no influence on the suction and saturation. This is shown by conducting a simple case study for a loamy sand column during rainfall infiltration with an intensity of q = 0.01 m/hour (Fig. 12). The soil column is 3 m high with a groundwater table at 1 m above ground surface. For the case including vegetation, six horizontal soil layers with increased cohesion are added (parameters from Table 1). The hydraulic parameters for the analysis have been evaluated by using the soil series from the international soil classification system (USDA).

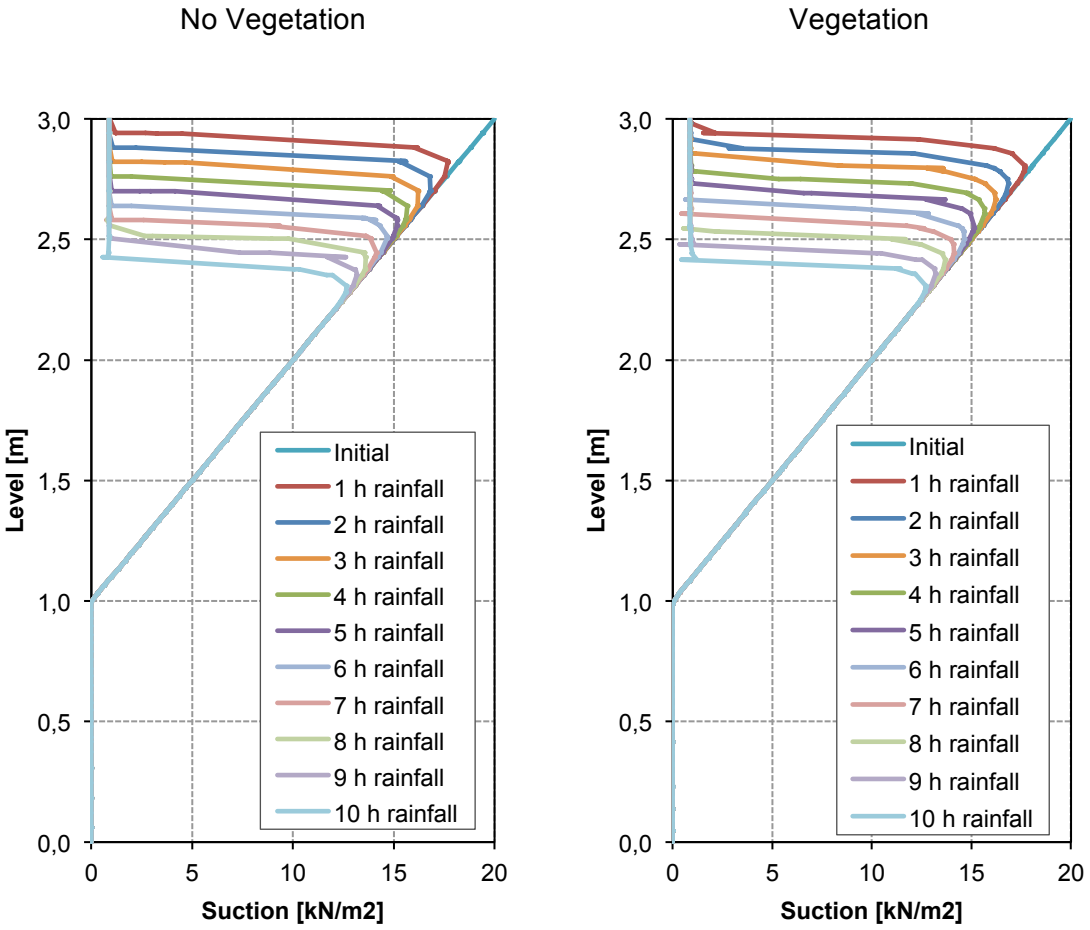

Fig. 12 Matric suction profile of a loamy sand column during infiltration (q = 0.01 m/hour)

Table 1 Parameters for the soil layers with increased cohesion, depths below ground surface

Depth [m]	0,25	0,5	0,75	1,0	1,25	1,5
c_R [kN/m^2]	64	55	46	37	28	19

2.4 Modeling vegetation in Finite Element Method (Plaxis)

In the past years a lot of researchers tried to investigate the beneficial effect of roots for erosion control and slope stability (Danjon et al. 2008, Preti & Giadrossich 2009, Islam & Shahin 2013, Lin et al. 2010, Pollen (2004, 2006) and Mickovski et al. 2011). In general there are two approaches for implementing roots into a numerical model.

2.4.1 Modeling single plant root architecture

One approach is to reproduce the plant root architecture with its physical properties into a three dimensional numerical model (Fig. 13). Therefore, the structure of the root system of the single plant has to be known and implemented into a numerical model. This requires a lot of effort since the plant has to be exempted from the soil and the topology and position coordinates of the root system have to be determined manually or by means of a 3-D digitizer method used by Danjon et al. (2008) in order to implement the data into the numerical model. Depending on how much plants are being modeled, the necessary time for computing will increase rapidly. On this account the mentioned method is commonly used for research and getting a better understanding of the soil-root interaction.

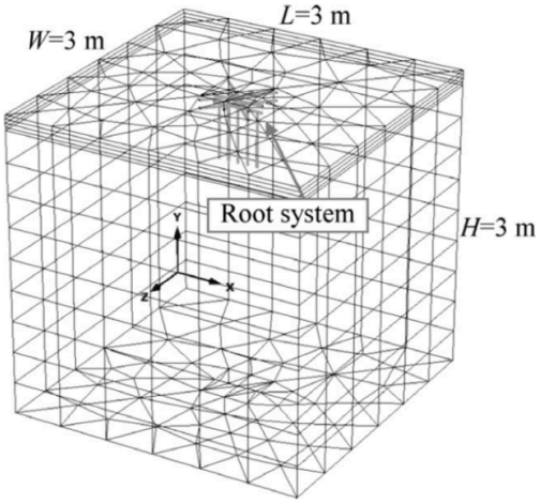

Fig. 13 3-D numerical modeling of a single root from the Makino bamboo soil-root system (Lin et al. 2010)

2.4.2 Simplification vegetation to a uniform layer of soil

A second approach is to assume that the increased strength for the slope due to the soil-root interaction is unchanged and uniform along the slope for specific depths.

This means that the spatial layout of the single specimens and its affect to the slope is simplified to a uniform layer of soil with increased strength (Fig. 14). In general, the amount of roots is decreasing by reaching greater soil depths. This results in a decreasing reinforcing effect of the roots and as a consequence the apparent cohesion is reducing. This effect can be applied in the model by establishing different soil layers with an associated apparent cohesion respective to the amount of roots. An advantage of this approach is that the single plant has not to be reproduced in the numerical model. As mentioned before, this would require the knowledge of a couple of parameters from the single plant. Thus, the required input parameter for the rooted soil is just the increased cohesion evaluated from a direct shear test or from using the formulations explained in chapter 2.1. Using these data the uncertainties like strength of the single roots, roots architecture and root diameter distribution can be avoided.

Attention while simplifying single plants to a uniform layer of soil should be payed since the spacing between the plants has an influence to the factor of safety (Fan &Lai 2014). That means that this method is more suitable for modelling vegetation with a more or less uniform root system like grasses and shrubs.

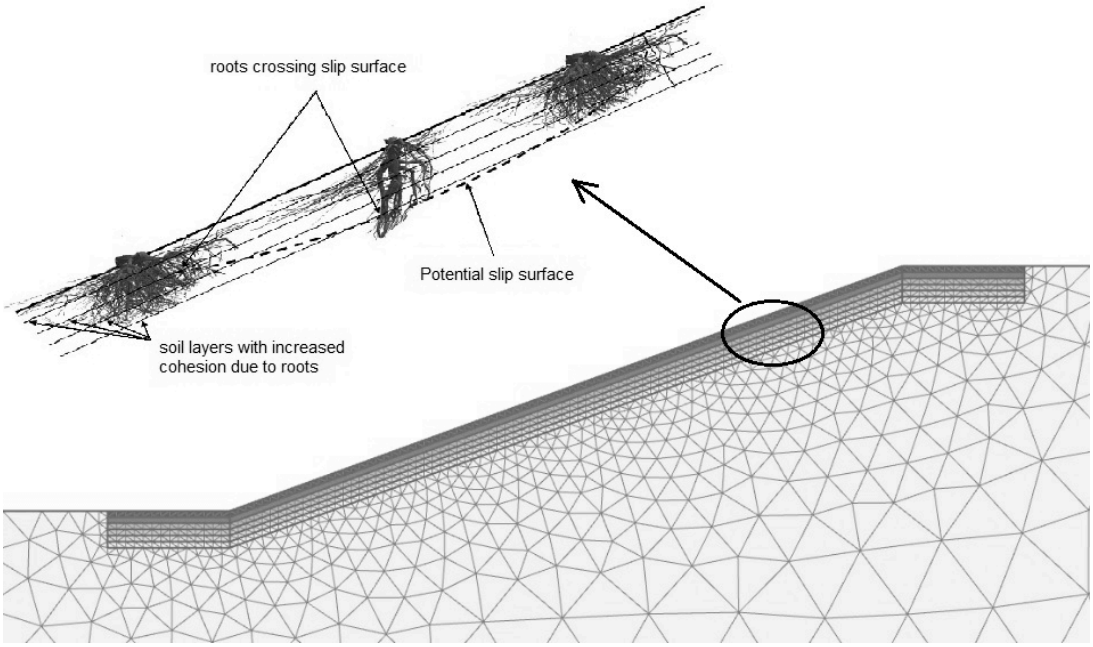

Fig. 14 Illustration of the simplification roots to soil layers with increased cohesion: Modified picture from Danjon et al. (2008)

3 Parameter study considering unsaturated soil behaviour

This chapter deals with the mechanical behaviour of vegetated slopes. Four case studies have been developed in order to analyse the effect of different parameters of influence (inclination, type of soil, water level, planted location and rainfall).

The vegetation is modelled by simplifying it to a uniform layer of soil with increased strength (Chapter 2.4.2). This approach is applied since the used vegetation for the case studies is a grass (Vetiver). Therefore, the mechanical behaviour of the single root is not relevant and the apparent cohesion (Chapter 3.2) is evaluated by using the perpendicular root model developed by Wu et. al (1979). Since the applied vegetation for the case studies is a grass, the weight of the vegetation is neglible and not considered in the analysis. However, if considering full-grown trees in the calculations, the weight should be taken into account as it represents a driving force.

The calculations are carried out by using the finite element program PLAXIS 2D AE.

Note that the water loss caused by transpiration and evaporation (chapter 2.2) is not considered in the following case studies.

3.1 Material model and stress analysis

In the following chapter 3.1.1 a short abstract about the applied material model and its material parameters for the slope stability analysis is shown. Chapter 3.1.2 gives a short overview about the stress analysis specially related to the calculation with PLAXIS 2D. Moreover, the influence of the constitutive model and parameters such as the dilatancy angle for the stress analysis is explained.

3.1.1 Mohr-Coulomb Model (MC)

The applied model for the slope stability calculation is the linear elastic perfectly plastic Mohr-Coulomb Model (MC). For the elastic range the model describes linear elasticity and for the plastic range perfect plasticity (development of irreversible strains) (Fig. 15).

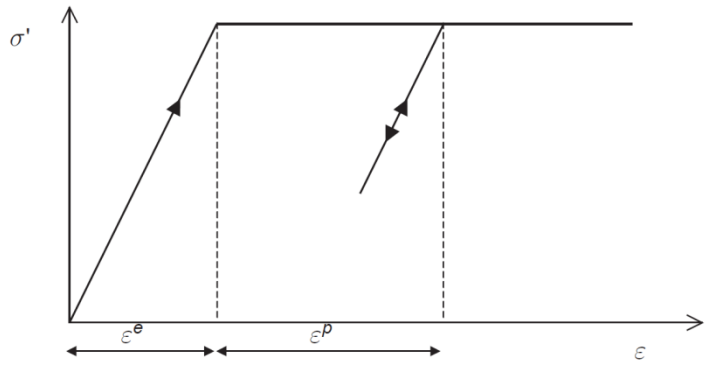

Fig. 15 Linear elastic perfect plastic model

Equation (26) shows that in the elastoplasticity strains and strain rates are decomposed into an elastic part and a plastic part.

$$\underline{\varepsilon} = \underline{\varepsilon}^e + \underline{\varepsilon}^p \tag{26}$$

For the MC model no hardening is occurring in the plastic range like advanced material models are describing it. Linear elastic perfectly plastic material behaviour is implemented in an FE calculation within six yield functions (*f*) (Eq. (27)) formulated in terms of principal stresses. The yield function defines whether or not plasticity occurs in a calculation. Furthermore, plastic yielding is related with the condition (f = 0). These six formulations represent a fixed hexagonal cone in principal stress space (Fig. 16).

$$\mathrm{f} = \frac{1}{2}(\sigma_1' - \sigma_3') + \frac{1}{2}(\sigma_1' - \sigma_3')\sin\varphi' - c'\cos\varphi' \leq 0 \tag{27}$$

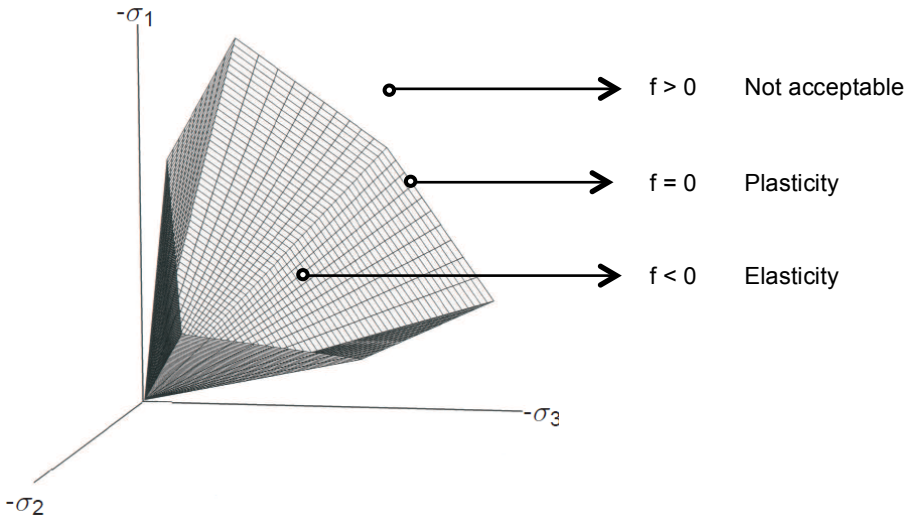

Fig. 16 Mohr-Coulomb yield surface in principal stress space (c = 0), modified picture from Brinkgreve et al. (2014a)

For cohesive soils (c > 0) the Mohr-Coulomb model allows tensile stresses, which are increase with cohesion. These behaviour is not representing the soil since it can sustain none or just very small tensile stresses. On this account using the tensile cut-off option in PLAXIS 2-D prohibits the occurrence of tensile stresses.

Special attention has to be paid when using an undrained analysis together with a positive dilatancy angle ($\Psi > 0$). This may lead to negative volumetric plastic deformations and as a result to unlimited deviatoric stress *(q)* (Fig. 17). This results in large shear strength.

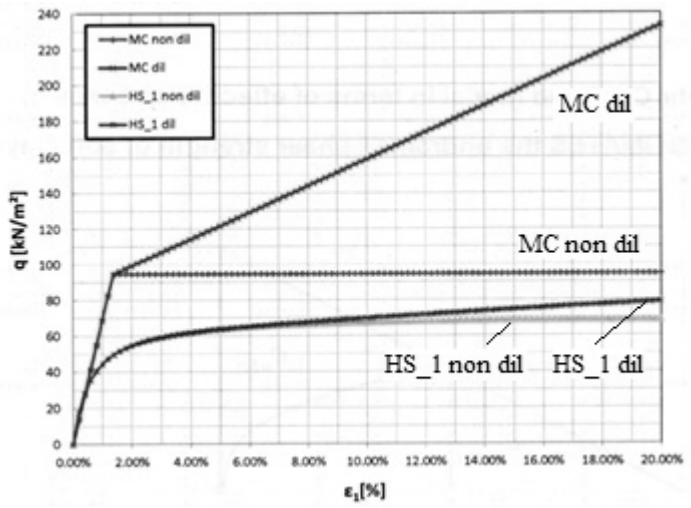

Fig. 17 Influence of Dilatancy – Simulation of undrained triaxial compression test – MC/HS model – *q* vs. ε_1 (Graz University of Technology, Institute of Soil Mechanics and Foundation Engineering 2014)

Bringreve et al. (2014a) recommend using a zero dilatancy angle for the undrained analysis.

The Mohr-Coloumb material model requires following five material parameters:

- **Elastic parameters**

E	[kN/m^2]	Young's modulus
v	[-]	Poisson's ratio

- **Shear parameters**

φ	[^{0}]	Effective friction angle
c'	[kN/m^2]	Effective cohesion
Ψ	[^{0}]	Dilatancy angle

Further information about the MC material model is provided by the PLAXIS Material Models Manual 2014 (Brinkgreve et al. 2014a).

3.1.2 Stress analysis

Depending on the soil characteristics and the loading conditions, pore water pressures can be generated which contributes to the total stress level. Equation (28) shows that total stresses σ can be divided into effective stresses σ' and pore pressures u (Terzaghi 1943).

$$\sigma = \sigma' + u \tag{28}$$

This principle of effective stress is applicable for fully saturated soils. By having an unsaturated condition, the soil is partially saturated what means that the pore volume is not fully filled by water, whereas the rest is covered by air. Therefore, Bishop (1959) has modified Terzaghi's classical effective stress theory by implementing a matric suction coefficient (χ) for the effective stress of unsaturated soils (Eq. (29)).

$$\sigma' = (\sigma - p_a) + \chi\,(p_a - p_w) \tag{29}$$

Where σ' and σ are the effective and total stress, p_a is the pore air pressure and p_w is the suction pore pressure. χ is the matric suction coefficient and varies between 0 to 1 depending on the degree of saturation. The term $(p_a - p_w)$ is called matric suction (see Chapter 2.2.1 for the determination of the suction pore pressure (p_w). For a fully saturated soil (χ = 1), the equation for the effective stress reads:

$$\sigma' = (\sigma - p_w) \tag{30}$$

and for a dry soil (χ = 1) the effective stress equation reads:

$$\sigma' = (\sigma - p_a) \tag{31}$$

The pore air pressure (p_a) is often neglected by assuming to be constant and small ($p_a \approx 0$). Therefore, for a dry soil, the effective stress is equal to the total stress. Since the determination of the suction coefficient is expensive, time consuming and difficult, Oberg & Sällfors (1997) and Vanapalli et al. (1996) suggested to replace the suction coefficient (χ) by the effective degree of saturation (S_e) (Eq. (32)). This is based on the fact that the shear strength of unsaturated soils is strongly related to the amount of water in the voids and therefore to the matric suction.

Consequently the effective stress equation can be simplified to:

$$\sigma' = \sigma - S_e\, p_w \tag{32}$$

By using a material with a high permeability, the drained analysis is more appropriate, since excess pore pressures can dissipate very fast due to the high permeability. On the contrary for a material with a low permeability and a high rate of loading (no consolidation) an undrained analysis is more appropriate.

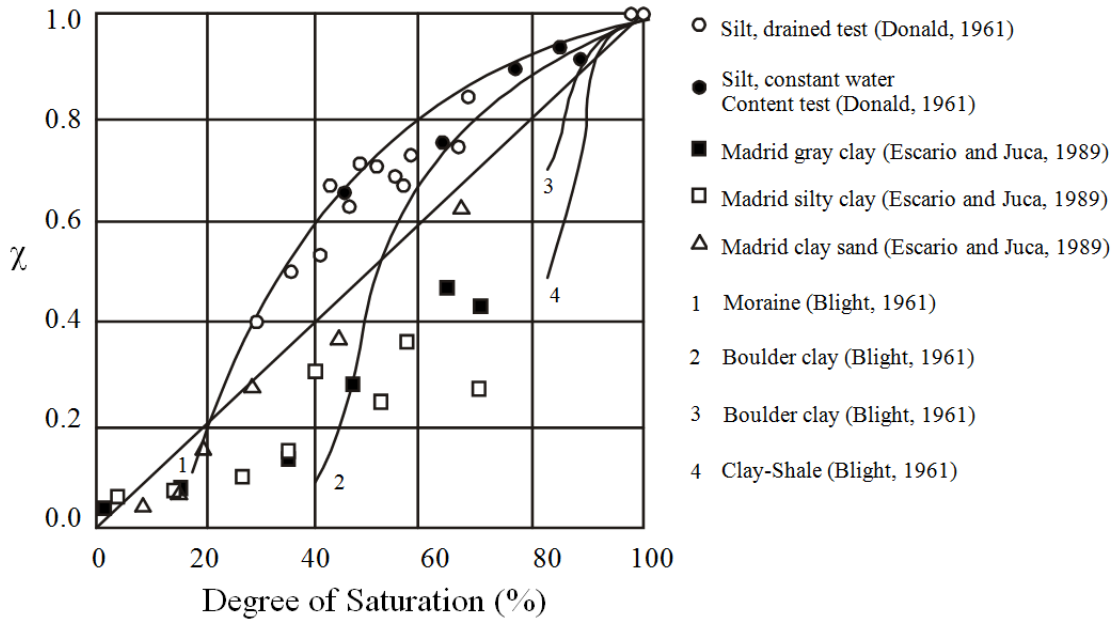

(a)

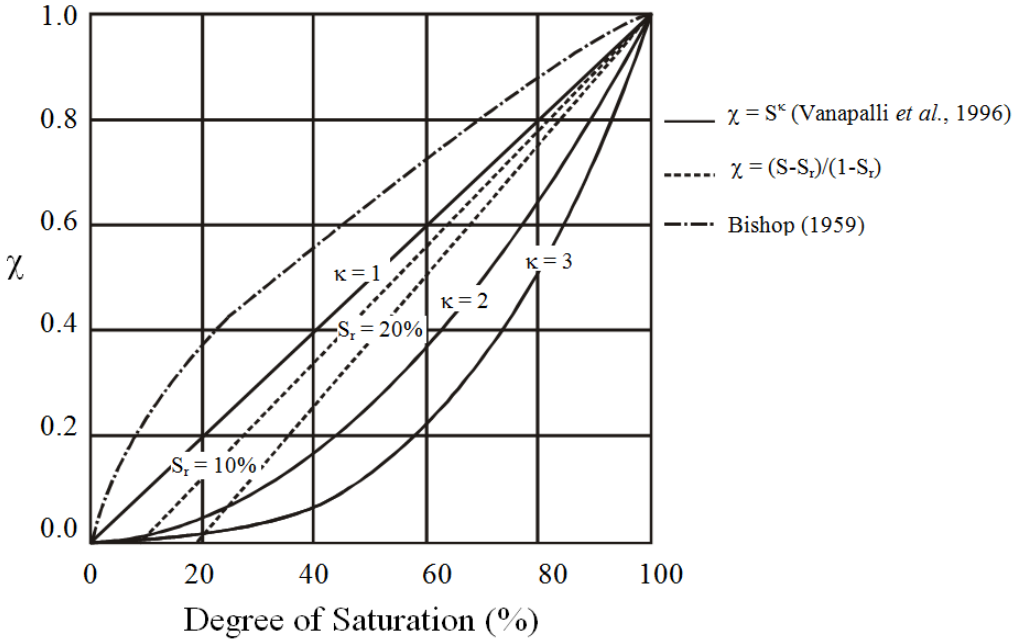

(b)

Fig. 18 Correlation between the matric suction coefficient (χ) and the saturation; (a) experimental data; (b) description by Vanapalli et al. (1996)

3.2 Determination of the apparent cohesion

As explained in chapter 2.4 there are two methods for determining the apparent cohesion for the rooted soil. First, by investigating the cohesion using direct shear tests and second, by using the arithmetical approach explained in chapter 2.1.

For the following parameter and sensitivity study the apparent cohesion is determined by calculating it with the perpendicular root model (Eq. (6)) from chapter 2.1. The data for the vegetation is taken from an experimental study carried out by Cazzuffi & Crippa (2005). For the type of the vegetation, the S-Vetiver plant is chosen (Fig. 3).

Vetiver (*Vetiveria* zizanioides) is a graminaceous densely tufted grass native in tropical and subtropical countries (Mickovski & Beek 2009). The most important characteristic of this plant is the highly branched rootstock composed of fibrous roots that can reach depths up to 3 m (Erskine 1992 and Truong 1999). The roots have a high tensile strength of around 85 ± 31.20 MPa with a ranging diameter of 0.66 ± 0.32 mm (Hengchaovanich 1998). Mickovski & Beek (2009) observed a near vertical orientation of the Vetiver roots (80˚ - 90˚). While having these near vertical orientated roots, the perpendicular root model (Eq. (6)) is suitable and therefore chosen to calculate the increased cohesion due to the presence of roots. Further information about the characteristics of the Vetiver plant is provided by Mickovski & Beek (2009).

According to Cazzuffi & Crippa (2005) the diameter of the Vetiver roots are ranging between 0.73 and 1.60 mm and can be correlated with equation (33). The tensile strength is represented by *y,* the root diameter by *x*.

$$y = 131.08 * e^{-1.077\,x} \tag{33}$$

$$y = 131.08 * e^{-1.077*1.16} = 37\ MPa$$

As there is no provided information about the diameter distribution over depth, a tensile strength of 37 MPa for an average diameter of 1.16 mm is calculated. For the distribution of the root area ratio (RAR) the linear formulation is used (Fig. 19) with a root area ratio distribution of RAR(z)=(1/400)*(2-z). Hengchaovanich & Nilaweera (1996) obtained that the computed values for the apparent cohesion are 3 times as high as the values from field experiments. As a consequence equation (34) is corrected by a factor of 0.33. According to a numerical case study from Chirico et al. (2013) a bias correction factor is assumed equal to 0.4.

$$c_R(z) = 0.33 * 1.2 * T_R \frac{A_R(z)}{A} \tag{34}$$

$$c_R(0.25) = 0.33 * 1.2 * 37 * \frac{1}{400} * (2 - 0.25)$$

$$= 64\ kN/m^2$$

Using these parameters gives following distribution for the apparent cohesion (c_R) over depth (c' is the cohesion of the soil without vegetation):

Table 2 Distribution of the apparent cohesion over depth for soil 1

Depth [m]	c' [kN/m²]	T_R [kN/m²]	A_R/A [-]	c_R [kN/m²]	c' + c_R [kN/m²]
0,25	0,2	37.000	0,00438	64	64
0,5	0,2	37.000	0,00375	55	55
0,75	0,2	37.000	0,00313	46	46
1,0	0,2	37.000	0,00250	37	37
1,25	0,2	37.000	0,00188	27	28
1,5	0,2	37.000	0,00125	18	19

Table 3 Distribution of the apparent cohesion over depth for soil 2

Depth [m]	c' [kN/m²]	T_R [kN/m²]	A_R/A [-]	c_R [kN/m²]	c' + c_R [kN/m²]
0,25	10	37.000	0,00438	64	74
0,5	10	37.000	0,00375	55	65
0,75	10	37.000	0,00313	46	56
1,0	10	37.000	0,00250	37	47
1,25	10	37.000	0,00188	27	37
1,5	10	37.000	0,00125	18	28

Table 4 Distribution of the apparent cohesion over depth for soil 3

Depth [m]	c' [kN/m²]	T_R [kN/m²]	A_R/A [-]	c_R [kN/m²]	c' + c_R [kN/m²]
0,25	10	37.000	0,00438	64	79
0,5	10	37.000	0,00375	55	70
0,75	10	37.000	0,00313	46	61
1,0	10	37.000	0,00250	37	52
1,25	10	37.000	0,00188	27	42
1,5	10	37.000	0,00125	18	33

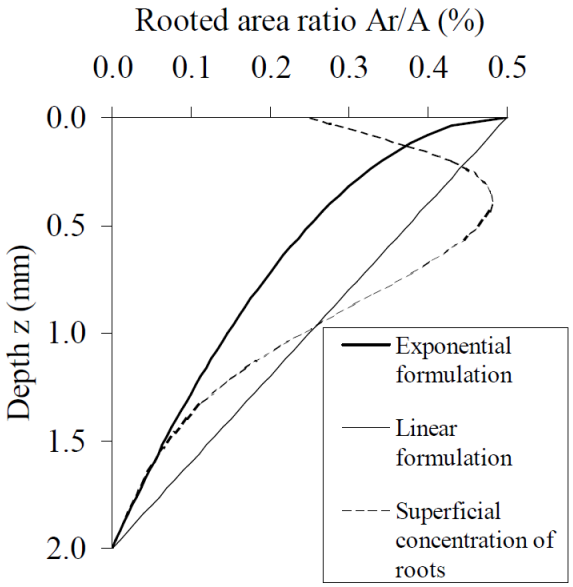

Fig. 19 Different hypothetical curves of rooted area ratio (A_R/A) distribution (Cazzuffi & Crippa 2005)

3.3 Safety analysis

The numerical determination of the factor of safety is done by performing a φ/c-reduction (Eq. (35)). Therefore, the strength parameter φ and c will be reduced in incremental steps until failure of the structure occurs. The staged construction for the influence of the inclination, influence of different drawdown levels and influence of the planted location consists of two calculation phases (Table 5). For simulating rainfall infiltration the days of rainfall have to be added to the calculation phase as well as the safety analysis for each day of rainfall (Table 6). The initial phase is computed by using gravity loading for calculating the initial stress states within the slope.

$$FoS = \frac{c_{available}}{c_{failure}} = \frac{\tan \varphi_{available}}{\tan \varphi_{failure}} \quad (35)$$

Table 5 Calculation phases for safety analysis without rainfall

Phase	Phase ID	Calculation type	Loading type
Phase 0	Initial Phase	Gravity loading	Staged construction
Phase 1	Safety analysis	φ/c-reduction	Incremental multiplier

Table 6 Calculation phases for safety analysis with two days of rainfall

Phase	Phase ID	Calculation type	Loading type
Phase 0	Initial Phase	Gravity loading	Staged construction
Phase 1	1st day of rainfall	Fully coupled flow-deformation	Staged construction
Phase 2	2nd day of rainfall	Fully coupled flow-deformation	Staged construction
Phase 3	FoS after 1st day of rainfall	φ /c-reduction	Incremental multiplier
Phase 4	FoS after 2nd day of rainfall	φ /c-reduction	Incremental multiplier

3.4 Influence of the inclination and different types of soil

In this chapter, slope stability analysis of unsaturated soils are carried out by analysing slopes without vegetation and slopes reinforced by vegetation for different inclinations and soils (soil 1, soil 2, soil 3). The inclination varies between 20 and 45 degrees with steps of 5 degrees. For the analysis, a simple case of homogeneous slope has been chosen. The mechanical and the hydraulic model are the Mohr-Coulomb failure criterion (chapter 3.3) and the Van Genuchten model respectively. The hydraulic parameters for the analysis have been evaluated by using the soil series from the international soil classification system (USDA).

3.4.1 Geometry, mesh coarseness and material properties

The height of the slope is 10 m and stays the same for all cases with different inclinations. The distance from the top of the slope to the left boundary and from the toe of the slope to the right boundary of the model is 15 m and stays the same for all cases. The dimensions for the cases with vegetation are the same than for the cases without vegetation.

For the vegetated slope six soil layers with increased strength parameters (apparent cohesion) are added. Each soil layer has a thickness of 25 cm and the vegetation penetrates in total 1.50 m deep into the slope (Fig. 20). The apparent cohesion has its highest value at the surface of the slope and decreases with depth (see values for the apparent cohesion at Table 2, Table 3 and Table 3).

Fig. 20 shows the geometry and the finite element mesh for a slope with an inclination of 30 degrees and reinforced with vegetation. The mesh is very fine and consists of 2446 15-noded elements. Special attention has been paid to ensure that the FE mesh has approximately the similar mesh fineness for both, the slope without vegetation and reinforced with vegetation.

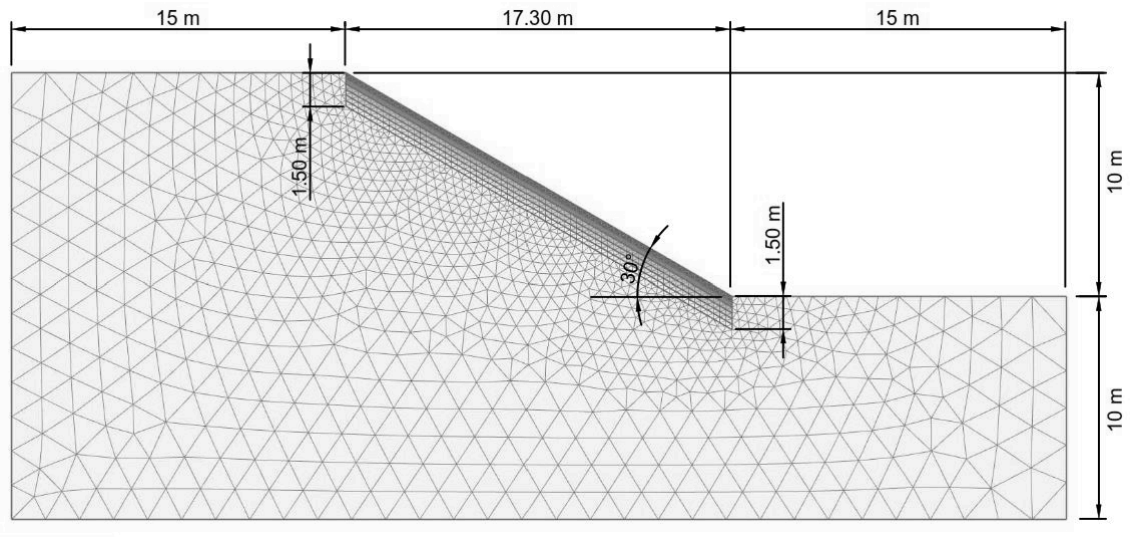

Fig. 20 Geometry and finite element mesh of the slope with vegetation, inclination 30 degree

Table 7 is showing the material parameters for the case study. To avoid numerical problems while using a cohesion less material, soil 1 was given a small cohesion of 0,2 kN/m^2.

Table 7 Material parameters for soil 1, soil 2 and soil 3

Parameter	Symbol	Soil 1	Soil 2	Soil 3	Unit
Soil unit weight unsaturated	γ_{unsat}	18	18	15	[kN/m^3]
Soil unit weight saturated	γ_{sat}	20	20	16	[kN/m^3]
Young's modulus	E_{ref}	30.000	10.000	4.300	[kN/m^2]
Poisson's ratio	v	0,30	0,30	0,33	[-]
Cohesion	c'	0,2	10	15	[kN/m^2]
Friction angle	φ'	40	20	27	[˚]
Dilatancy angle	Ψ	10	0	0	[˚]
Permeability	k_{sat}	8,3*10^{-5}	6,9*10^{-6}	5,5*10^{-7}	[m/s]

3.4.2 Boundary conditions

The global water table was assumed to be at the toe of the slope. The left and the right boundary are permeable and the bottom of the model is impermeable. Suction is taken into account and the calculation is performed using a drained analysis for soil 1 and an undrained analysis for soil 2 and soil 3.

3.4.3 Results

Table 8 and Fig. 21 show the influence of the inclination on the factor of safety. Considering soil 1, it can be seen that vegetation has a positive effect on the stability of the slope. For an inclination of 20 degree the difference in the FoS between the soil and reinforced with vegetation is around 4% and is increasing up to 25% for an inclination of 40 degrees. From a mechanical point of view a difference in the FoS can only be seen, if the shear plane is intersecting with the vegetated part of the soil. Therefore, for deep failure surfaces the influence of the vegetation is small to non-existent. As it can be seen at Fig. 22, for soil 1 with an increasing inclination, the failure surface is shifting shallower to the surface. On this account, the increasing difference in the FoS can be explained for soil 1. Above an inclination of 40 degree the slope is not in equilibrium and collapse is predicted.

Same as soil 2, soil 3 is not showing any significant difference in the FoS between the soil without vegetation and reinforced with vegetation for different inclinations. The reason is that the failure surface due to the cohesion is deeper than for soil 1 (Fig. 23 and Fig. 24) and not intersecting with the reinforced part of the soil. From Fig. 23 and Fig. 24 it can be seen that the failure mechanism for the soil without vegetation and reinforced with vegetation has the similar shape and therefore this is an indication for no or low reinforcing influence of the vegetation.

Table 8 Factor of safety for different inclinations and various types of soils (*) Drained analysis; (**) Undrained analysis

Inclination [°]	FoS					
	Soil 1 (*)		Soil 2 (**)		Soil 3 (**)	
	Soil	Vegetation	Soil	Vegetation	Soil	Vegetation
20	2,36	2,45	1,48	1,48	2,23	2,23
25	1,86	2,00	1,37	1,38	2,10	2,10
30	1,49	1,67	1,29	1,29	2,00	2,00
35	1,22	1,47	1,23	1,24	1,93	1,93
40	0,98	1,30	1,18	1,19	1,87	1,87
45	*Collapse*	1,17	1,13	1,14	1,81	1,81

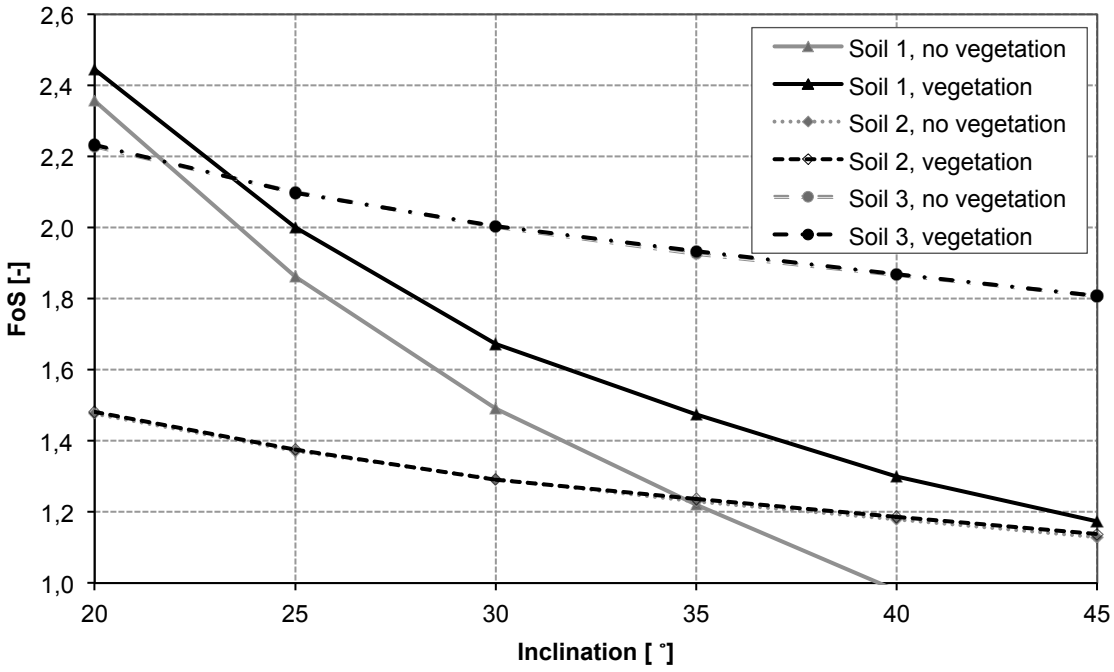

Fig. 21 Variation of the factor of safety for different inclinations and various types of soil

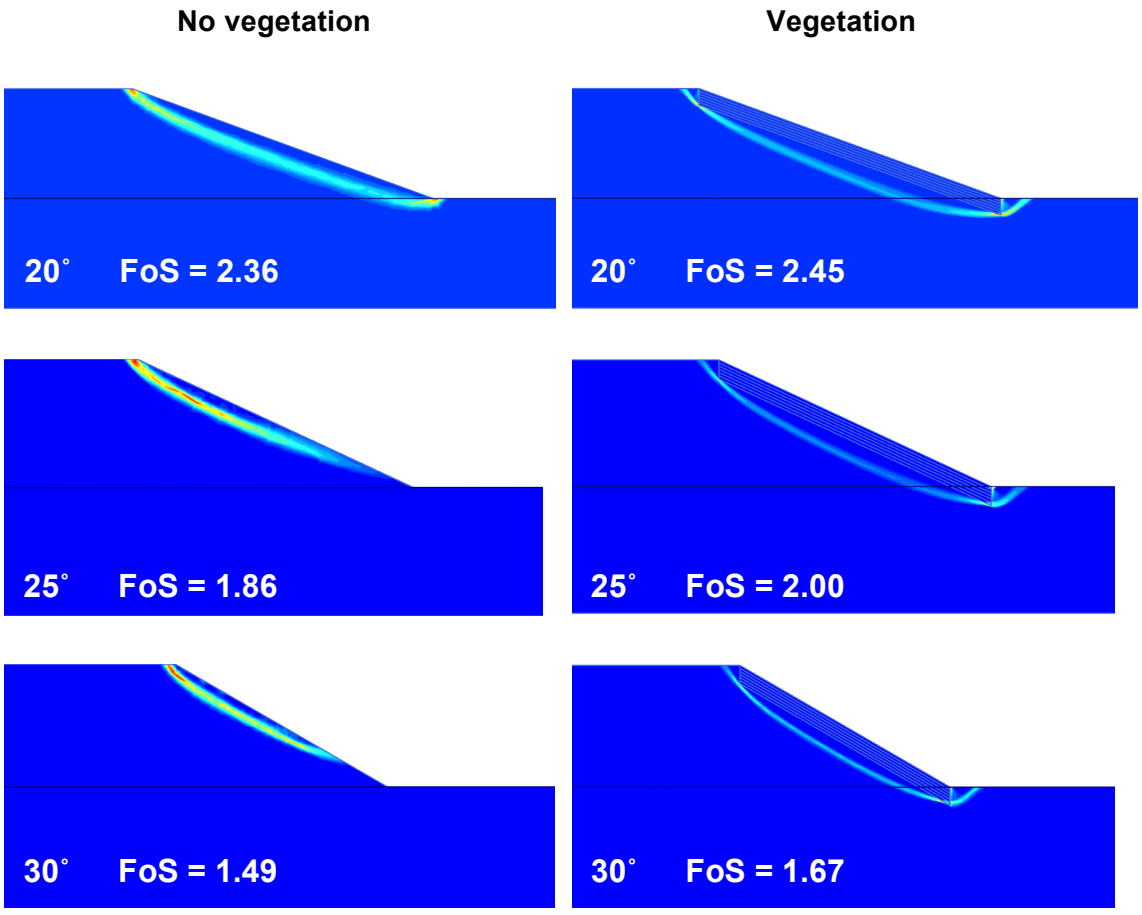

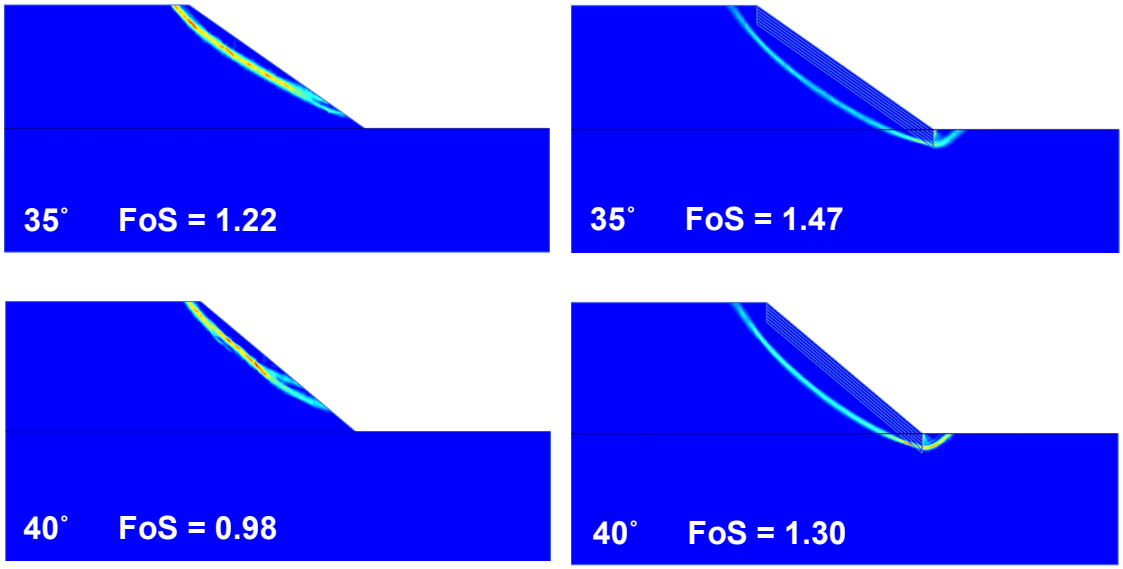

Fig. 22 Failure mechanism (incremental deviatoric strain) for soil 1 and different inclinations, left side no vegetation, right side with vegetation

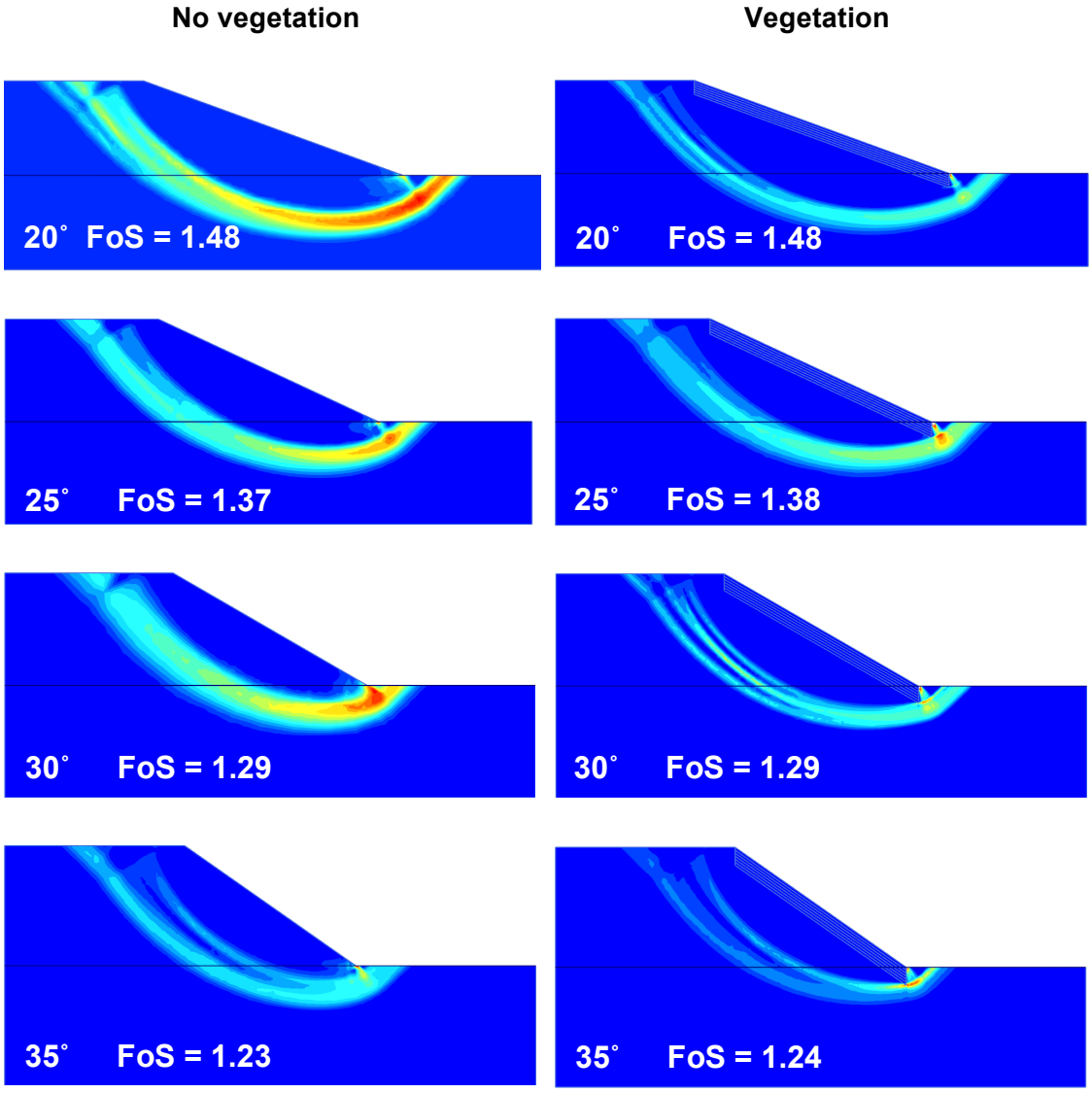

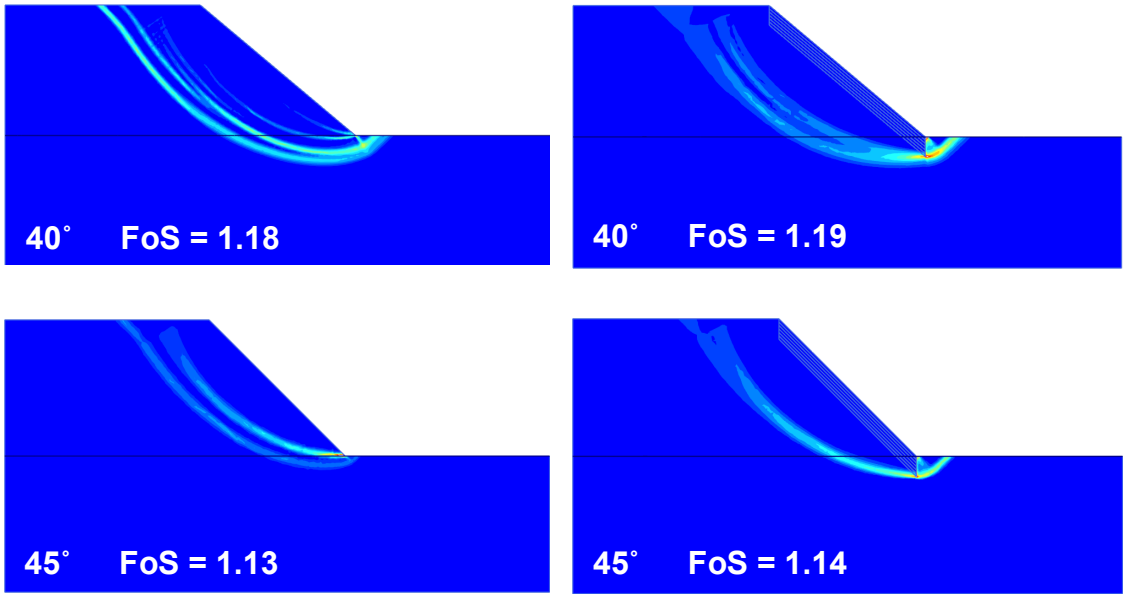

Fig. 23 Failure mechanism (incremental deviatoric strain) for soil 2 and different inclinations, left side no vegetation, right side with vegetation

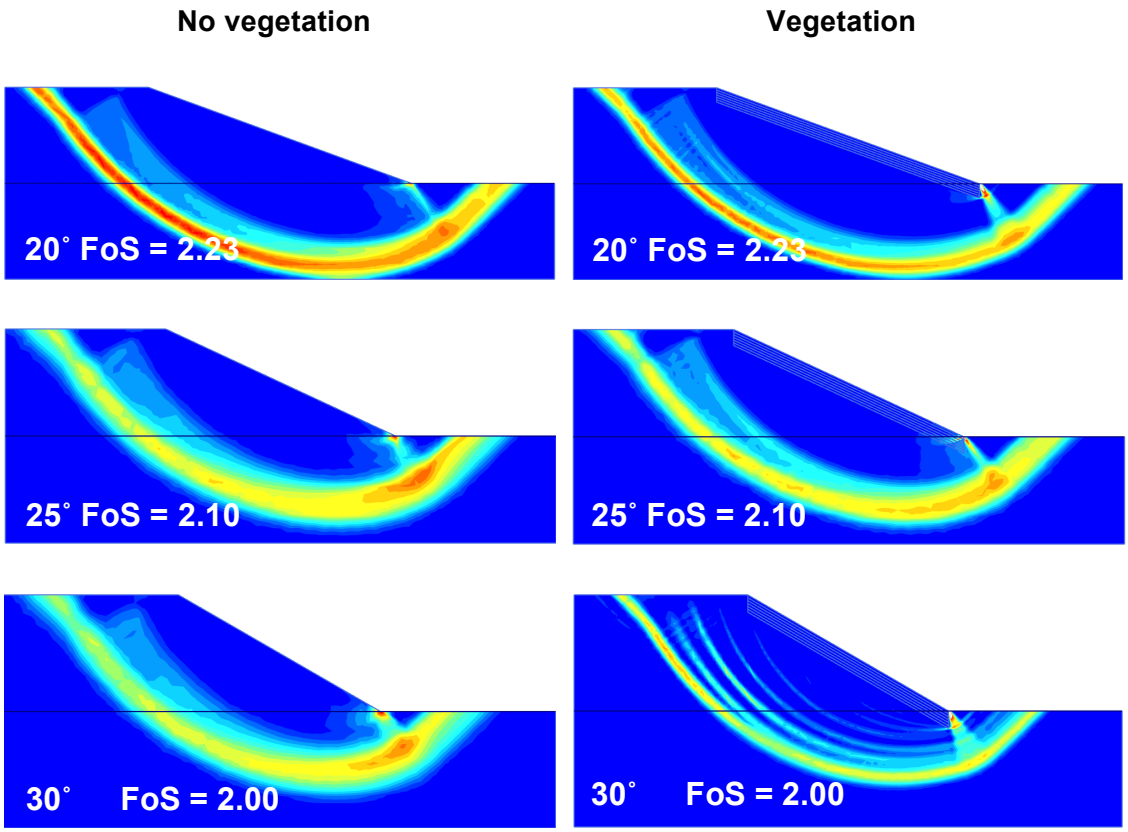

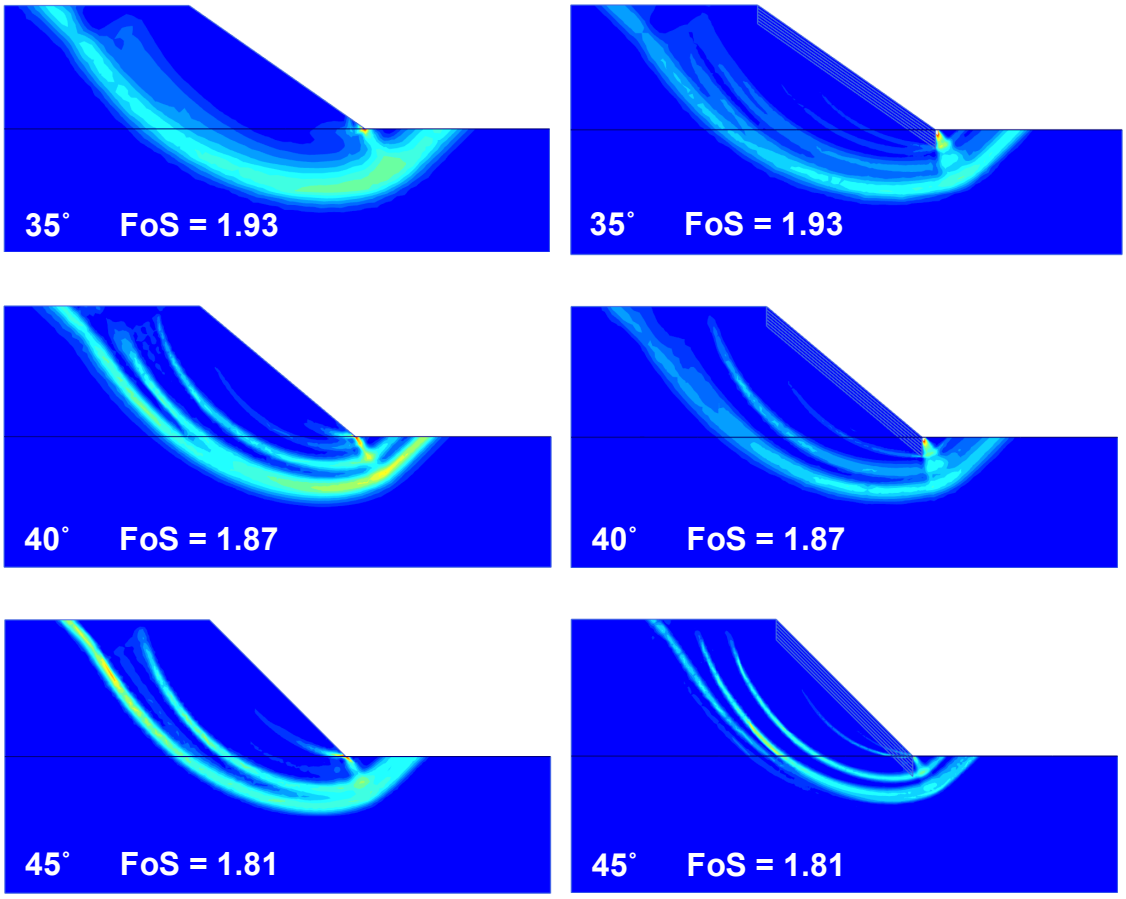

Fig. 24 Failure mechanism (incremental deviatoric strain) for clay and different inclinations, left side no vegetation, right side with vegetation

3.5 Influence of different water levels

Vegetation is often used for erosion control and stabilizing stream-banks. According to Simon & Collison (2002) vegetation is not only providing ecological benefits, it is also increasing the stability of stream-banks. As already explained in chapter 2.1 the beneficial effect of vegetation can be divided into a mechanical and a hydrological effect. After Pollen (2006) the mechanical effects take the most part of the beneficial influence of vegetation to stream-bank stability. It should be noted that the mechanical behaviour of vegetation for different water levels is studied in this chapter and hydrological influences caused by transpiration and evaporation are neglected.

For the analysis, a simple case of homogeneous slope has been chosen. The mechanical and the hydraulic model are the Mohr-Coulomb failure criterion (chapter 3.3) and the Van Genuchten model respectively. The hydraulic parameters for the analysis have been evaluated by using the soil series from the international soil classification system (USDA). The analysis was performed for soil 1 and soil 2 with slope inclinations of 25 and 35 degrees.

3.5.1 Geometry, mesh coarseness and material properties

The height of the slope is 10 m and stays the same for all cases with inclinations of 25 and 35 degrees. The distance from the top of the slope to the left boundary and from the toe of the slope to the right boundary of the model is 15 m and the same for all cases. The dimensions for the cases with vegetation are the same than for the cases without vegetation.

For the vegetated slope six soil layers with increased strength parameters (apparent cohesion) are added. Each soil layer has a thickness of 25 cm and the vegetation penetrates in total 1.50 m deep into the slope (Fig. 25). The apparent cohesion has its highest value at the surface of the slope and decreases with depth (see values for the apparent cohesion at Table 2 and Table 3).

Fig. 25 shows the geometry and the finite element mesh for a slope with an inclination of 30 degrees and reinforced with vegetation. The mesh is very fine and consists of 2446 15-noded elements. It has to be ensured that the FE mesh has approximately the similar mesh fineness for both, the slope without vegetation and reinforced with vegetation.

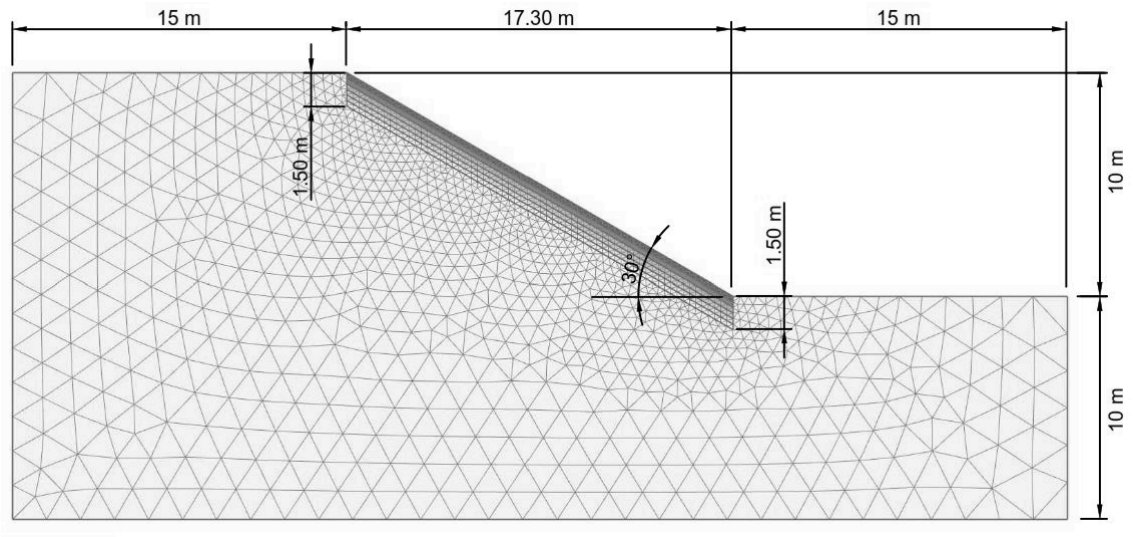

Fig. 25 Geometry and finite element mesh of the slope with vegetation, inclination 30 degree

Table 7 shows the material parameters for the case study. To avoid numerical problems while using a cohesion less material, soil 1 was given a small cohesion of 0,2 kN/m^2.

Table 9 Material parameters for soil 1 and soil 2

Parameter	Symbol	Soil 1	Soil 2	Unit
Soil unit weight unsaturated	γ_{unsat}	18	18	[kN/m^3]
Soil unit weight saturated	γ_{sat}	20	20	[kN/m^3]
Young's modulus	E_{ref}	30.000	10.000	[kN/m^2]
Poisson's ratio	v	0,30	0,30	[-]
Cohesion	c'	0,2	10	[kN/m^2]
Friction angle	φ'	40	20	[˚]
Dilatancy angle	Ψ	10	0	[˚]
Permeability	k_{sat}	8,3*10^{-5}	6,9*10^{-6}	[m/s]

3.5.2 Boundary conditions

The influence of various depths of horizontal water tables, on the stability of slopes, has been evaluated. Therefore, the ground water table was assumed to be horizontal at a certain depth (d) (Fig. 26). The analyses were performed with d/H ratios between 0.0 and 2.0.

The left and the right boundary are permeable and the bottom of the model is impermeable. Suction is taken into account and the calculation is performed using a drained analysis for soil 1 and an undrained analysis for soil 2 and soil 3.

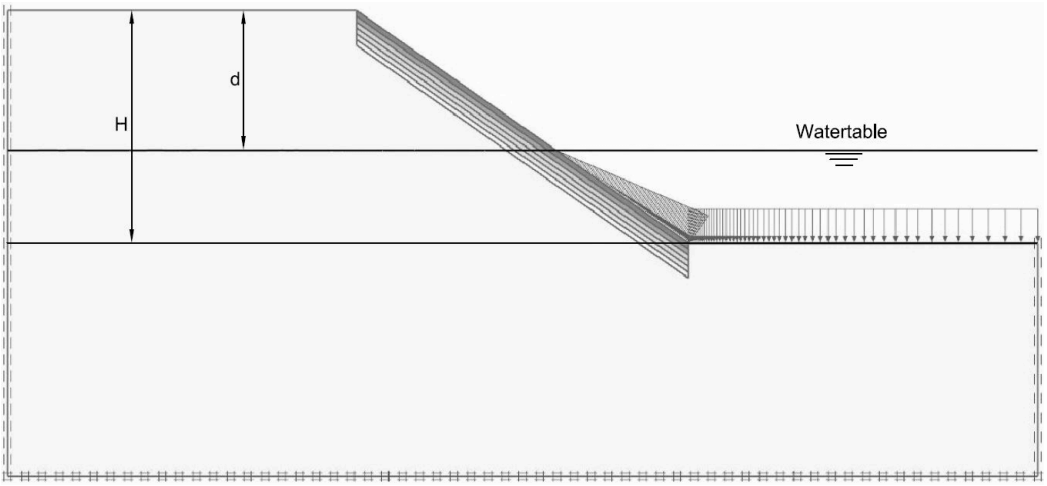

Fig. 26 Boundary conditions of the model

3.5.3 Results

From Table 10, Fig. 27 and Fig. 28 it can be seen that soil 2 compared to soil 1 is more sensitive to different water levels. Considering the case study for an inclination of 25 degree (Fig. 27), no significant reinforcing effect for soil 2 can be distinguished. This can be explained by having a deep failure surface for soil 2, which is not intersecting with the reinforced part of the slope. The vegetated slope for soil 2 has a FoS of 1.84 with a water level at the top and reach the minimum FoS of 1.33 for a d/H ratio of ~0.8 (d = 8 m).

Compared to soil 2, soil 1 is showing a significant difference between the soil without vegetation and reinforced by vegetation. The highest FoS (2.19) can be observed if the water table is at the top of the slope (d/H = 0.0) and the smallest FoS of 1.9 for a d/H ratio of ~0.6 (d = 6 m). Below a water table of d/H = 1.2 the reinforced soil 1 is not showing any significant influence.

Table 10 Factor of safety for different water levels (*) Drained analysis; (**) Undrained analysis

d/H	FoS							
	Inclination 25°				Inclination 35°			
	Soil 1(*)		Soil 2(**)		Soil 1(*)		Soil 2(**)	
	Soil	Vegetation	Soil	Vegetation	Soil	Vegetation	Soil	Vegetation
0,0	1,87	2,19	1,83	1,84	1,24	1,66	1,43	1,45
0,2	1,81	2,07	1,53	1,58	1,20	1,57	1,28	1,31
0,4	1,75	1,96	1,42	1,43	1,17	1,47	1,20	1,23
0,6	1,74	1,90	1,34	1,35	1,16	1,42	1,17	1,20
0,8	1,75	1,91	1,33	1,33	1,19	1,43	1,18	1,20
1,0	1,86	2,00	1,36	1,36	1,23	1,47	1,23	1,24
1,2	1,85	2,16	1,54	1,54	1,24	1,60	1,38	1,40
1,4	1,85	2,16	1,74	1,74	1,23	1,60	1,55	1,57
1,6	1,85	2,18	1,95	1,95	1,24	1,60	1,63	1,65
1,8	1,85	2,16	2,10	2,11	1,23	1,60	1,70	1,72
2,0	1,85	2,16	2,18	2,18	1,22	1,60	1,77	1,79

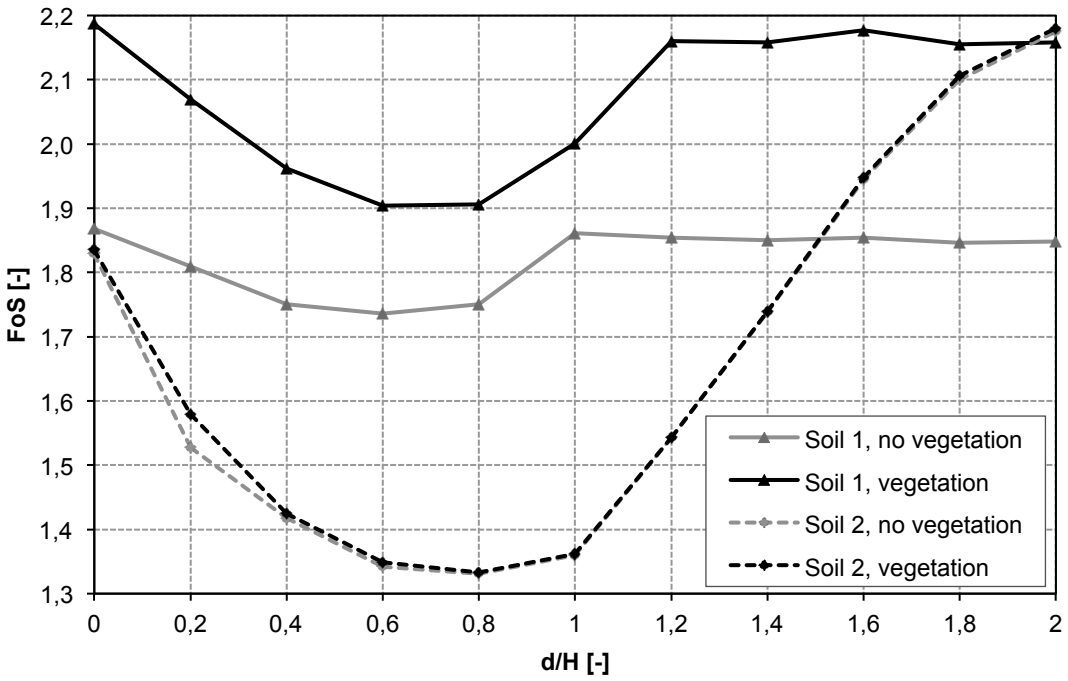

Fig. 27 Variation of the factor of safety for different water levels, slope inclination 25°

Considering the case study for an inclination of 35 degree (Fig. 28) the slope with vegetation for soil 1 and soil 2 is showing a similar behaviour compared to the case study with an inclination of 25 degree. For soil 1 with vegetation the highest FoS (1.66) can be observed if the water table is at the top of the slope (d/H = 0.0) and the smallest FoS of 1.42 for a d/H ratio of ~0.6 (d = 6 m). Below a water table of d/H = 1.2 the reinforced soil 1 is not showing any significant influence. For an inclination of 35

degree, the vegetated slope for soil 2 is showing a small reinforcing effect. A FoS of 1.45 can be observed by having a water level at the top of the slope and a minimum FoS of 1.20 is reached for a d/H ratio of ~0.6 - 0.8 (d = 6 - 8 m). The maximum FoS of 1.79 is reached by having a water table at the bottom of the model (d/H = 2.0).

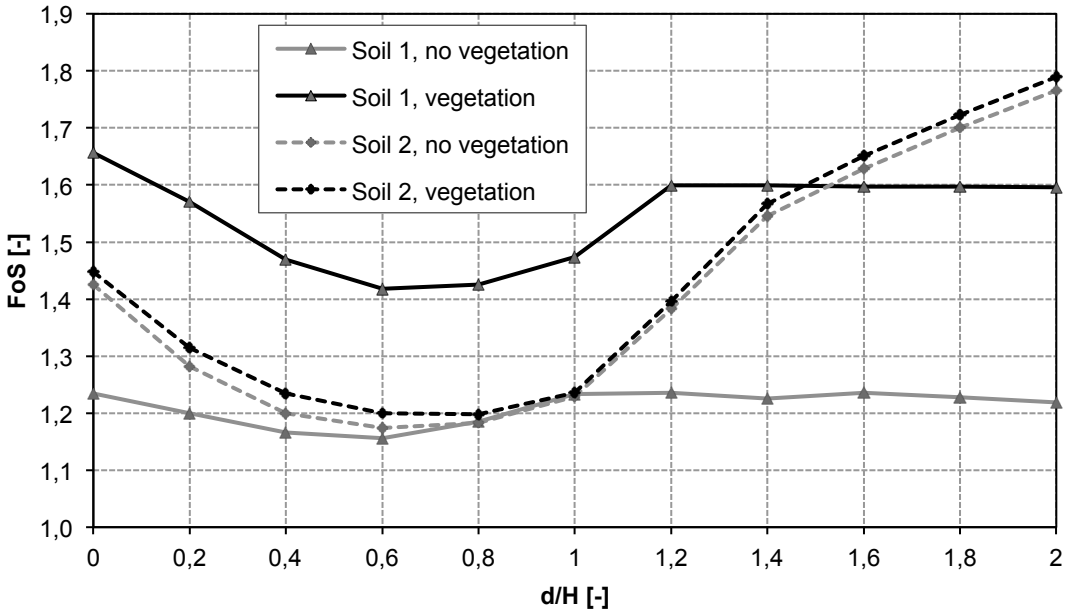

Fig. 28 Variation of the factor of safety for different water levels, slope inclination 35°

The FoS for the reinforced soil 1 is in average 9% smaller for a slope inclination of 25 degrees compared to a slope inclination of 35 degrees. Soil 2 is showing a small average difference of 1% between the slope with an inclination of 25 degree and 35 degree (Fig. 29).

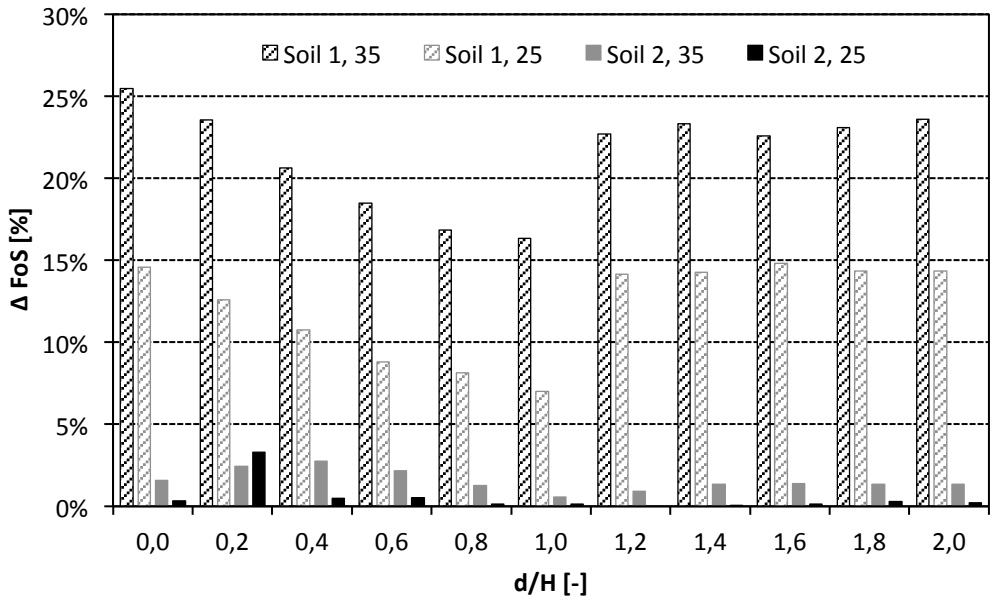

Fig. 29 Reinforcing effect of vegetation for different water levels

Failure mechanism for soil 1 and soil 2 for an inclination of 25 degree is shown in the appendix (Fig. 51 and Fig. 52).

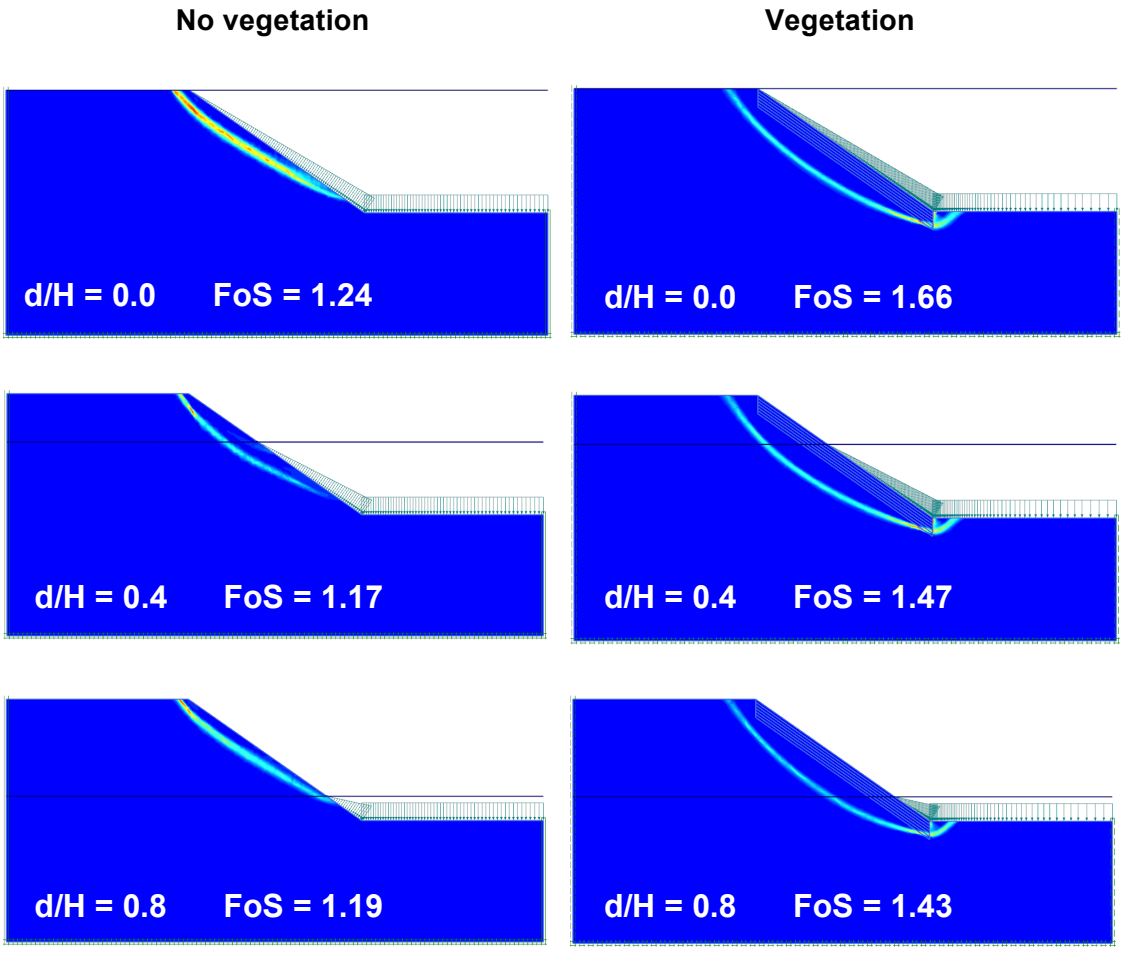

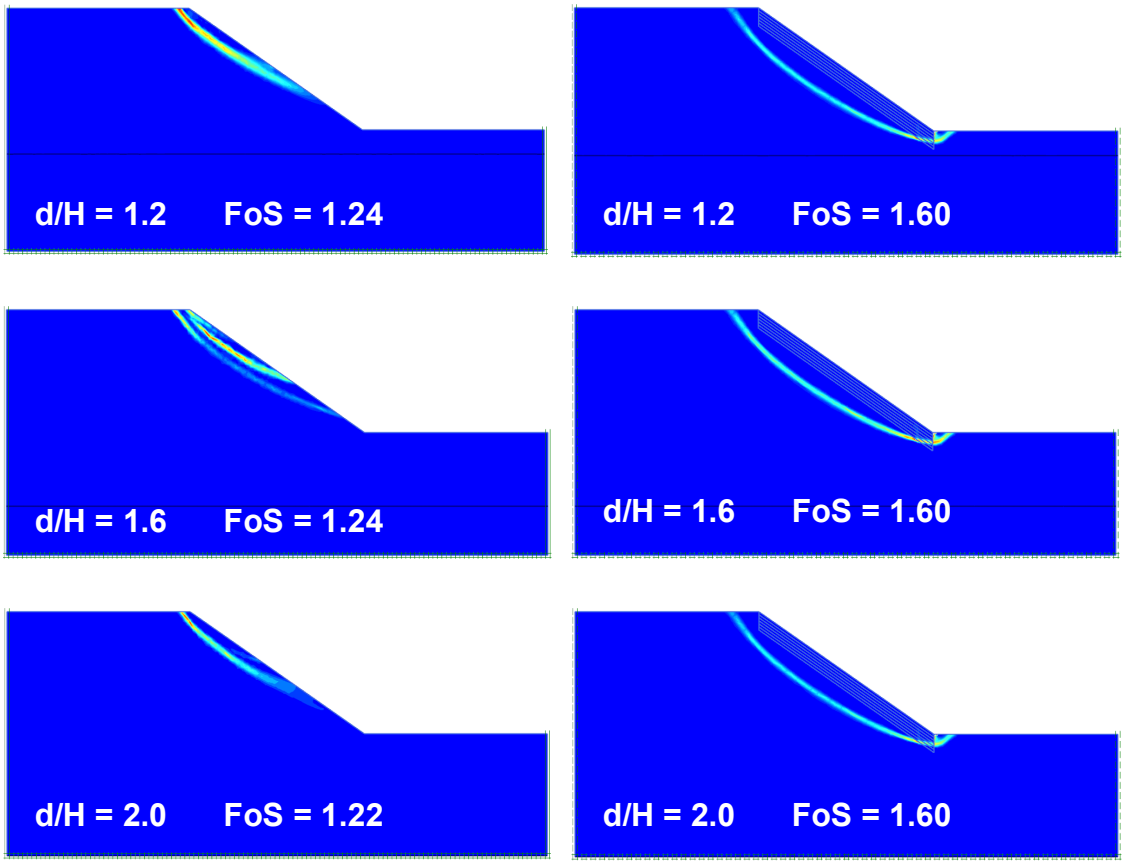

Fig. 30 Failure mechanism (incremental deviatoric strain) for soil 1, inclination 35 degree, left side no vegetation, right side with vegetation

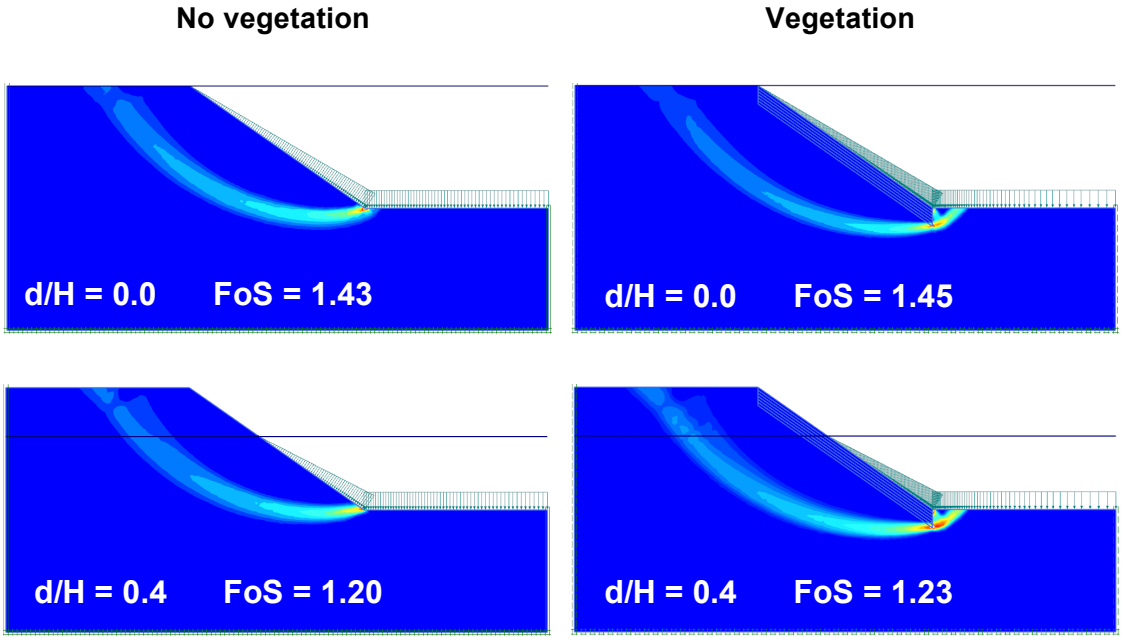

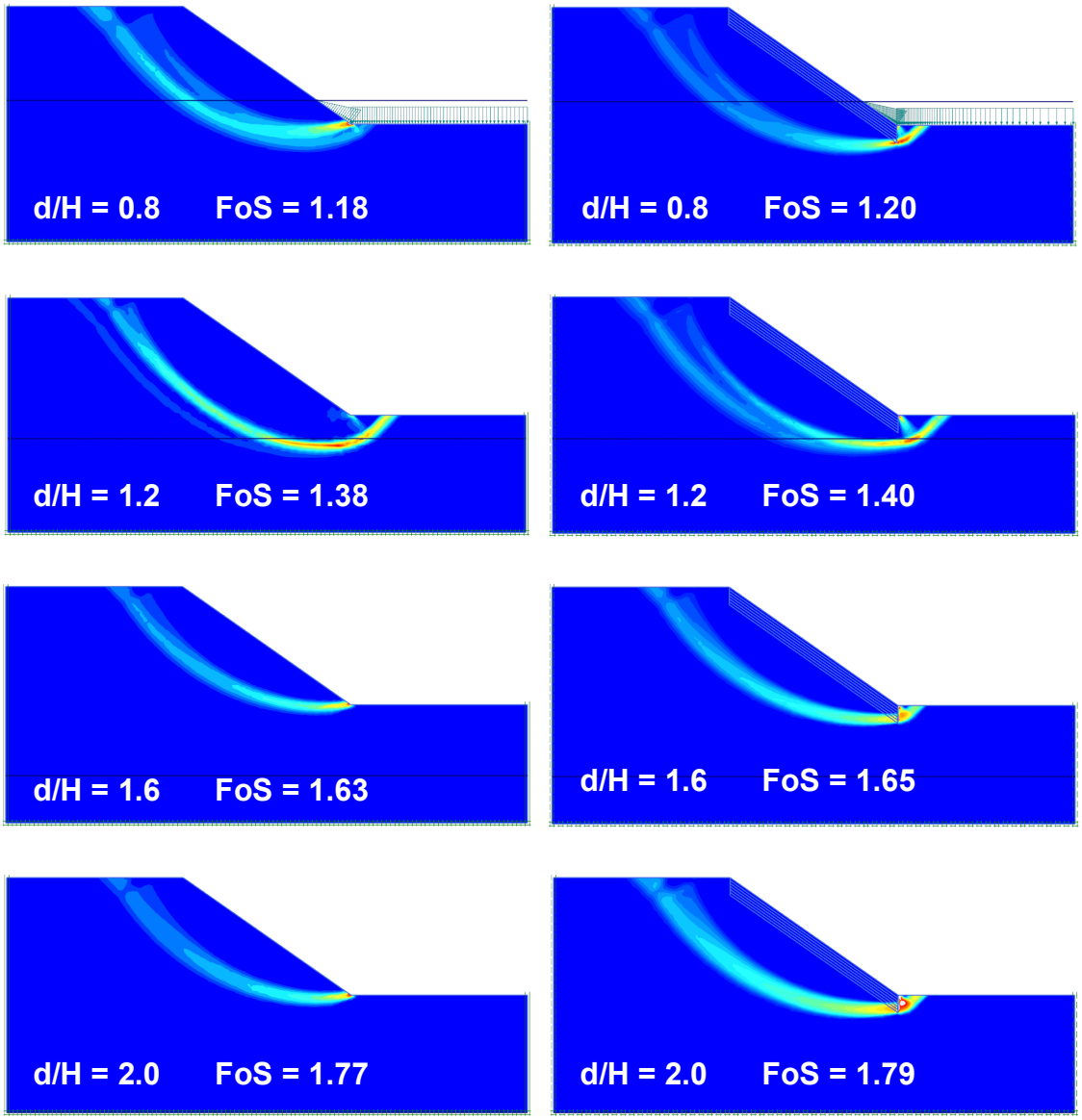

Fig. 31 Failure mechanism (incremental deviatoric strain) for soil 2, inclination 35 degree, left side no vegetation, right side with vegetation

3.6 Influence of the planted location

In this section the influence of different layouts of the planted location is studied. Especially for artificial slopes, the toe and the top section of the slope can be covered by vegetation. This can be seen often at stream banks or flood detention basins.

Therefore, three case studies (Fig. 32) have been conducted for the analyses.

- **Slope:** Just the slope is covered with vegetation (a)
- **Slope + toe:** Slope and 5 m of horizontal vegetation at the toe of the slope (b)
- **Entire surface:** Slope and 5 m of horizontal vegetation at the toe and the head of the slope (c)

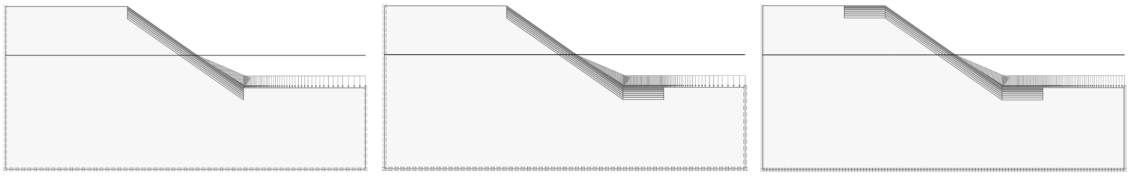

(a) (b) (c)

Fig. 32 Geometry of the case studies: (a) Slope; (b) Slope+toe; (c) Entire surface

For the analysis, a simple case of homogeneous slope has been chosen. The mechanical and the hydraulic model are the Mohr-Coulomb failure criterion (chapter 3.3) and the Van Genuchten model respectively. The hydraulic parameters for the analysis have been evaluated by using the soil series from the international soil classification system (USDA). The analysis was performed for soil 1 and soil 2 with a slope inclination of 35 degrees. The mesh was refined until the FoS wasn't changing anymore.

3.6.1 Geometry, mesh coarseness and material properties

The height of the slope is 10 m and the distance from the top of the slope to the left boundary and from the toe of the slope to the right boundary of the model is 15 m. The dimensions for the cases with vegetation are the same as for the cases without vegetation.

For the vegetated slope six soil layers with increased strength parameters (apparent cohesion) are added. Each soil layer has a thickness of 25 cm and the vegetation penetrates in total 1.50 m deep into the slope (Fig. 33). The apparent cohesion has its

highest value at the surface of the slope and decreases with depth. The values for the apparent cohesion are shown in table 1 and table 2.

Fig. 33 shows the geometry and the finite element mesh for a slope with an inclination of 35 degrees and reinforced with vegetation. The mesh is very fine and consists of 2914 15-noded elements. It has to be ensured that the FE mesh has approximately the similar mesh fineness for both, the slope without vegetation and reinforced with vegetation.

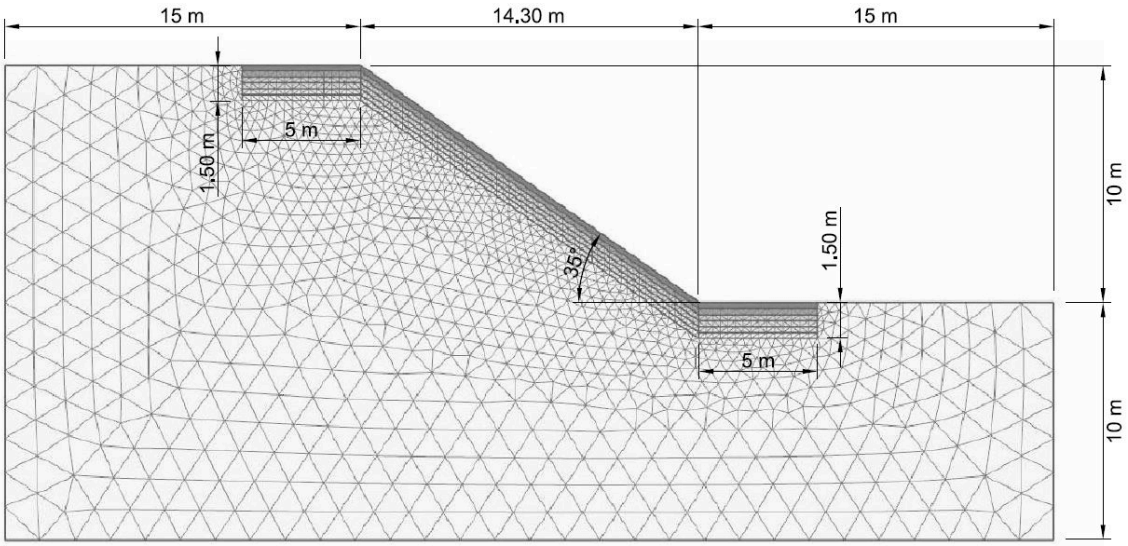

Fig. 33 Geometry and finite element mesh of the slope with additional vegetation at the toe and the head, inclination 35 degree

Table 11 shows the material parameters for the case study. To avoid numerical problems while using a cohesion less material, soil 1 was given a small cohesion of 0,2 kN/m^2.

Table 11 Material parameters for soil 1 and soil 2

Parameter	Symbol	Soil 1	Soil 2	Unit
Soil unit weight unsaturated	γ_{unsat}	18	18	[kN/m^3]
Soil unit weight saturated	γ_{sat}	20	20	[kN/m^3]
Young's modulus	E_{ref}	30.000	10.000	[kN/m^2]
Poisson's ratio	v	0,30	0,30	[-]
Cohesion	c'	0,2	10	[kN/m^2]
Friction angle	φ'	40	20	[˚]
Dilatancy angle	Ψ	10	0	[˚]
Permeability	k_{sat}	8,3*10^{-5}	6,9*10^{-6}	[m/s]

3.6.2 Boundary conditions

The influence of various depths of horizontal water tables for different configurations of the vegetation, on the stability of the slope, has been evaluated. Therefore, the ground water table was assumed to be horizontal at a certain depth (d) (Fig. 34). The analyses were performed with d/H ratios between 0.0 and 2.0.

The left and the right boundary are permeable and the bottom of the model is impermeable. Suction is taken into account and the calculation is performed using a drained analysis for soil 1 and an undrained analysis for soil 2.

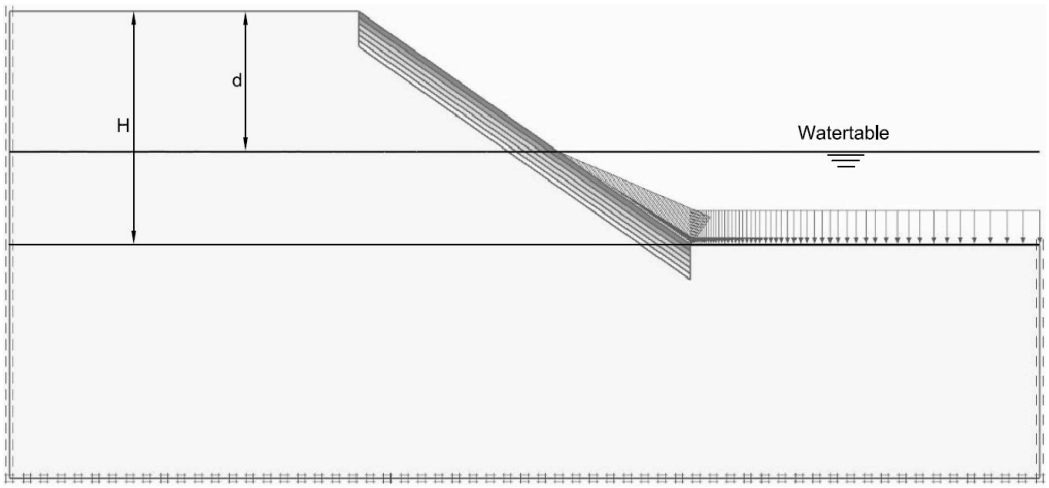

Fig. 34 Boundary conditions of the model

3.6.3 Results

Table 12, Fig. 37 and Fig. 38 show the results from the analysis with different water levels and planted locations. From the results of the previous chapter 3.5.3 it was shown that the reinforcing effect of vegetation has a significant influence on the FoS.

Considering soil 1 and adding a horizontal layer of vegetation at the toe of the slope (Fig. 32 picture (b)) the FoS can be increased again for a maximum of 13% (d/H = 0.0). If the head of the slope is also covered with a horizontal layer of vegetation (Fig. 32 picture (c)) the influence on the factor of safety is small and around 1% in average. This represents the main output of this analysis. A reinforced section at the toe of the slope is much more effective than a reinforced section at the head of the slope. This can be explained by having a failure surface with a pointed angle relative to the vegetated part at the head of the slope and displacements more or less plane parallel to the surface (Fig. 35 and Fig. 36). This results in tension stresses that the soil can't significantly resist.

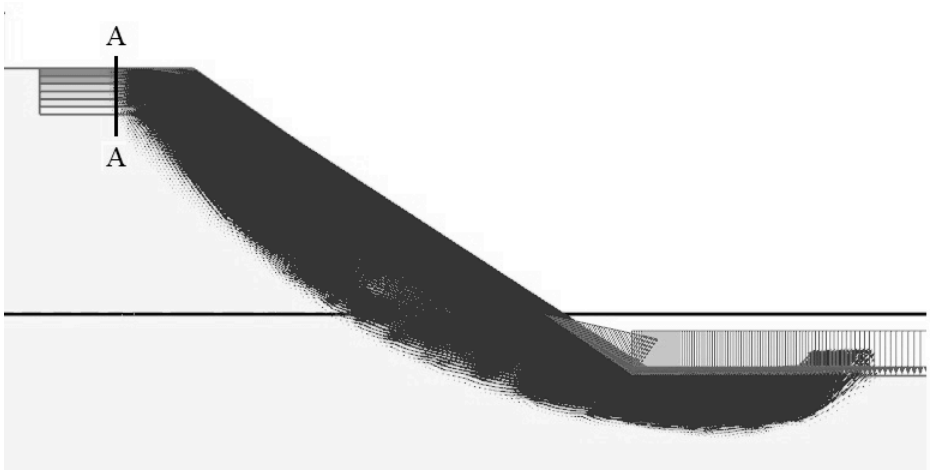

Fig. 35 Total displacement indicated with black arrows (not in scale)

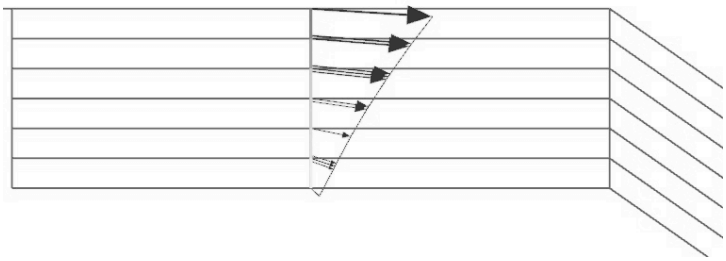

Fig. 36 Cross section A-A: Detail of the total displacement in the failure plane

At Fig. 41 it can be seen that due to the vegetation at the toe of the slope the failure surface shifts more to the right side or is forced to shear the vegetated part of the slope.

Therefore, two mechanisms can be observed which are increasing the FoS. First, a shifting of the failure surface that is also enlarged (at the toe of the slope) and second, a shearing trough the vegetated part of the slope with higher shear strength. The highest FoS (2.02) for case (b) (Fig. 32) can be observed if the water table is at the top of the slope (d/H = 0.0) and the smallest FoS of 1.65 for a d/H ratio of ~0.8 (d = 8 m). Below a water table of d/H = 1.2 soil 1 with vegetation is not showing any significant influence.

As it can bee seen at Fig. 37 a vegetated part at the toe of the slope is significantly increasing the stability and can be heightened by using trees with a deep-rooted root system planted at the toe of the slope. Especially for high cohesive slopes with a deep failure surface, roots from fully-grown trees can reach such depths. But care has to be taken by having heavy trees at the head of the slope. They have a contrary effect and

are destabilizing the slope due to its self-weight. Furthermore, the roots are not significantly increasing the stability of the slope.

Table 12 Factor of safety for different water levels (*) Drained analysis; (**) Undrained analysis

d/H	FOS							
	Soil 1(*)				Soil 2(**)			
	Soil	Slope	Slope+toe	Entire surface	Soil	Slope	Slope+toe	Entire surface
0,0	1,24	1,66	2,02	2,03	1,43	1,45	1,55	1,55
0,2	1,20	1,57	1,87	1,89	1,28	1,31	1,41	1,40
0,4	1,17	1,47	1,75	1,77	1,20	1,23	1,32	1,31
0,6	1,16	1,42	1,69	1,70	1,17	1,20	1,27	1,27
0,8	1,19	1,43	1,65	1,67	1,18	1,20	1,25	1,25
1,0	1,23	1,47	1,69	1,70	1,23	1,24	1,27	1,26
1,2	1,24	1,60	1,80	1,83	1,38	1,40	1,43	1,42
1,4	1,23	1,60	1,79	1,83	1,55	1,57	1,62	1,62
1,6	1,24	1,60	1,79	1,83	1,63	1,65	1,77	1,77
1,8	1,23	1,60	1,79	1,83	1,70	1,72	1,85	1,85
2,0	1,22	1,60	1,79	1,83	1,77	1,79	1,91	1,92

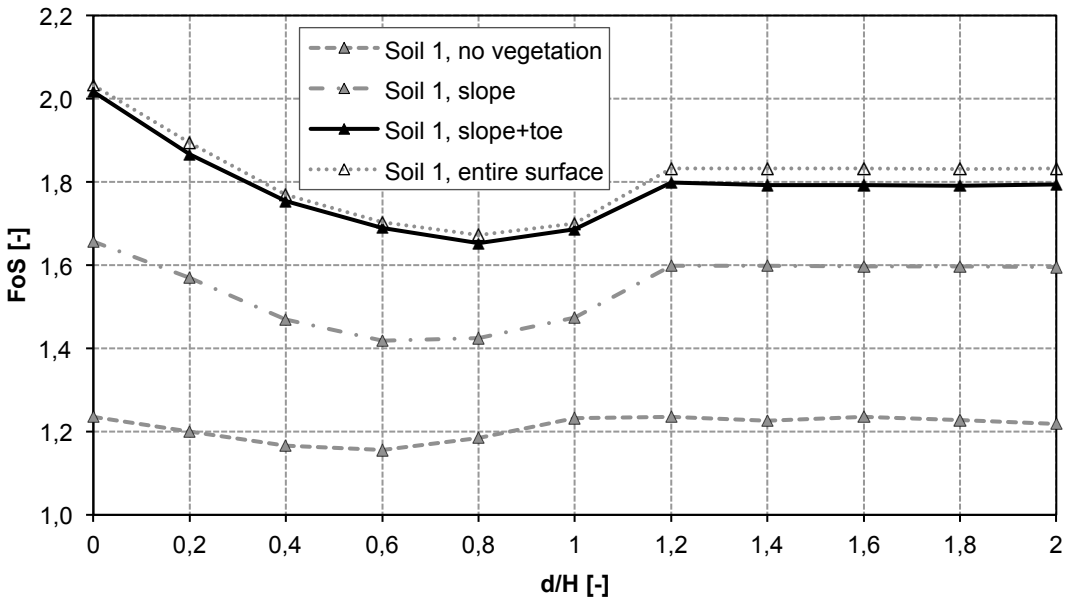

Fig. 37 Variation of the factor of safety for different water levels and planted locations for soil 1, slope inclination 35°

Considering the case study for soil 2 (Fig. 38) the results show a similar behaviour, in terms of the negligible effect of a reinforced head of the slope, compared to the case study for soil 1. No significant difference can be observed if the head of the slope is reinforced in addition to a reinforced section at the toe of the slope (Fig. 40). For case

(b) (Fig. 32) a FoS of 2.02 can be observed if the water table is at the top of the slope (d/H = 0.0) and reaches a minimum FoS of 1.25 for a d/H ratio of ~0.8 (d = 8 m).

The same reinforcing effect as for soil 1 can be observed for soil 2. Fig. 42 shows a shifting of the failure surface, due to the vegetation at the toe of the slope, to the right section of the model or a failure surface that is forced to shear the vegetated part of the slope.

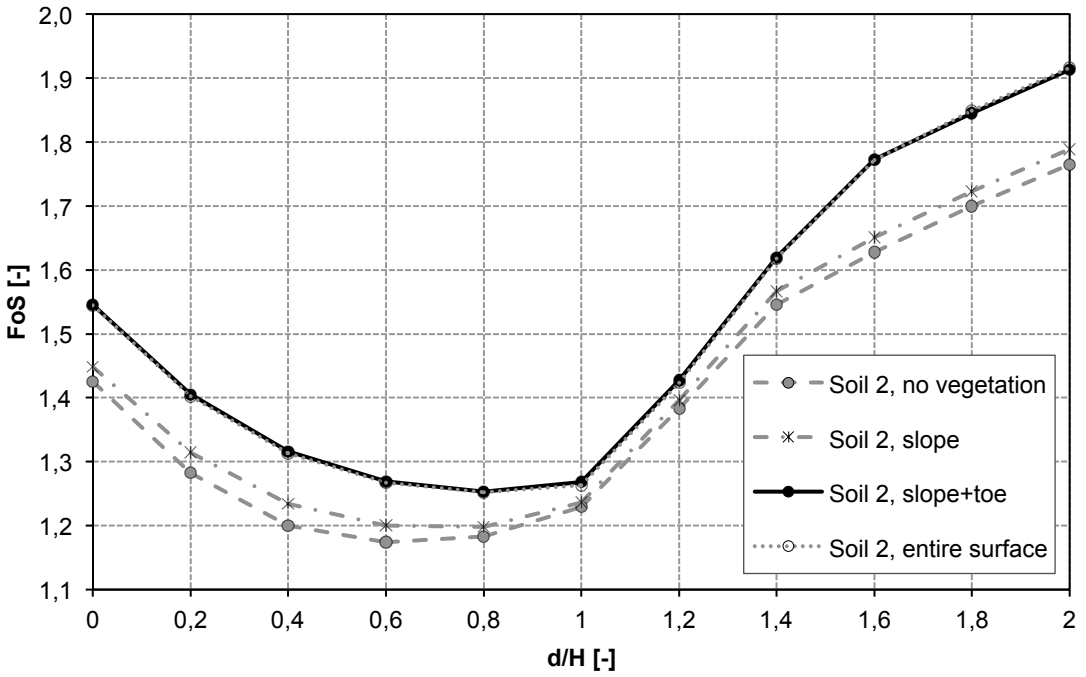

Fig. 38 Variation of the factor of safety for different water levels and planted locations for soil 2, slope inclination 35˚

Fig. 39 shows the reinforcing effect of the vegetation for soil 1 and different planted locations with the soil without vegetation as reference. For case study (b) (Fig. 32) a FoS that is in average 11% higher can be observed. The difference between case (b) and case (c) is small and in average 1%.

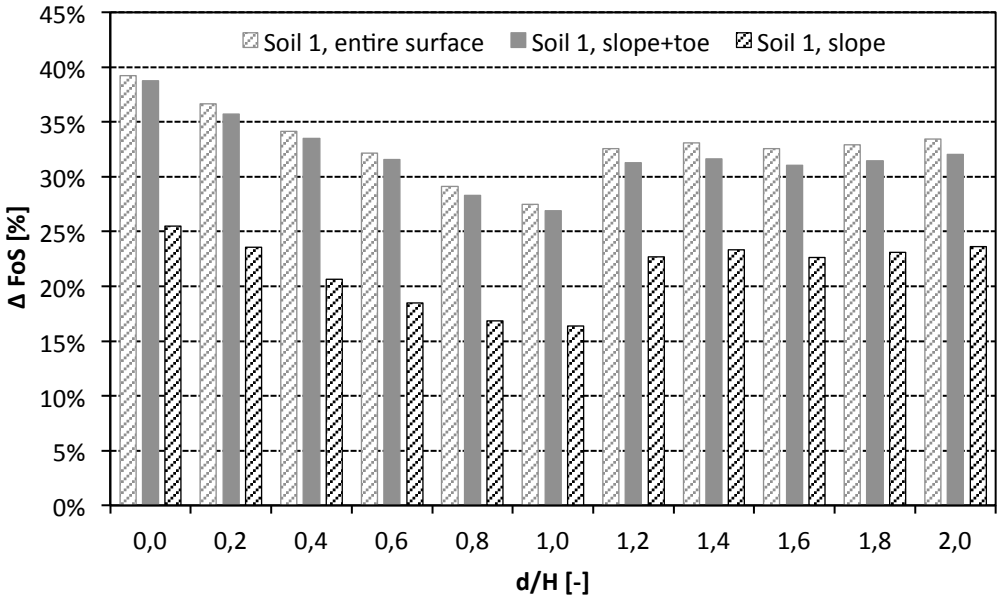

Fig. 39 Reinforcing effect of the vegetation for different water levels; soil 1

Fig. 40 is showing the reinforcing effect for soil 2 for different planted locations with the soil without vegetation as reference. For case study (b) (Fig. 32) a FoS that is in average 6% higher can be observed. The difference between case (b) and case (c) is negligible and smaller than 1%.

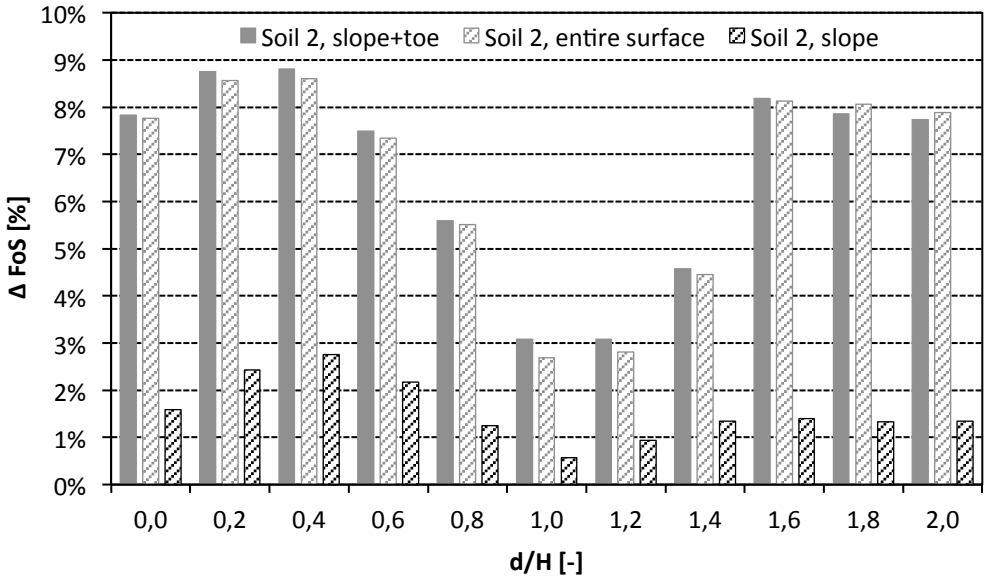

Fig. 40 Reinforcing effect of the vegetation for different water levels, soil 2

Fig. 41 Failure mechanism (incremental deviatoric strain) for soil 1, inclination 35 degree, left column vegetated slope, middle column slope + toe, right column entire surface vegetated

Fig. 42 Failure mechanism (incremental deviatoric strain) for soil 2, inclination 35 degree, left column vegetated slope, middle column slope + toe, right column entire surface vegetated

3.7 Tension crack

Developed tension cracks of expansive soils, in combination with rain infiltration, are a key problem in slope stability since they produce a local weakness in shear resistance and increase the infiltration rate. An expansive soil is a special unsaturated soil, characterized by having a significant swell-shrink characteristic (Shi et al. 2014).

The wet-dry cycle can be seen as the main triggering factor that leads to development of tension cracks. Expansive soils swell in a wetting cycle and shrink in a drying cycle. Drying causes negative volumetric strain that results in tensile stress. If the tensile stress exceeds the soils resistance to tension (own cohesion), the soil body will crack. Shi et al. (2014) is reporting that the development of a tension crack is not a result of one wet-dry cycle. Moreover, it is a result of cumulating deformations due to wet-dry cycles. Therefore, the water conditions (moisture content) in the soil as well as the climatic conditions (temperature, thermal radiation, wind, precipitation) at the surface of the slope are the main factors of influence.

Tension cracks also develop by having deformations in the slope (creeping slope). Therefore, tensions are generated in the upper part of the slope, which the soil cannot resist and cracks.

The result from the rainfall infiltration analysis for a cohesive (no tension crack) soil (Fig. 43) is not showing a significant reinforcing effect of the vegetation. This can be explained by having a deep failure mechanism, which is not intersecting with the root system. The rain infiltration lasted for 72 hours with an intensity of 15 mm/hour. With the presence of a tension crack it will be studied whether or not the tension crack is influencing the stability of the slope and if the failure surface is shifting to shallower depths because of a higher infiltration rate and therefore accelerated decrease of the matric suction.

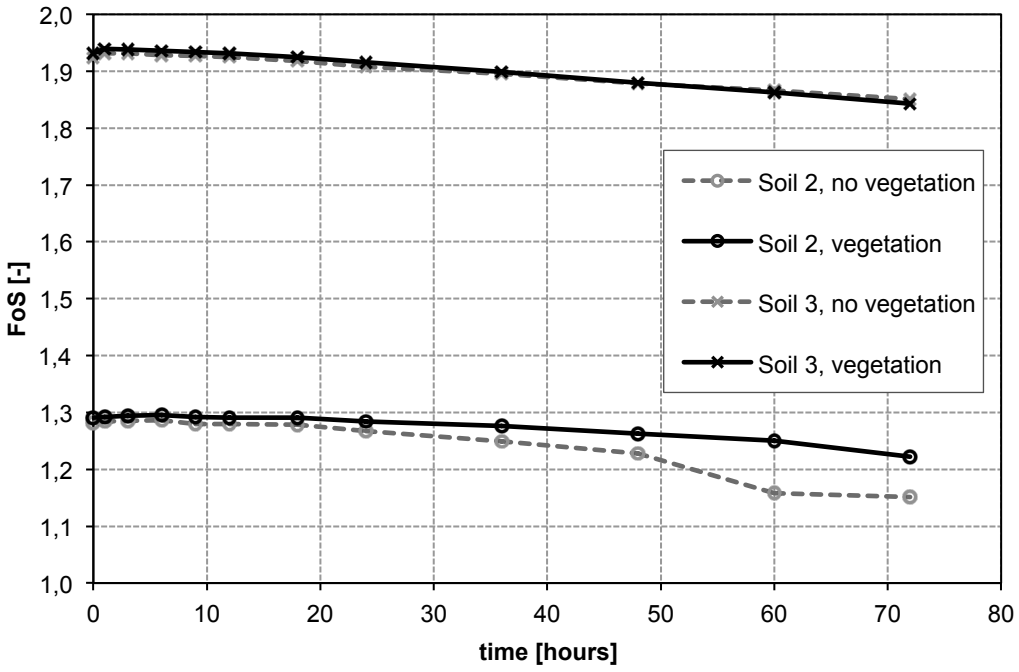

Fig. 43 Factor of safety for soil 2 and soil 3 with rainfall intensity of 15 mm/hour, slope inclination 30˚

3.7.1 Geometry, mesh coarseness and material properties

The analysis of the slope including tension cracks is conducted for soil 2 and soil 3 for a slope inclination of 30 degrees. The hydraulic parameters for the analysis have been evaluated by using the soil series from the international soil classification system (USDA). Soil 2 was defined as silt and soil 3 as sandy clay. The mesh is very fine with an additional refinement for the non-vegetated soil. The water table was assumed to be horizontal at the toe of the slope. The location of the tension crack and the mesh coarseness for the case studies is listed at Table 13.

The width of the crack is 10 cm and the same for soil 2 and soil 3. Sand with a high permeability of $k = 1.4*10^{-4}$ m/s was defined for the filling of the crack.

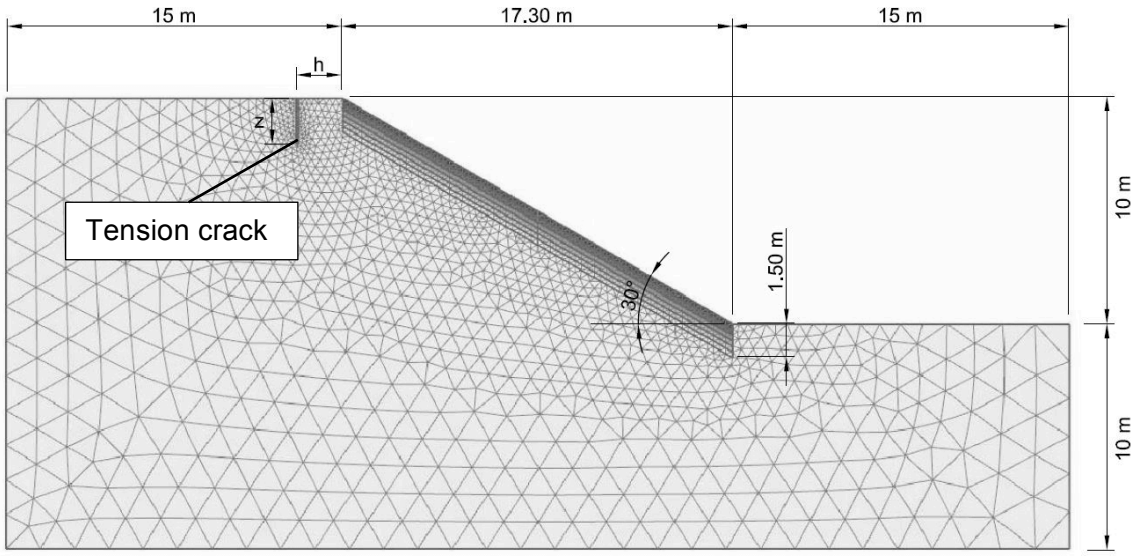

Fig. 44 Geometry, finite element mesh and location of the tension crack, (*z*) depth of the tension crack, (h) distance from the upper edge of the slope, slope inclination 30˚

Following case studies have been conducted in order to analyse the influence of the tension crack:

Table 13 Case studies for the influence of tension cracks

	Soil material	Distance from crest (h)	Depth of crack (z)	Mesh coarseness
Case (a)	Soil 2	1 m	2 m	Elements: 2096 Nodes: 17041
Case (b)	Soil 2	2 m	2 m	Elements: 2803 Nodes: 22751
Case (c)	Soil 3	1 m	2 m	Elements: 3829 Nodes: 31027
Case (d)	Soil 3	2 m	2 m	Elements: 2803 Nodes: 22751

3.7.2 Boundary conditions

A global water table was assumed to be at the toe of the slope. The left, right and bottom boundary is impermeable (Fig. 45). Suction is taken into account for the analysis. The maximum pore pressure head (ψ_{max}) and the minimum pore pressure head (ψ_{min}), relative to the elevation of the boundary, are set by default and are 0.1 and -1.0 respectively. That means if the rainfall intensity is higher than the saturated hydraulic conductivity of the soil, not all of the water can infiltrate and a part remains at the surface. The water accumulates at the surface and the maximum pore pressure head (ψ_{max}) defines the threshold level at which point surface run-off takes place.

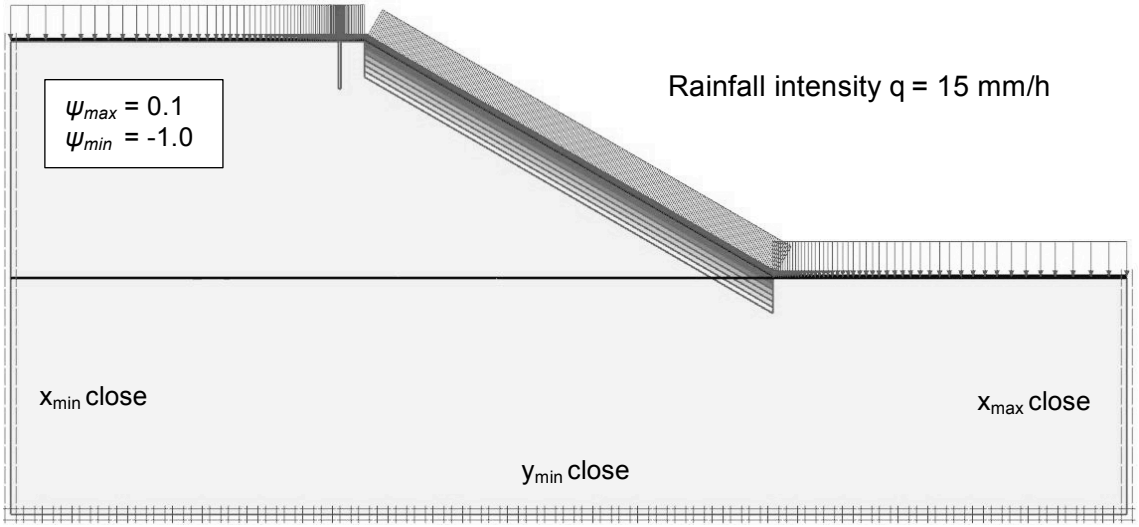

Fig. 45 Boundary conditions, slope with vegetation and tension crack

3.7.3 Pore pressure analysis

The behaviour of the pore pressure and the saturation, influenced by a higher infiltration rate through a tension crack, is studied. The saturation is analysed in a vertical cross section through the tension crack from the top of the slope till the water table at the toe of the slope (case (b)). The analysis is performed for both, a vegetated slope with no tension crack and a vegetated slope including a tension crack in order to compare the results.

As it can be seen at figure Fig. 46 the tension crack is significantly increasing the infiltration rate. While for the slope without a tension crack (Fig. 46 (b)) fully saturated conditions are reached in 3 m depth below ground surface after 72 hours rainfall, the slope with a tension crack (Fig. 46 (a)) reaches the fully saturated condition in 3 m depth after half of the time (36 hours rainfall).

Fig. 47 shows the suction pattern (case (b)) for a slope with a tension crack compared to a slope without a tension crack for particular times of rainfall infiltration (initial condition, 12 hours, 24 hours, 48 hours and 72 hours rainfall). The crack forms a saturated soil column around the crack. The moisture content clearly increases around a tension crack and reduces the matric suction that contributes to decreasing shear strength.

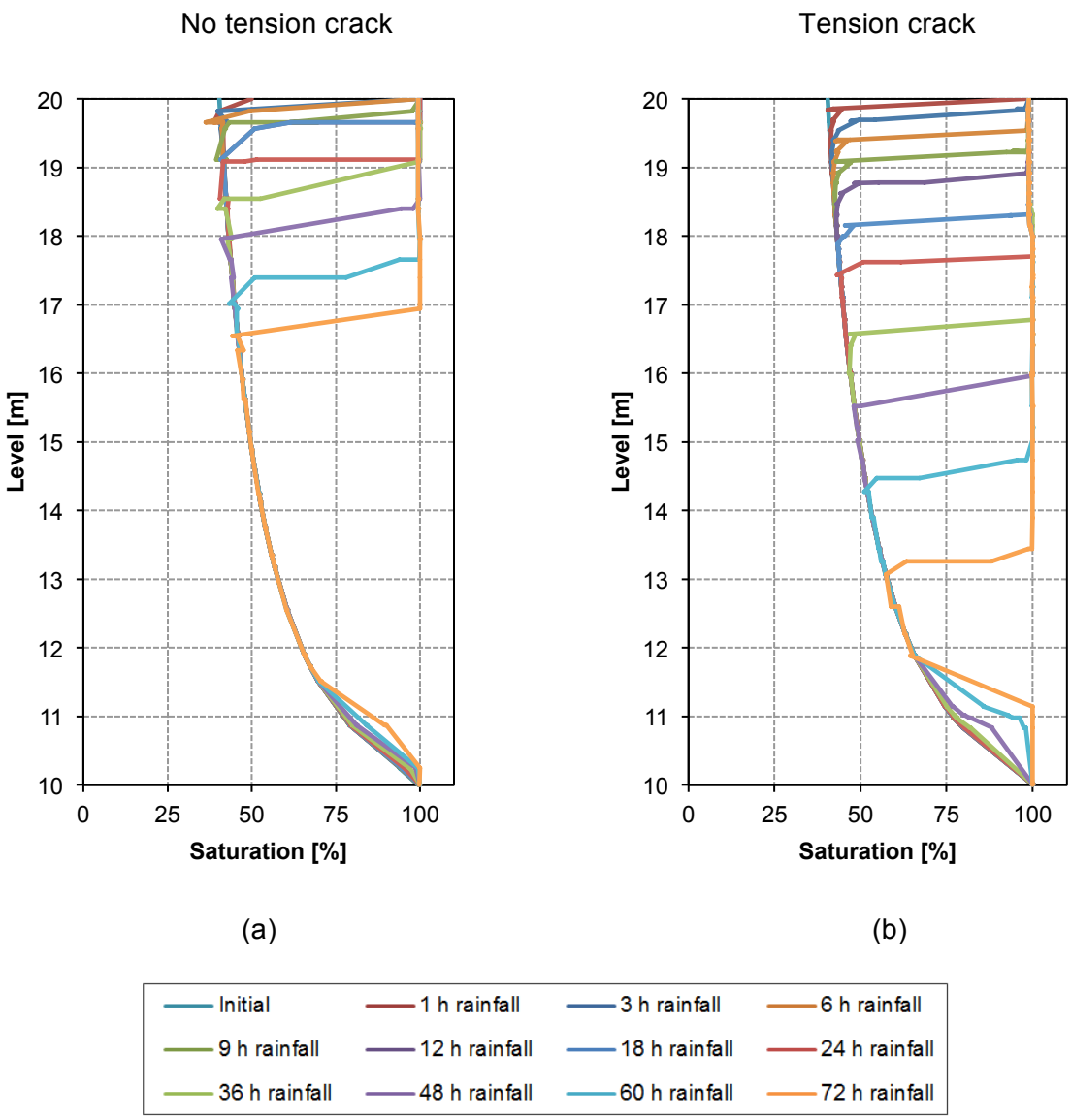

Fig. 46 Saturation profile for case (b) in a vertical cross section plane vertical through the tension crack, 20 m represents ground surface at top of the slope: (a) no tension crack, (b) tension crack

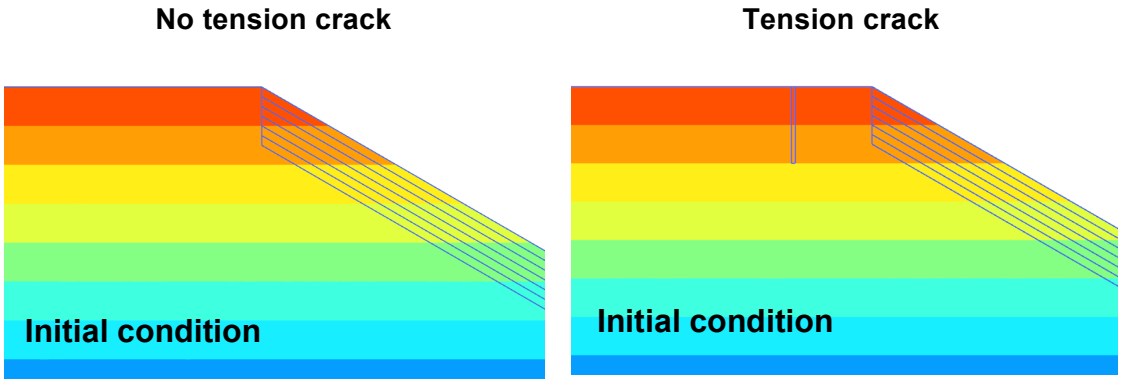

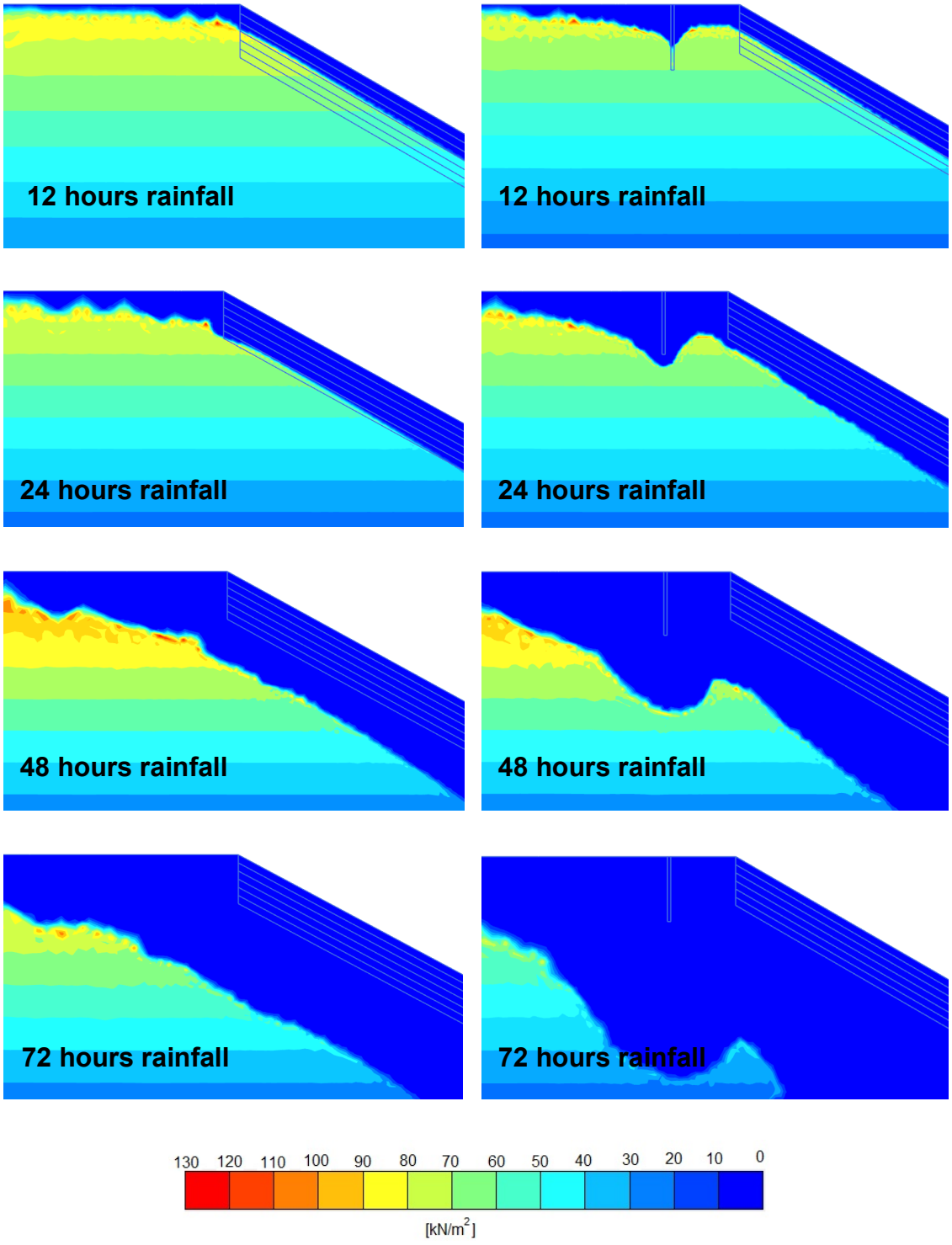

Fig. 47 Suction profile for case (b) for particular times of rainfall infiltration; left no tension crack, right with tension crack

3.7.4 Stability analysis

As shown before in Fig. 46 and Fig. 47, a tension crack is increasing the infiltration rate, which results in a different saturation and suction pattern compared to a case with no crack. Now, the influence of the tension crack on the stability of the slope is studied. Soil 2 (case (a), case (b)) and soil 3 (case (c), case (d)) was taken for the analysis with a rainfall intensity of 15 mm/h. For the soil 3 the rainfall intensity is higher than the saturated hydraulic conductivity and surface run-off takes place (see Fig. 11).

Table 14 shows the results from the stability analysis. For the initial condition and the first few hours of rainfall, when the soil is slightly saturated through the crack, the FoS with a tension crack is approximately the same than without a tension crack. As a conclusion it can be said that from a mechanical point of view the tension crack has no significant influence because of the different mechanical properties of the crack. That means that the main factor of influence is the accelerated saturation and reduced shear strength because of a higher saturation caused by the crack. At Fig. 48 and Fig. 49 it can be seen that with a progressive rainfall infiltration the FoS for the cases with a tension crack is decreases more than without a crack.

Table 14 Factor of safety with tension crack and rainfall infiltration

Rainfall [hour]	FoS					
	Soil 2			Soil 3		
	Veg. no crack k_{sat}=6,94E-06 [m/s]	Case (a) k_{sat}=6,94E-06 [m/s]	Case (b) k_{sat}=6,94E-06 [m/s]	Veg. no crack k_{sat}=3,3E-06 [m/s]	Case (c) k_{sat}=3,3E-06 [m/s]	Case (d) k_{sat}=3,3E-06 [m/s]
0	1,29	1,29	1,28	1,93	1,93	1,93
1	1,29	1,30	1,29	1,94	1,94	1,93
3	1,29	1,30	1,29	1,94	1,94	1,94
6	1,30	1,30	1,28	1,94	1,94	1,93
9	1,29	1,29	1,28	1,93	1,93	1,93
12	1,29	1,29	1,28	1,93	1,93	1,93
18	1,29	1,28	1,27	1,93	1,93	1,92
24	1,28	1,28	1,27	1,92	1,92	1,91
36	1,28	1,25	1,24	1,90	1,90	1,89
48	1,26	1,21	1,21	1,88	1,88	1,85
60	1,25	1,17	1,18	1,86	1,83	1,81
72	1,22	1,15	1,16	1,84	1,79	1,77

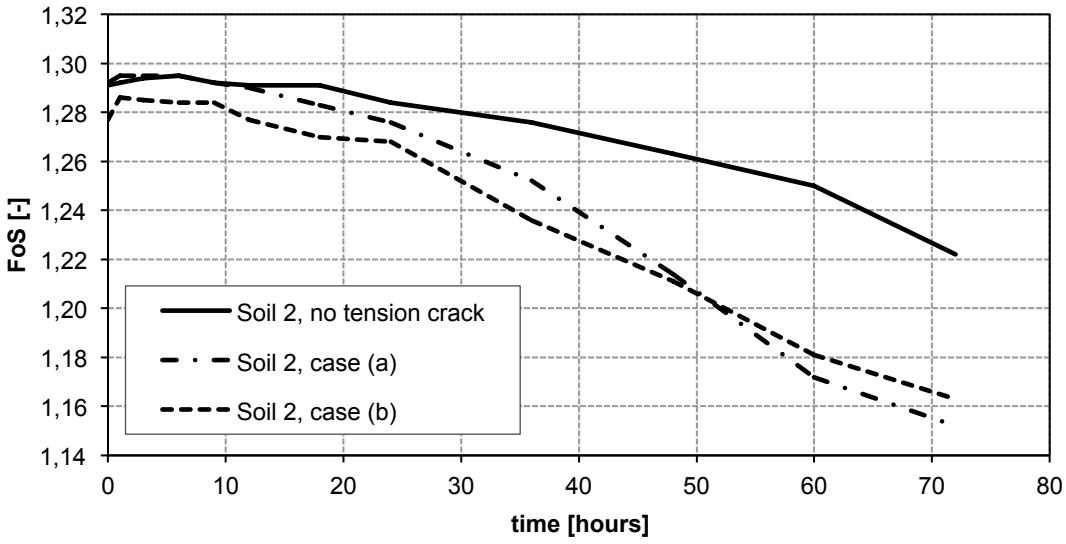

Fig. 48 Factor of safety for soil 2 with tension crack; case (a) and case (b)

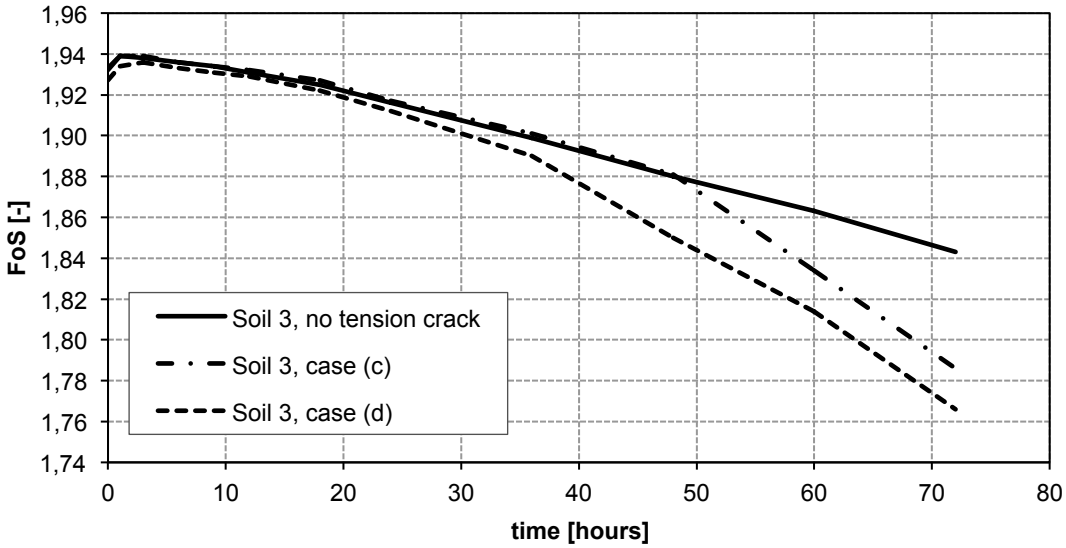

Fig. 49 Factor of safety for soil 3 with tension crack; case (c) and case (d)

Fig. 50 shows the saturation profile and the incremental deviatoric strain for specific durations of rainfall for (a) case with- and without a tension crack.

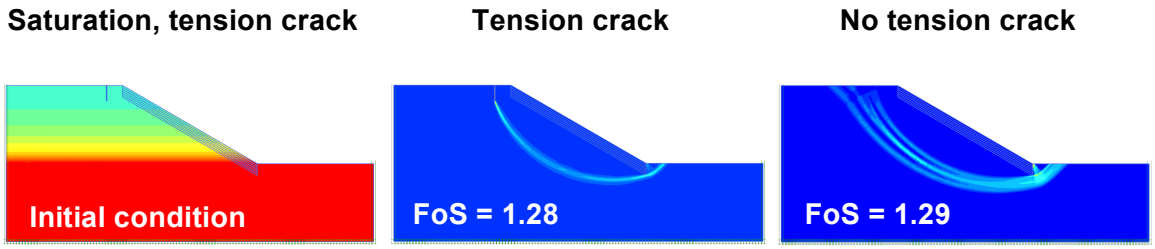

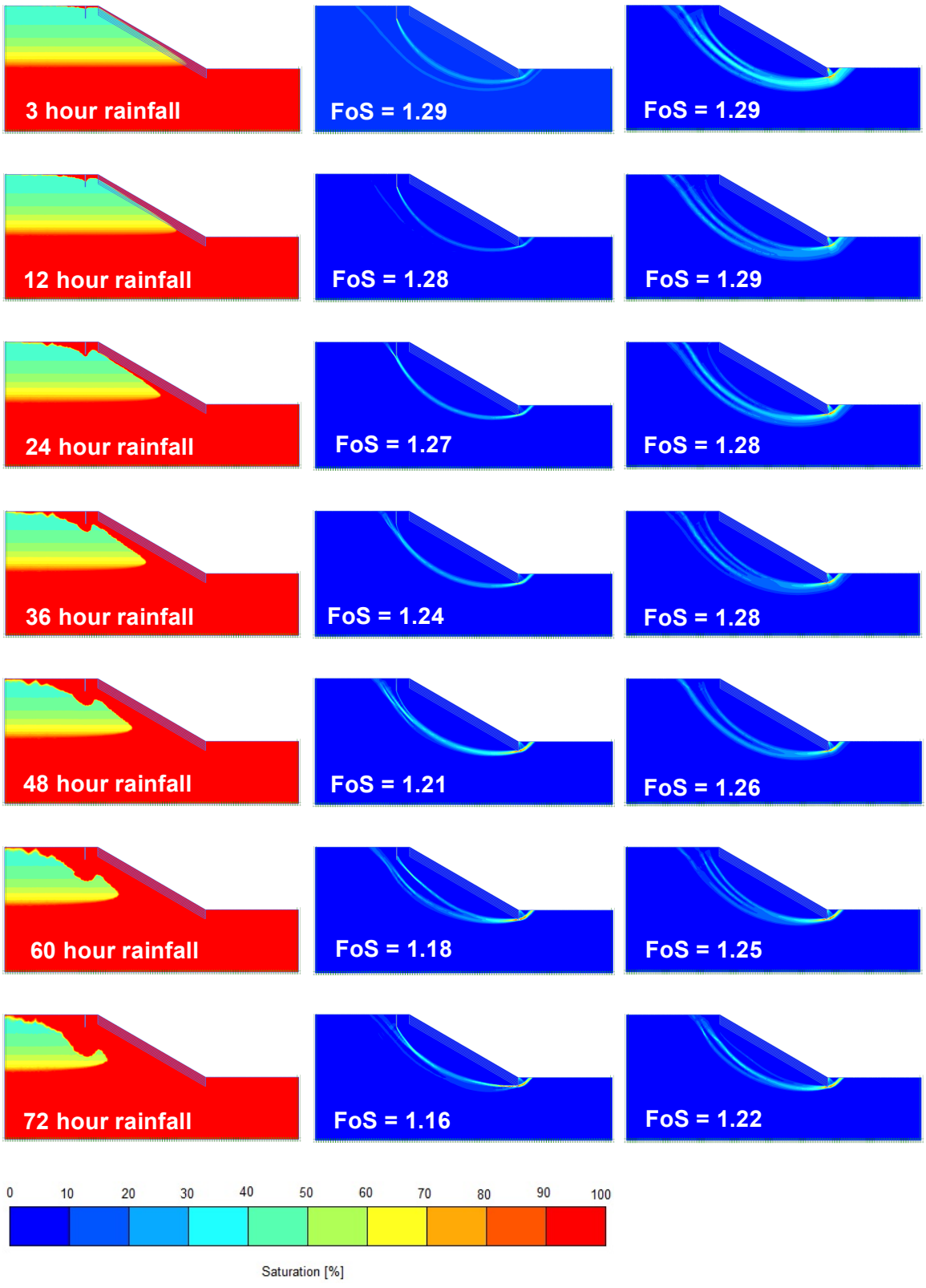

Fig. 50 Saturation and failure mechanism (incremental deviatoric strain) for soil 2 case (a), inclination 30 degree, left column saturation, middle column failure mechanism with tension crack, right column failure mechanism without tension crack

4 Summary and Conclusion

In this thesis the perpendicular root model is explained and applied for the slope stability analysis. It constitutes a simplified root model for calculating the apparent cohesion and requires two input parameters (tensile strength of the single root and the root area ratio). However, it should be considered that the model is based on simplifications and tends to overestimate the apparent cohesion. A second approach to determine the parameters of a rooted soil is the use of a direct shear test. The advantage of this approach is that in situ data can be used for the stability calculation in order to overcome the simplifications, required from the perpendicular root model.

Next to a mechanical strengthening of a rooted soil, vegetation also has a beneficial hydrological impact as it decreases the soil moisture content through transpiration. Therefore, matric suction is increased and contributes towards higher shear strength. For calculating the root water uptake, a linear one-dimensional model is shown. This model requires two plant specific parameters: the maximum root depth and a metrological parameter. As the water extraction is dependent on the pore water pressure in the soil, the water uptake can't be included in the finite element program PLAXIS and is not considered. However, for long term stability analysis the water uptake should be considered and included in the calculations.

The results of the stability analysis for different types of soil, inclinations and water tables show that the reinforcing effect of vegetation is strongly dependent on the failure mechanism. The main difference is obtained for non-cohesive soils with a shallow failure surface that intersects with the vegetated part of the slope. On the contrary, cohesive soils with a deep failure surface display a small or not significant reinforcing effect.

By analysing the influence and effectiveness of the location of the vegetation the main output is that a reinforced section at the toe of the slope is much more effective than a reinforced section at the head of the slope. The effect can be altered by using trees with a deep-rooted root system located at the toe of the slope. The self-weight of the vegetation is not taken into account since the applied species is grass with negligible self-weight. The use of fully grown trees at the head of the slope has a destabilising effect due to their self-weight and should be considered separately.

The slope stability analysis with a tension crack shows a higher infiltration rate because of the crack. In this case the slope indicates a different saturation and suction pattern compared to a case without a crack. In addition, the results show that the main influence is the accelerated saturation caused by the crack and therefore reduced shear strength because of the higher saturation. The analysis also shows that the local weakness in strength due to the crack has no significant influence since the FoS is approximately the same for the initial condition and the first few hours of rainfall.

5 Literature

Ali, A., Huang, J., Lyamin, A., Sloan, S., & Cassidy, M. (2014). Boundary effects of rainfall-induced landslides. *Computers and Geotechnics 61 (2014) 341-354* .

Allen, R., Pereira, L., Raes, D., & Smith , M. (1998). Crop evapotranspiration - Guidelines for computing crop water requirements. *FAO- Food and Agriculture Organization of the United Nations, Rome* .

Bishop, A. (1959). The principle of effective stress. *Teknisk Ukeblad, 106(39), 859-863*.

Brinkgreve, R., Engine, E., & Swolfs, W. (2014a). PLAXIS 2D Scientific Manual (Universary Edition). *PLAXIS bv, Delft, Netherlands* .

Brinkgreve, R., Enging, E., & Swolfs, W. (2014 a). PLAXIS 2D Material Models Manual (Universary Edition). *PLAXIS bv, Delft, Netherlands* .

Cazzuffi, D., & Crippa, E. (2005). Contribution of Vegetation to Slope Stability: An Overview of Experimental Studies Carried Out on Different Types of Plants. *Erosion of Soils and Scour of Foundations* .

Chirico, G. B., Borga, M., Preti, F., Rigon, R., & Tarolli, P. (2013). Role of vegetation on slope stability under transient unsaturated conditions. *Procedia Environmental and Sciences 19, 932-941* .

Danjon, F., Barker, D., Drexhage, M., & Stokes, A. (2008). Using Three-dimensional Plant Root Architecture in Models of Shallow-slope Stability. *Oxford University Press, Annuals of Botany 101: 1281-1293* .

Eching, S., & Moellenberndt, D. (2000). *CIMIS Agriculture Resource Book.* Sacramento: California Departement of Water Resources.

Erskine, J. (1992). Vetiver grass: its potential use in soil and moisture conservation in Southern Africa. *S Afr J Sci, 88:298-299* .

Faisal, H., & Normaniza, O. (2008). Shear strength of soil containing vegetation roots. *Soils and Foundation, 48(4), pp. 587-596* .

Fan, C.-C., & Lai, Y.-F. (2014). Influence of the spatial layout of vegetation on the stability of slopes. *Plant and Soil, 377:83-95* .

Fatahi, B. (2007). Modelling of infleunce of matric suction induced by native vegetation on sub-soil improvement. *PhD thesis, School of Cicil, Mining and Environmental Engineering, University of Wollong* .

Feddes, R., Kowalk PJ., & Zaradny, H. (1978). *Simulation of field water use and crop yield.* New York: Halsted Press, John Wiley & Sons.

Fredlund, D. (1996). The emergence of unsaturated soil mechanic. *The Fourth Spencer J. Buchanan Lecturer, College Station, Texas, A & M University Press, p.39.* .

Gavin, K., & Xue, J. (2008). A simple method to analyze infiltration into unsaturated soil slopes. *Computer and Geotechnics, 35, 223-230* .

Gentile, F., Elia, G., & Elia, R. (2010). Analysis of the stability of slopes reinforced by roots. *Design and Nature V* .

Gentile, F., Romano, G., & Trisorio-Liuzzi, G. (1998). L'uso della vegetazione negli intervendi di difesa del suolo in ambiente mediterraneo. *Genio Rurale, 2, pp. 42-51* .

Graz University of Technology. (2015). Computational Geotechnics, Script. *Institute of Soil Mechanics and Foundation Engineering, Graz University of Technology* .

Hamdhan, I. (2012). A Contribution to Slope Stability Analysis with the Finite Elemente Method. *PhD thesis, Institute for Soil Mechanics and Foundation Engineering, Graz University of Technology* .

Harry, S.-A., Toll, D., & Phoon, K.-K. (2007). *Rainfall Induced Landslides - Why they occur and some mitigating measures.* Retrieved 06 28, 2015, from http://www.cces.ethz.ch/latsis2007/program/CCES_Latsis_extended_abstract_Siew_Ann_Tan.pdf

Hengchaovanich, D. (1998). Vetiver grass for slope stabilization and erosion control. *Tech. Bull., No. 1998/2, PrVN/ORDPB, Bangkok, Thailand* .

Hengchaovanich, D., & Nilaweera, N. (1996). An Assesement of Strength Properties of Vetiver Grass Roots in Relation to Slope Stabilisation. *International Conference on Vetiver, Chain Kai, Thailand* .

Hough, M., & Jones, J. (1997). The United Kingdom meteorological office rainfall and evaporation calculation system: MORECS version 2.0 - and overview. *Hydrol Earth Syst Sci; V1(2):227-39* .

Hough, M., Palmer, S., Weir, A., Lee, M., & Barrie, I. (1997). The meteorological office rainfall and evaporation calculation System: MORECS version 2.0 (1995). An update to hydrological memorandum 45. *Meteorological Office* .

Islam, M., & Shahin, H. (2013). Reinforcing effect of Vetiver (Vetiveria zizanioides) root in geotechnical structures - experiments and analyses. *Geomechanics and Engineering, Vol. 5 No. 4 , 313-329* .

Likitlersuang, Suched; Lohwongwatana, Boonrat; Vanno, Sirintra; Boonyananta, Soamshine;. (2015). Laboratory investigation of Vetiver root reinforcement for slope protection.

Lin, D.-G., Huang, B.-S., & Lin, S.-H. (2010). 3-D numerical investigations into the shear strength of the soil-root system of Makino bamboo and its effect on slope stability. *Ecological Engineering, 36, 992-1006* .

Mickovski, S., & Beek, L. (2009). Root morphology and effects on soil reinforcement and slope stability of young vetiver (Vetiveria zizanioides) plants grown in semi-arid climate. *Plant and Soil, 324:43-56* .

Mickovski, S., Stokes, A., van Beek, R., Ghestem, M., & Fourcaud, T. (2011). Simulation of direct shear tests on rooted and non-rooted soil using finite element analysis. *Ecological Engineering 37, 1523-1532* .

Ng, C., & Pang, Y. (2000). Influence of stress state on soil-water characteristics and slope stability. *Journal of Geotechnical and Geoenvironmental Engineering, Vol. 22 (1), 1-28* .

Nyambayo, V., & Potts, D. (2009). Numerical simulation of evapotranspiration using a root water uptake model. *Computers and Geotechnics 37, 175-186* .

Oberg, A., & Sällfors, G. (1997). Determination of shear strength parameters of unsaturated silts and sands based on the water retention curve. *ASTM Geotechnical Testing Journal, Vol. 20(1), 40-48* .

Pollen, N. (2006). Temporal and spatial variability in root reinforcement of streambanks: Accounting for soil shear strength and moisture. *Channel and Watershed Processes Research Unit, USDA-ARS National Sedimentation Laboratory* .

Pollen, N. (2004). The Effects of Riparian Vegetation on streambank stability: Mechanical and Hydrological interactions. *Ph.D. Thesis, King's College, University of London, 320 pp.*

Pollen, N., & Simon, A. (2005). Estimating the mechanical effects of riparian vegetation on streambank stability using fiber bunde model. *Water Resources Research 41, W07025* .

Prasad, R. (1988). A linear root water uptake model. *Hydrol, 99:297-306* .

Preti, F., & Giadrossich, F. (2009). Root reinforcement and slope bioengineering stabilization by Spanish Broom (Spartium junceum L.). *Hydrology and Earth Sciences, 13, 1713-1726* .

Sasekaran, M. (2011). Impact of Permeability and Surface cracks on Soil Slopes. *Master thesis, Faculty of Engineering and Physical Science, University of Manchester* .

Schwarz, M., Preti, F., Giadrossich, F., Lehmann, P., & Or, D. (2009). Quantifying the role of vegetation in slope stability: A case study in Tuscany (Italy). *Ecological Engineering, 285-291* .

Selby, M. (1993). Hillslope Materials and Processes. *Oxford University Press* .

Shi, B.-X., Chen, S.-s., Han, H.-q., & Zheng, C.-f. (2014). Expansive Soil Crack Depth under Cumulative Damage. *The Scientific World Journal, Articel ID 498437* .

Simon, A., & Collison, J. (2002). Quantifying the Mechanical and Hydrologic Effect of Riparian Vegetation on Streambank Stability. *Earth Surface Processes Landforms 27, 527-546* .

Terzaghi, K. (1943). Theoretical Soil Mechanics. *John Wiley and Sons, New York* .

Thomas, R., & Pollen, N. (2009). Modeling root-reinforcement with a fiber-bundle modeland Monte Carlo simulation. *Ecological Engineering 36 (2010) 47-61* .

Truong, P. (1999). Vetiver grass technology for land stabilisation, erosion and sediment control in the Asia Pacific region. In: Proc. First Asia Pacific Conference on Ground and Water Bioengineering for Erosion Control and Slope Stabilisation, Manila, Philippines. *Int Eros Control Assoc, Steamboat Springs, USA* .

Van Genuchten, M. (1980). A closed-form equation for predicting the hydraulic conductivity of unsaturated soils. *Soil Science Society of America Journal, Vol. 44 (5), 892-898* .

Vanapalli S. K., Fredlund, D., Pufahl, D., & Clifton, A. (1996). Model for the prediction of shear strength with respect to soil suction. *Canadian Geotechnical Journal, Vol. 33 (3), 379-392* .

Vanapalli, S., Fredlund, D., Pufahl, D., & Clifton, A. (n.d.). Model for the prediction of shear strength with respect to soil suction. *Canadian Geotechnical Journal, Vol. 33 (3), 379-392* .

Waldron, L. (1977). The shear resistance of root-permeated homogeneous and stratified soil. *Journal of the Soil Science Society of Amerika, 41, 843-849* .

Waldron, L., & Dakessian, S. (1981). Soil reinforcement by roots: calculation of increased soil shear resistance from root properties. *Soil Science, 427-435* .

Wu, T., Beal, P., & Lan, C. (1988). In situ shear test of soil-root system. *Journal of Geotechnical Engineering, 114, pp. 1351-1375* .

Wu, T., McKinnell, I., & Swanston, D. (1979). Strength of tree roots and landslides on Prince of Wales Island, Alaska. *Canadian Geotechnical Journal 16, 19-33* .

6 APPENDIX

Failure mechanism for soil 1 with an inclination of 25 degrees (according to chapter 3.5)

No vegetation	Vegetation
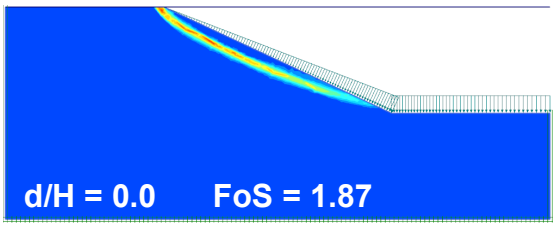	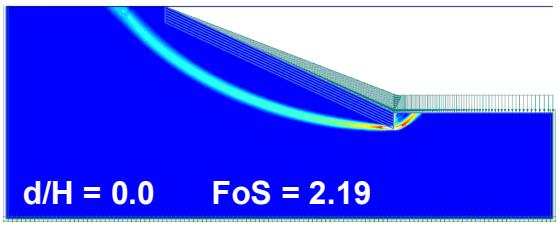
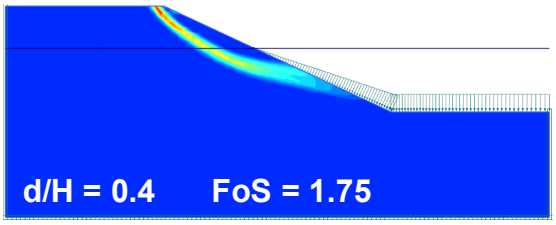	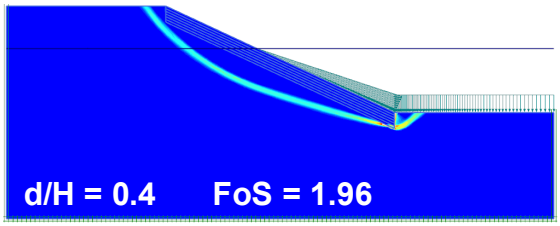
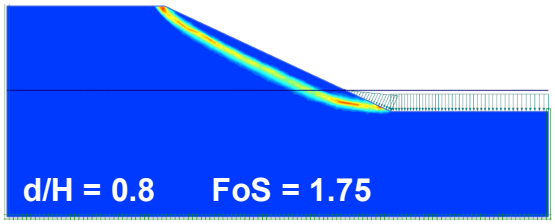	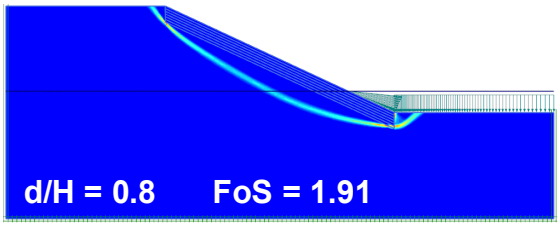
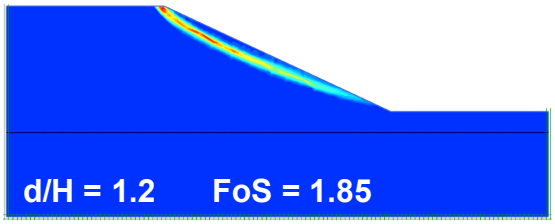	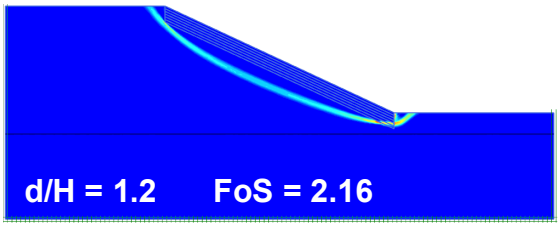
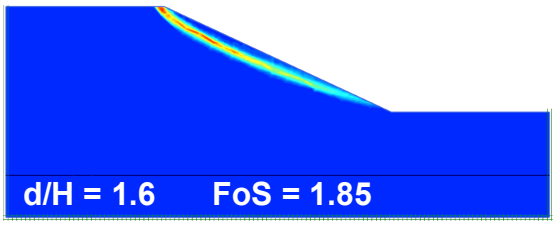	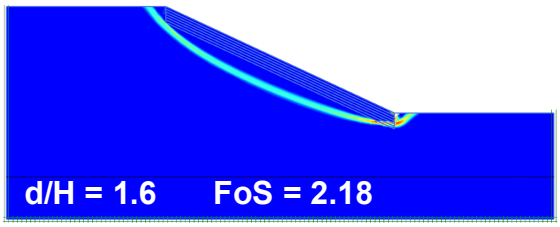

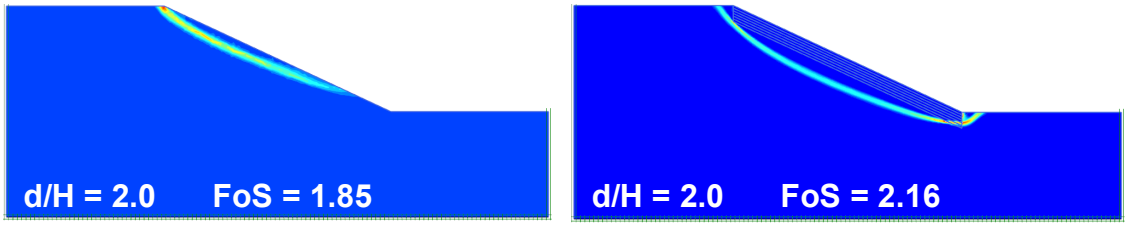

Fig. 51 Failure mechanism (incremental deviatoric strain) for soil 1, inclination 25 degree, left side no vegetation, right side with vegetation

Failure mechanism for soil 2 with an inclination of 25 degrees (according to chapter 3.5)

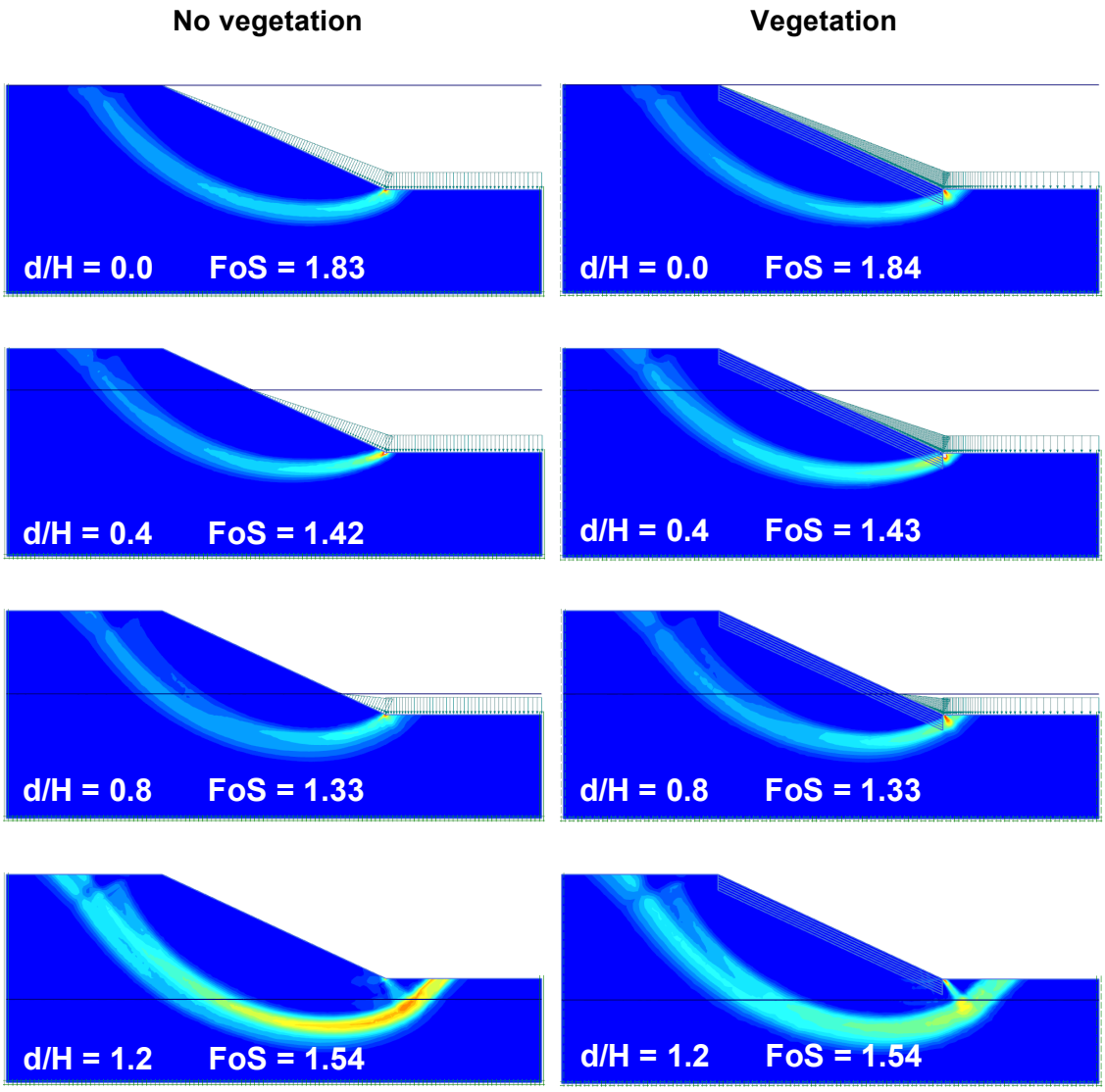

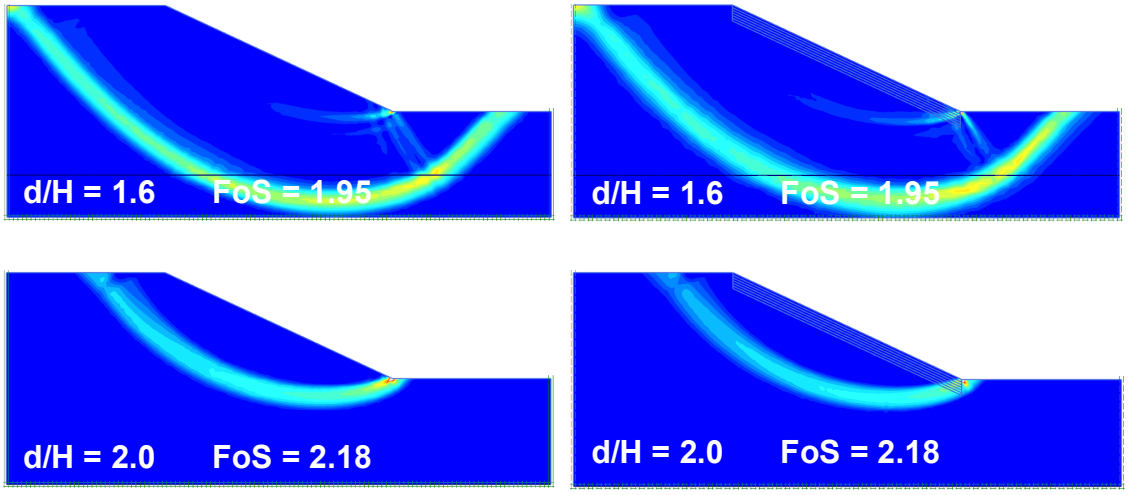

Fig. 52 Failure mechanism (incremental deviatoric strain) for soil 2, inclination 25 degree, left side no vegetation, right side with vegetation